이학박사 학위논문

Synthesis of Well-Defined 1-Dimensional Polymers by Ring-Opening Metathesis Polymerization: Conformation and Mechanochemistry

고리개환복분해중합에 의한 정교한 1차원 고분자의 합성: 구조 및 기계화학

2020년 2월

서울대학교 대학원

화학부 유기화학 전공

방 기 택

Abstract

Synthesis of Well-Defined 1-Dimensional Polymers by Ring-Opening Metathesis Polymerization: Conformation and Mechanochemistry

Ki-Taek Bang

Department of Chemistry

The Graduate School

Seoul National University

Synthesis of complex macromolecules with well-defined architecture has been a goal of polymer chemistry to mimic and move beyond the natural polymers. In particular, this is the case of graft polymers, consisting of linear polymers as side groups grafted on the main-chain polymers. However, there are still issues to control the polymer architecture precisely because of defects issues and dispersity of the polymeric side groups. Following the three chapters describe the synthesis of the well-defined macromolecules and their characteristics.

Chapter 2 describes the synthesis of the high generation dendronized polymers (denpols), which are the unique macromolecules composed of a backbone with dendritic side groups (dendrons). We prepared denpols containing ester dendrons up to the sixth generation (G6) by ring-opening metathesis polymerization (ROMP). It is the highest generation ever polymerized among denpols prepared by grafting-through approach. The combination of size exclusion chromatography multi-angle laser light scattering (SEC-MALLS) small-angle neutron scattering (SANS) techniques revealed their detailed structure in solution and the relationship between the size of the dendron, grafting density, and conformation.

Charter 3 reports the synthesis of the denpols having polyphenylene dendrons and their mechanochemistry. We prepared the series of denpols with high molecular weight up to 1484 kDa with narrow dispersity below 1.30. The successful preparation enabled us to unravel their mechanochemical reaction which was investigated by ultrasound-induced degradation technique. We were able to find a quantitative relationship between the chain extension and the rate of degradation.

Chapter 4 presents the synthesis of carbon nanodot polymers. We were able to prepare the defect-free polymers by polymerizing a norbornene having nanographene moiety. Grubbs 3rd generation catalyst provided the molecular weight control of polymers ranging from 32 to 164 kDa with narrow dispersity below 1.40. The controlled polymerization led us to synthesize the block copolymer containing HBC for the first time.

Keywords: Ring-opening metathesis polymerization, dendronized polymer, multi-angle laser light scattering, conformation, mechanochemistry, nanographene.

Student Number: 2014-21252

Table of Contents

Chapter 1. Introduction

1.1 Backgrounds

Ring opening metathesis polymerization (ROMP) for complex macromolecules

The ring-opening metathesis polymerization (ROMP) is one of chain-growth polymerization where the cyclic olefin is opened to generate a polymer chain by metathesis reaction[1]. It has been emerged as a powerful tool to synthesize complex macromolecules such as block copolymers,[2-4] graft-polymers,[5,6] metallopolymer[7] and dendronized polymers.[2,8-10] Norbornene (NB) derivatives has used the typical monomer because the release of their ring strain provide strong driving force to overcome the steric hindrance caused by the bulky pendant group during the propagation. Moreover, high reactive fast-initiating Grubbs 3rd catalyst[11] having extraordinary functional group tolerance enabled the synthesis of complex polymers in a living manner, ensuring the molecular weight control with low dispersity.

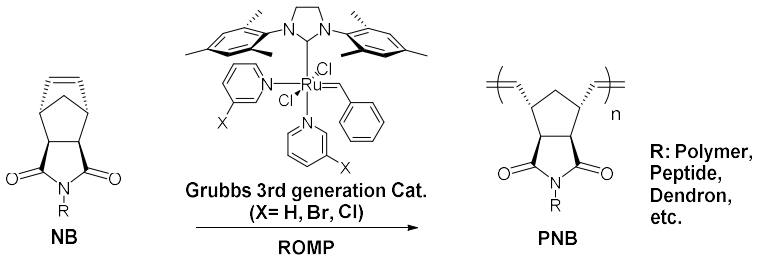

Scheme 1.1. Ring-opening metathesis polymerization of norbornene

Endo-tricyclo[4.2.2.0]deca-3,9-diene (TD)

Endo-tricyclo[4.2.2.0]deca-3,9-diene (TD)s are unique molecules which are also capable of ROMP like NB due to the cyclobutene moiety having high ring strain (Scheme 1.1a). They have been much less

studied since their propagation rate (k_p) is much slower than those of NB[12]. However, one of the advantage of TD is that one can achieve the highly grafted polymer compared to poly(NB) (PNB) analogues given that the repeat unit length of poly(TD) (PTD) is shorter than that of PNB (Scheme 1.2b).[2,13,14] Moreover, our group reported that rate of initiation(k_i) for TD monomer is much faster compared to NB derivatives.[15] Furthermore, the intermediate of the propagating species for PTD where the Ru carbene is chelated to adjacent olefin was observed by NMR analysis and X-ray crystallography.[16] The formation of the chelated Ru complexes during the polymerization plays an important role to stabilize propagating species and increase k_i / k_p ratio which are necessary for living polymerization. Thus, TD monomers are highly desirable to obtain the densely grafted polymers with controlled molecule weight and narrow dispersity.

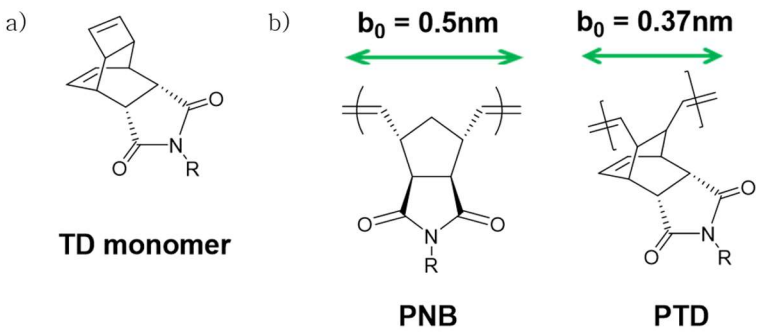

Scheme 1.2 a) structure of a TD monomer b) unit length(b_o) of PTD and PNB

Dendronized polymers

Dendronized Polymer(denpol) is the unique macromolecule having the branched unit dendron as a pendant group. One of the most distinct

features of denpol is its extended conformation whereas conventional polymers such as poly(styrene) adapts the entangled conformation. Besides, one can design a polymer with a precisely controlled molecular architecture and desired properties by tuning the polymer backbone and the dendritic unit[17]. The structural versatility of denpols is an attractive feature that has led scientists to examine their behavior in a variety fields, inlcuding photonics[3], electronics[8], biomaterial[18], self-assembly[19], drug delivery[20], waste treatment[21], energy storage[22], and rheology[23]. However, the main obstacle towards the synthesis of large denpols is the precise incorporation of the bulky pendant with high fidelity.

Synthetic approaches for denpols

To overcome the synthetic hurdle, many approaches have been investigated for the preparation of denpols. For example, grafting-to method[24-29], (coupling dendrons to the precursor polymers directly) or most widely used grafting-from approach[10,30-33] (step by step dendronization of every generation onto the precursor polymer chain) have been successful to prepare denpols carrying up to 8th generation dendrons.[33,34] However, these methods lead to some defects and analysis to confirm their structure can be tedious, especially for high generations.

The alternative approach is grafting-through or macromonomer approach[2,9,15,35-42] via directly polymerizing macromonomers containing the defect-free dendrons. Although this allows the synthesis of highly pure denpols, it is the most challenging method as the steric hindrance between the bulky dendrons greatly retards the

polymerization. Fortunately, recent advances of ring-opening metathesis polymerization (ROMP)[43-45] has provided an excellent solution to overcome this challenge. For example, we reported denpols of poly(endo-tricycle[4.2.2.0]deca-3,9-diene) (PTD) containing up to 4th generation dendrons[2] and poly(norbornene) (PNB) containing up to 5th generation dendrons[9], as well as their block copolymers and gradient copolymers[2] by ROMP.

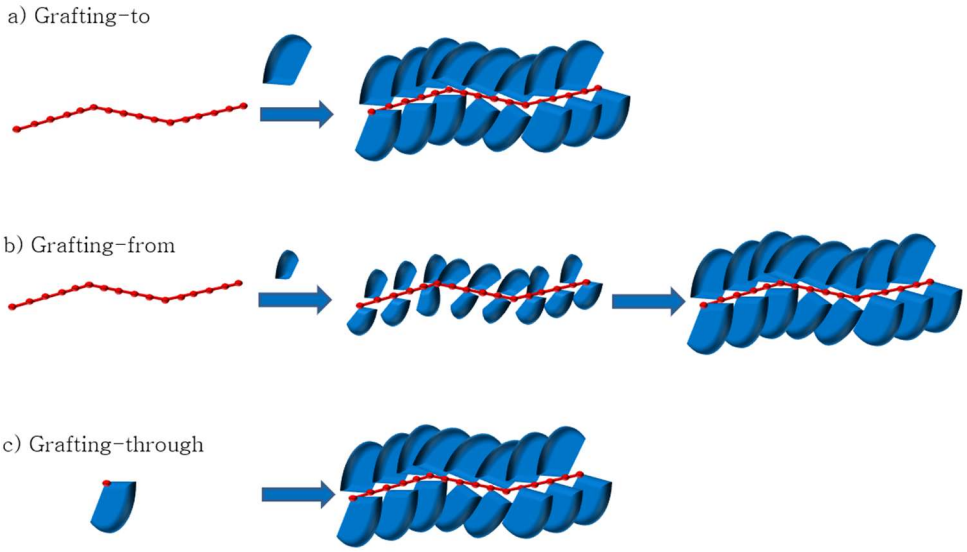

Figure 1.1 Synthetic strategies for the denpols a) Grafting-to b) Grafting-from c) Grafting-through approach.

1.2 Reference

(1) Sutthasupa, S.; Shiotsuki, M.; Sanda, F. *Polymer Journal* 2010, *42*, 905.

(2) Kim, K. O.; Choi, T.-L. *Macromolecules* 2013, *46*, 5905.

(3) Piunova, V. A.; Miyake, G. M.; Daeffler, C. S.; Weitekamp, R. A.; Grubbs, R. H. *Journal of the American Chemical Society* 2013, *135*, 15609.

(4) Isarov, S. A.; Lee, P. W.; Pokorski, J. K. *Biomacromolecules* 2016, *17*, 641.

(5) Kammeyer, J. K.; Blum, A. P.; Adamiak, L.; Hahn, M. E.; Gianneschi, N. C. *Polymer Chemistry* 2013, *4*, 3929.

(6) Kawamoto, K.; Zhong, M.; Gadelrab, K. R.; Cheng, L.-C.; Ross, C. A.; Alexander-Katz, A.; Johnson, J. A. *Journal of the American Chemical Society* 2016, *138*, 11501.

(7) Gu, H.; Ciganda, R.; Hernandez, R.; Castel, P.; Zhao, P.; Ruiz, J.; Astruc, D. *Macromolecules* 2015, *48*, 6071.

(8) Kim, J.; Yun, M. H.; Lee, J.; Kim, J. Y.; Wudl, F.; Yang, C. *Chemical Communications* 2011, *47*, 3078.

(9) Kim, K. O.; Choi, T.-L. *ACS Macro Letters* 2012, *1*, 445.

(10) Lee, C. C.; Fréchet, J. M. J. *Macromolecules* 2006, *39*, 476.

(11) Choi, T.-L.; Grubbs, R. H. *Angewandte Chemie International Edition* 2003, *42*, 1743.

(12) Charvet, R.; Novak, B. M. *Macromolecules* 2001, *34*, 7680.

(13) Dutertre, F.; Bang, K.-T.; Vereroudakis, E.; Loppinet, B.; Yang, S.; Kang, S.-Y.; Fytas, G.; Choi, T.-L. *Macromolecules* 2019, *52*, 3342.

(14) Dutertre, F.; Bang, K.-T.; Loppinet, B.; Choi, I.; Choi, T.-L.; Fytas, G. *Macromolecules* **2016**, *49*, 2731.

(15) Kim, K. O.; Shin, S.; Kim, J.; Choi, T.-L. *Macromolecules* **2014**, *47*, 1351.

(16) Song, J.-A.; Park, B.; Kim, S.; Kang, C.; Lee, D.; Baik, M.-H.; Grubbs, R. H.; Choi, T.-L. *Journal of the American Chemical Society* **2019**, *141*, 10039.

(17) Schlüter, A. D.; Rabe, J. P. *Angewandte Chemie International Edition* **2000**, *39*, 864.

(18) Deng, J.; Zhou, Y.; Xu, B.; Mai, K.; Deng, Y.; Zhang, L.-M. *Biomacromolecules* **2011**, *12*, 642.

(19) Feng, S.; Xiong, X.; Zhang, G.; Xia, N.; Chen, Y.; Wang, W. *Macromolecules* **2009**, *42*, 281.

(20) Wen, L.; Dalin, W.; Dieter, S. A.; Afang, Z. *Journal of Polymer Science Part A: Polymer Chemistry* **2009**, *47*, 6630.

(21) Roeser, J.; Heinrich, B.; Bourgogne, C.; Rawiso, M.; Michel, S.; Hubscher-Bruder, V.; Arnaud-Neu, F.; Méry, S. *Macromolecules* **2013**, *46*, 7075.

(22) Chakrabarti, A.; Juilfs, A.; Filler, R.; Mandal, B. K. *Solid State Ionics* **2010**, *181*, 982.

(23) Costanzo, S.; Scherz, L. F.; Schweizer, T.; Kröger, M.; Floudas, G.; Schlüter, A. D.; Vlassopoulos, D. *Macromolecules* **2016**, *49*, 7054.

(24) Karakaya, B.; Claussen, W.; Gessler, K.; Saenger, W.; Schlüter, A. D. *Journal of the American Chemical Society* **1997**, *119*, 3296.

(25) Helms, B.; Mynar, J. L.; Hawker, C. J.; Fréchet, J. M. J. *Journal of the American Chemical Society* **2004**, *126*, 15020.

(26) Mynar, J. L.; Choi, T.-L.; Yoshida, M.; Kim, V.; Hawker, C. J.; Frechet, J. M. J. *Chemical Communications* **2005**, 5169.

(27) Gao, M.; Jia, X.; Kuang, G.; Li, Y.; Liang, D.; Wei, Y. *Macromolecules* **2009**, *42*, 4273.

(28) Gössl, I.; Shu, L.; Schlüter, A. D.; Rabe, J. P. *Journal of the American Chemical Society* **2002**, *124*, 6860.

(29) Shu, L.; Göossl, I.; Rabe, J. P.; Dieter Schlüter, A. *Macromolecular Chemistry and Physics* **2002**, *203*, 2540.

(30) Shu, L.; Schlüter, A. D.; Ecker, C.; Severin, N.; Rabe, J. P. *Angewandte Chemie International Edition* **2001**, *40*, 4666.

(31) Yoshida, M.; Fresco, Z. M.; Ohnishi, S.; Fréchet, J. M. J. *Macromolecules* **2005**, *38*, 334.

(32) Grayson, S. M.; Fréchet, J. M. J. *Macromolecules* **2001**, *34*, 6542.

(33) Yu, H.; Schlüter, A. D.; Zhang, B. *Macromolecules* **2014**, *47*, 4127.

(34) Messmer, D.; Kröger, M.; Schlüter, A. D. *Macromolecules* **2018**, *51*, 5420.

(35) Kasëmi, E.; Zhuang, W.; Rabe, J. P.; Fischer, K.; Schmidt, M.; Colussi, M.; Keul, H.; Yi, D.; Cölfen, H.; Schlüter, A. D. *Journal of the American Chemical Society* **2006**, *128*, 5091.

(36) Malkoch, M.; Carlmark, A.; Woldegiorgis, A.; Hult, A.; Malmström, E. E. *Macromolecules* **2004**, *37*, 322.

(37) Zhang, A.; Zhang, B.; Wächtersbach, E.; Schmidt, M.; Schlüter, A. D. *Chemistry – A European Journal* **2003**, *9*, 6083.

(38) Kang, E.-H.; Lee, I.-H.; Choi, T.-L. *ACS Macro Letters* **2012**, *1*, 1098.

(39) Ossenbach, A.; Rüegger, H.; Zhang, A.; Fischer, K.; Schlüter, A. D.; Schmidt, M. *Macromolecules* **2009**, *42*, 8781.

(40) Zhang, A.; Okrasa, L.; Pakula, T.; Schlüter, A. D. *Journal of the American Chemical Society* 2004, *126*, 6658.
(41) Cheng, C.; Schmidt, M.; Zhang, A.; Schlüter, A. D. *Macromolecules* 2007, *40*, 220.
(42) Sun, X.; Lindner, J.-P.; Bruchmann, B.; Schlüter, A. D. *Macromolecules* 2014, *47*, 7337.
(43) Novak, B. M.; Risse, W.; Grubbs, R. H. In *Polymer Synthesis Oxidation Processes*; Springer Berlin Heidelberg: 1992; Vol. 102, p 47.
(44) Ivin, K. J. M., J. C. *Olefin Metathesis and Metathesis Polymerization*; Academic Press: San Diego, 1997.
(45) Buchmeiser, M. R. *Chemical Reviews* 2000, *100*, 1565.

Chapter 2. Synthesis of Up to Sixth Generation Dendronized Polymers via Graft-Through Approach by ROMP: Interplay between Dendron, Grafting Density and Conformation

2.1 Abstract

Well-defined dendronized polymers (denpols) bearing high-generation dendron are attractive nano-objects as high persistency provides distinct properties, contrast to the random coiled linear polymers. However, their syntheses via graft-through approach have been very challenging due to their structural complexity and steric hindrance retarding polymerization. Here, we report the first example of the synthesis of poly(norbornene) (PNB) containing ester dendrons up to the sixth generation (G6) by ring-opening metathesis polymerization (ROMP). This is the highest generation ever polymerized among dendronized polymers prepared by graft-through approach, producing denpols with molecular weight up to 1960 kg/mol. Combination of size-exclusion chromatography, light scattering and neutron scattering allowed a thorough structural study of these large denpols in dilute solution. A semi-flexible cylinder model was successfully applied to represent both the static and dynamic experimental quantities yielding persistent length (l_p), cross-sectional radius (R_{CS}) and contour length (L). The denpol persistency seemed to increase with generation, with l_p reaching 27 nm (Kuhn length 54 nm) for PNB-G6, demonstrating a rod-like conformation. Poly (endo-tricycle[4.2.2.0]deca-3,9-diene) (PTD) denpols exhibited larger persistency than the PNB analogs of the same generation presumably due to the higher grafting density of the PTD denpols.

2.2 Introduction

One of the most interesting features of denpols is their extended or persistent conformation due to large steric repulsion among the dendrons[1,2]. However, to what extent the polymer chains extend is often overlooked in most applications[3-6] although chemists would agree that the denpols could transform from Gaussian coil to rod-like structures by increasing the generation of the dendron[7]. The connection between dendron size (cross-section radius) and chain rigidity has been rarely investigated[8,9].

It leads us to study the chain conformation in systemic manner. Denpols are suitable for the investigation since their excellent control on the pendants at the molecular level can eliminate dispersity and defects issues, which are inevitable for graft polymers where the linear polymer attached to the polymer backbone as a side group. Therefore, it is much easier to modulate their cross-section profile and conformation by tuning the sizes of the dendrons with high fidelity and precision. In this context, recent theoretical work suggests that the main difference between denpols and graft polymers[10] should arise from the higher density in dendritic architectures compared to linear polymer chains.

Persistence length (l_p) has been mostly used for quantifying the conformational rigidity of the polymer backbone and can be controlled by grafting density, size of the graft, and length of the main chain backbone[11]. Although atomic force microscopy (AFM) analysis could determine l_p of denpols,[12] one should be aware that AFM can overestimate because adsorption could induce stretching on the

substrates[13]. Alternatively, scattering techniques[8] have been used for more reliable estimation of l_p in solution, eliminating surface effects. For instance, l_p ranges between 1-10 nm in polymers containing up to 2nd generation[14] carbosilane dendrons. On the other hand, l_p of 30 nm was reported for the denpol containing fifth generation aromatic amide dendrons[8,9]. We have reported l_p values around 6-8 nm for polynorbornene (PNB) and poly (endo-tricycle[4.2.2.0]deca-3,9-diene) (PTD) containing 3rd generation ester dendrons in dilute regime by the combination of static light scattering (SLS) and dynamic light scattering (DLS)[15]. However, the impact of even higher dendron generation on the denpols conformation remains largely unexplored for denpols, obtained by graft-through approach, due to the lack of good synthetic access to them.

Herein, we report the synthesis of large denpols (up to G6 on PNB and G5 on PTD, Scheme 1) having molecular weight up to 1960 kDa along with their unique conformational analysis in solution. The consistent determination of the configurational quantities obtained from the combination of size exclusion chromatography multi-angle laser light scattering (SEC-MALLS) and small-angle neutron scattering (SANS) techniques revealed the effect of backbone structure and generation on the conformation. The high persistence l_p up to 27 nm strongly suggests a rod-like conformation of the high generation denpols.

2.3 Result and Discussion

2.3.1 Synthesis of the Denpols

To achieve well-defined denpols by grafting-through approach, we

selected highly reactive monomers such as NB[16] and TD[17]. The release of their ring strain is essential to overcome the steric hindrance during the propagation of a polymer chain. It should be noticed that the comparison of the PNB and PTD chain conformation would lead to a deeper insight on the effect of the backbone structures because of their unit length(b_o) difference. We also incorporate the rigid biphenyl linker between the active monomer and dendron to reduce the steric hindrance during the propagation compromising the slight loss of chain rigidity[16,17]. For the systematic investigation of the relationship between dendron generation and conformation, we prepared PNB with G3, G4, and G5 ester dendrons and PTD with G3 and G4 dendron using Grubbs 3rd generation catalyst (A) (Table 1, entry 3-10 and 15-18).[16,17] Both PNB and PTD containing 2-ethyl-1-hexyl side chain[18] were prepared as reference material for comparison with the denpols (Table 1, entry 1,2 and entry 14). The obtained polymers have weight-average molecular weights (M_w) ranging from 79 to 1847 kg/mol and relatively narrow dispersity except for entry 10.

To push the limit of the synthesis beyond the state of the art, we attempted to synthesize PTD containing G5 dendron and even larger PNB containing the largest G6 dendron via ROMP. Synthesis of these extremely large denpols was extremely challenging as such huge denpols have not been prepared by grafting-through approach. The synthesis of those monomers, NB-G6 and TD-G5, were successfully carried out by following the reported procedure[16]. Their structures were confirmed by NMR and matrix-assisted laser desorption/ionization mass spectroscopy (See Experimental Section for more details). With those macromonomers in hands, we attempt the

polymerization. However, initial attempts to polymerize TD- G5 and NB-G6 by using **A** did not yield the desired polymers even at 50°C presumably due to the low reactivity of the congested propagating species. On the other hand, ROMP of NB-G6 using highly active and thermally stable 2nd generation Grubbs catalyst (**B**) in toluene at 70°C afforded the denpols with moderate weight average degree of polymerization ($DP_w = M_w/M_{mon}$ where M_{mon} is the molecular weight of a monomer) of 78 and dispersity of 1.45 (Table 1, entry 11).

Encouraged by this initial result, we further optimized this ROMP in THF at 60 °C where the faster ROMP was reported compared to toluene[19] and the M_w increased to 1145 kg/mol with DP_w of 128 (Table 1, entry 12). Further trials to obtain higher molecular weight polymers by increasing reaction concentration, changing the solvent from THF to 1,2-dichloroethane (DCE) and increasing temperature to 70 °C were not satisfactory (Table S2.1).

As an alternative strategy, we switched the catalyst to the recently developed Ru-catalysts bearing cyclic (alkyl)(amino)carbine (CAAC), which showed even higher activity toward ring-closing metathesis (RCM)[20] and cross metathesis (CM)[21] reaction, hoping that it would do the same to ROMP. Indeed, after several trials using several catalysts including **C**, we obtained the denpols having larger fraction of high molecular weight despite the broader dispersity (Table S2.1), and fortunately, fractionating out their low molecular weight portion via preparative-SEC successfully provided the denpol having M_w of 1960 kg/mol with DP_w of 220 and narrow dispersity (Table 1, entry 13) (See Table S1). Notably, this enables us to explore the behaviour of high molecular weight G6 denpols in the dilute solution for the first time.

Likewise, using the new optimized condition to prepare PNB-G6, ROMP of TD-G5 using G2 in THF at 60°C afforded the PTD-G5 with high M_w of 938 kg/mol, DP_w of 205 and moderate dispersity of 1.39 (Table 1, entry 19). Furthermore, using CAAC catalyst (**D**) and fractionalization (Table S2.2) afforded the PTD-G5 denpols having even higher M_w of 1699 kg/mol corresponding to DP_w of 369 with moderate dispersity (Table 1, entry 20).

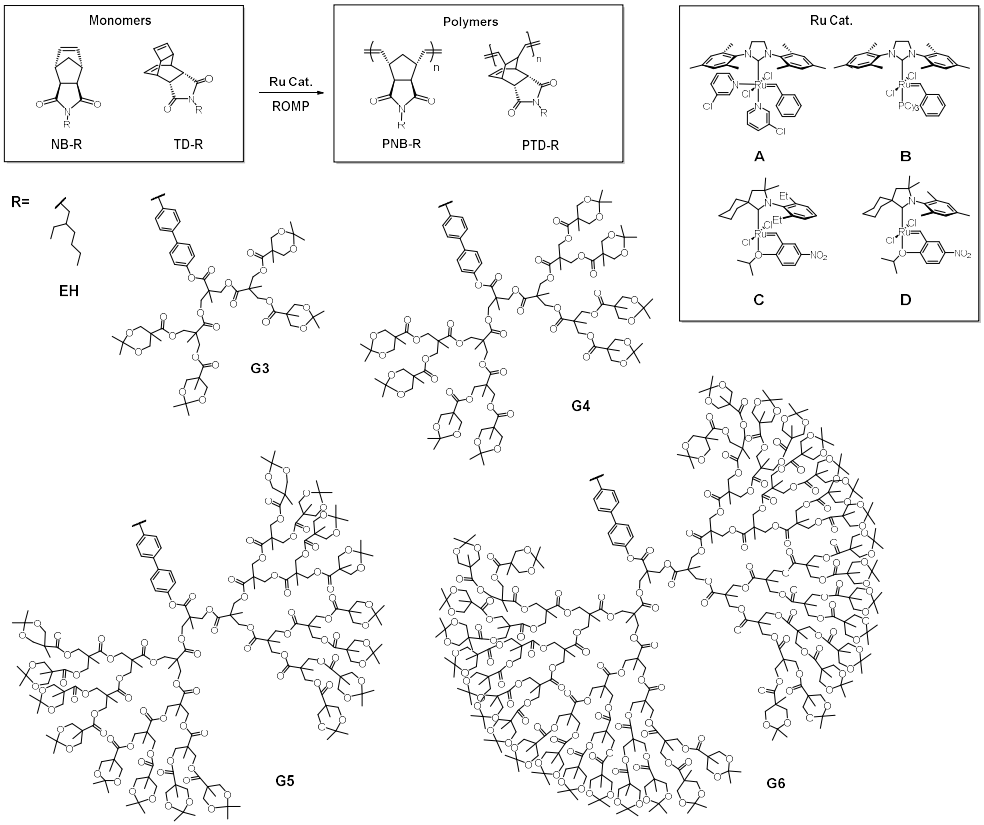

Scheme 1. Synthesis of the denpols via ROMP using various monomers and catalysts

Table 2.1: Characterizations of the polymers

PNB				PTD			
Entry	Name[a]	M_w[b] (kg/mol)	$Đ$[b]	Entry	Name[a]	M_w[b] (kg/mol)	$Đ$[b]
1	PNB-EH-287	79	1.06	14	PTD-EH-931	292	1.16
2	PNB-EH-1587	437	1.19			-	-
3	PNB-G3-510	666	1.26	15	PTD-G3-1060	1424	1.25
4	PNB-G3-750	978	1.55	16	PTD-G3-1376	1847	1.20
5	PNB-G3-1257	1640	1.48			-	-
6	PNB-G4-301	720	1.25	17	PTD-G4-257	626	1.17
7	PNB-G4-475	1136	1.37	18	PTD-G4-630	1532	1.15
8	PNB-G5-148	678	1.28	19[c]	PTD-G5-205	938	1.39
9	PNB-G5-208	949	1.45	20[d,e]	PTD-G5-369	1699	1.41
10	PNB-G5-295	1350	1.76				
11[c]	PNB-G6-78	698	1.45				
12[c]	PNB-G6-128	1145	1.77				
13[d]	PNB-G6-220	1960	1.33				

[a]Numbers at the end of the label indicate calculated N_w. [b]M_w and $Đ$ were determined by SEC-MALLS in chloroform. [c]2nd generation Grubbs catalyst (**B**) was used. [d]The polymer was fractionated using preparative-SEC. [e]Catalyst **D** was used.

2.3.2 Quantifying the Chain Extension by SEC-MALLS Analysis

To estimate the chain extension, we analyzed the denpols by SEC-MALLS, providing the M_w and the radius of gyration (R_g) The relationship between M_w and R_g provides a basis to calculate persistence length (l_p) using standard worm-like chain models. Notably, these quantities are obtained on monodisperse elution by SEC-MALLS so that polydispersity effects can be ignored. The

evolution of R_g with the of effective contour length (L=$b_o DP_w$) within each fraction of the PNB and PTD denpols is depicted in the double logarithmic plot (Figure 1a and b) where the slope represents flory exponent (ν). The parameter ν is related to the conformation of the polymer, with a value of 0.5 indicating a random coil and 1.0 indicating a rigid rod[22]. Clearly, PNB-G6 and PTD-G5 approached the rod regime (solid red lines), whereas denpols with low generation falls near the flexible-chain regime (dotted black lines in Figure 2.1a and 2.1b). This general trend is consistently reflected in the increase of l_p (from 3.5 nm to 27 nm) in THF (Table 2.2), demonstrating the rod-like conformation of the high generation denpols. AFM images showing single chains further support their rigid conformations inferred from the scattering data in solution (Figure 2.2 and S2.7). The same analysis in chloroform solution gave the similar trend (Table S2.4), which is concordance with the observed one.

Notably, we also measured the second virial coefficient(A_2) by SLS to determine the solvent quality. The observed low values ($A_2 < 10^{-4}$ mol.cm^3.g^{-2}) for denpols indicates that both CF and THF are nearly theta solvent.

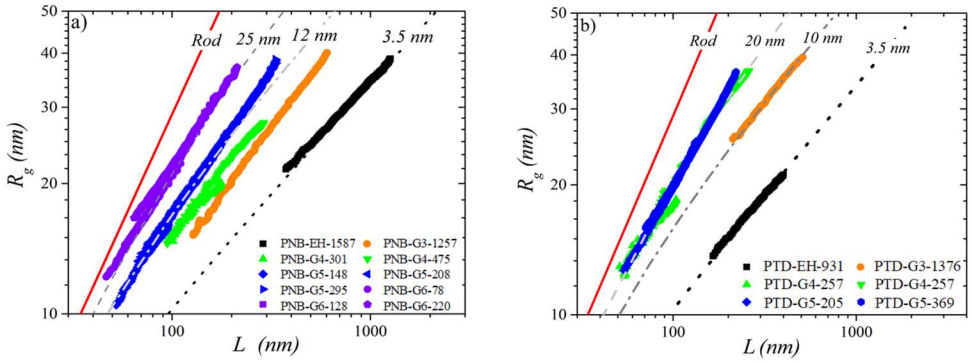

Figure2.1: Radius of gyration (R_g) as a function of weight-averaged contour length (L), obtained from MALLS-SEC measurement, in THF, for PNB-Gn denpols (a) and PTD-Gn denpols (b).The various dashed lines represent the Benoit-Doty model (eq. S1) for different values of persistence length. The solid red lines in a) and b) represents the rod scaling behavior.

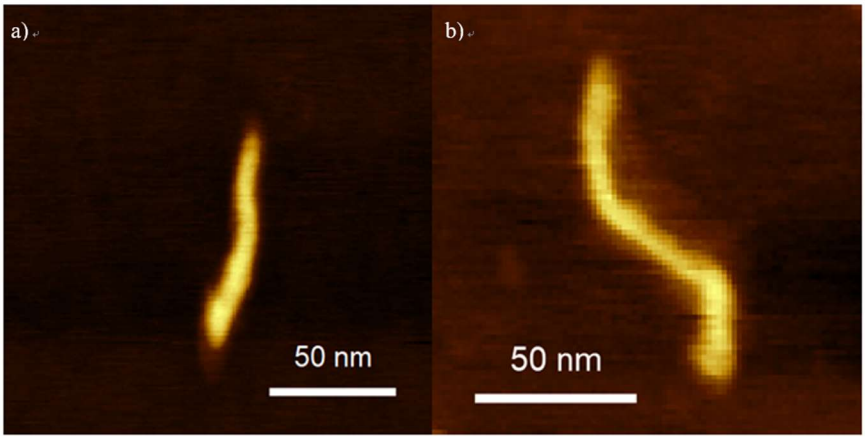

Figure 2.2 Representative AFM images of a)PNBG6-220 and b) PTDG5-369

2.3.3. SANS analysis to Estimate the Cross Section Radius

In order to access to the internal structure of the denpols in dilute solutions, we further characterize the denpols by the SANS, providing higher resolution ($2*10^{-3}$ to $4nm^{-1}$). Kholodenko model was used because it is recognized to be the best adapted for the description of semi-flexible cylinder[23-25]. The model provides persistence length $l_{p,k}$ and cross-sectional radius R_{cs} (Table 2.2 and Figure 2.3a). Notably, R_{cs} cannot be obtained by SEC-MALLS, enabling access only to the low wave-vector fraction of the form factor enough to determine R_g.

Table 2.2: Molecular Parameters for selected polymers in dilute solutions in THF.

Code	SANS		GPC-MALLS
	l_K[a] (nm)	R_{CS}[a] (nm)	l_p[b] (nm)
PNB-EH-287	2.0 ± 0.5	N/A	-[c]
PNB-G3-1257	6.0 ± 0.8	1.8	9.9
PNB-G4-301	6.4 ± 0.8	1.9	8.0
PNB-G5-295	10.2 ± 1.0	2.3	13.5
PNB-G6-128	15.0 ± 1.5	2.8	27.3
PTD-G3-1060	13.7 ± 1.4	2.2	11.3
PTD-G4-630	24.2 ± 2.4	2.4	20.1
PTD-G5-205	14.3 ± 1.4	2.8	20.2

[a] cross section radius R_{CS} and persistence length l_K were obtained from the representation of the SANS form factor by Kholodenko model [50,51]. [b] Obtained from SEC-MALLS data fitting using Benoit Doty equation. [c] R_g (< 10 nm) is too small to be measured by MALLS detector.

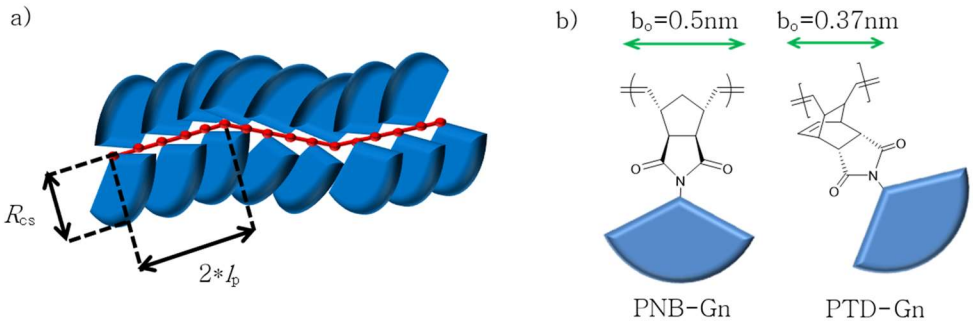

Figure 2.3 a) Schematic representation of a) a denpol chain b) unit length of PNB and PTD

2.3.4 The relationship between the Cross-Section Radius, Molecular Weight of Dendrons and Persistence Length

The study on the PNB and PTD systems provided insight into the effect of increasing dendron generation on the conformation of the denpols. First, we observed that the increase of both R_{cs} and l_p with the dendron molecular weight (M_{sc}) as described in the log-log presentation of R_{cs} vs M_{sc} (Figure 2.5 and 2.6a). Interestingly, we found that both PTD and PNB denpols show a rather weak increase of R_{cs} with generation that conforms to $R_{cs} \sim M_{sc}^{0.25}$. It contradicts to the theoretical prediction for bottlebrush polymer where R_{cs} is expected to grow as $M_{sc}^{0.5}$in theta solvent[26] and $M_{sc}^{0.75}$ in good solvent.[13] The weak increase with generation of the dendron indicates that the high generation denpols are denser than the lower generation denpols rendering their shape close to colloidal nano-objects. It might also imply densely packing near to the polymer main chain. It should be noticed that the R_{cs} of the PTD is larger than that of PNB at the same generation because of the higher grafting density of the PTD than PNB PTD as a result of the compact monomer structure; b_o of PTD-Gn

(b_o=0.37nm) is smaller than that of PNB-Gn (b_o=0.5nm) (Figure 2.3b).[15] Hence, the grafting density of PTD-Gn is about 25% larger than for PNB-Gn.

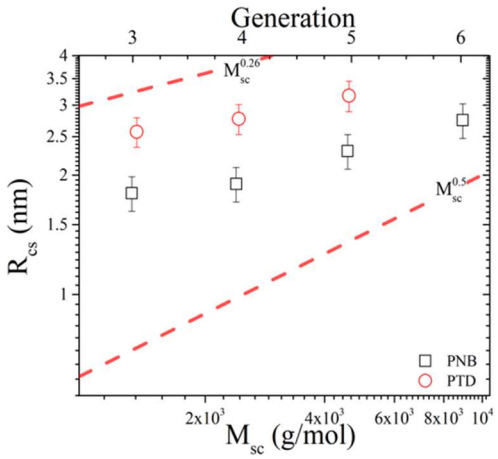

Figure 2.5 A log-log plot of the cross-section radius vs dendron generation or equivalently the side chain molecular weight. The two dashed lines represent different power law dependencies indicated in the plot.

Next, the persistence lengths obtained from SEC-MALLS (opened symbols) and from SANS (filled symbols) with each generation are reported as a function of M_{sc} (Figure 2.6a) to compare them with the theoretical calculation for bottlebrush polymers where l_p is expected to proportional to M_{sc}.[27] The excess persistency ($l_{p,0}$ = 3.5 nm being the persistence length of the linear chain "precursor") increases with generation reaching the value of 27 nm for PNB-G6. Importantly, l_p of the PTD is larger than that of PNB over the same generation, indicating that PTD is more persistent than PNB as expected based on the grafting density difference. However, the trend seems not to follow $l_p \sim M_{sc}^{x}$ relationship based on the observation.

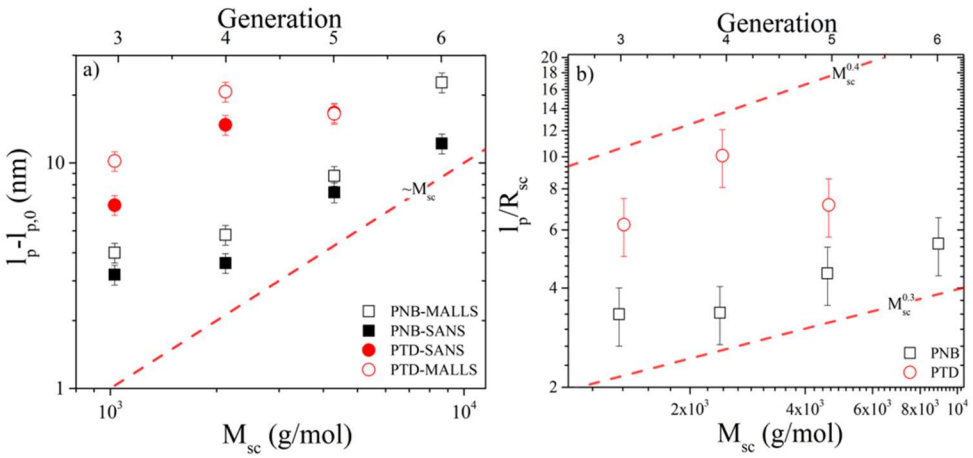

Figure 2.6 a) Excess persistence length obtained from SANS (filled symbols) and MALLS-GPC analysis (opened symbols). Dash line represents a linear scaling. $l_{p,0}$ is the persistence length of the linear chain. b) The ratio of the persistence length to the cross-section radius as a function of generation in log-log presentation.

To gain further insight into the internal structure of the denpols, we presented the aspect ratio (l_p/R_{cs}) as a function of M_{sc}. Since l_p/R_{cs} was found to increase with generation for both PTD and PNB backbones as displayed in Figure 2.6b, the persistence length should increase faster than R_{cs}. The higher aspect ratio of the PTD in the same generation is observed as expected, considering their unit length difference.

2.4 Conclusions

The dendronized PNB containing up to 6th generation and PTD containing up to 5th generation dendrons were synthesized by ROMP via grafting-through method for the first time. Successful preparation of unique series of denpols with huge molecular weight up to 1960 kDa

enabled us to unravel their structure in solution. The results from SEC-MALLS and SANS experiments can be well understood using a semi-flexible cylinder model with three characteristic sizes: a contour length, a persistence length l_p and a cross-sectional radius R_{cs}.

The high generation denpols display a rod-like conformation, with grafting induced l_p of up to 27nm. The increase of l_p with generation appears to be governed by the molecular weight of the dendron. Compared to l_p, R_{cs} displays a weaker increase with generation resulting in an increase of aspect ratio l_p/R_{cs} with generation. Interestingly, the PTD denpols are clearly more persistent than the PNB denpols of the same generation due to the more compact structure and higher grafting density in the PTD.

2.5 Experimental section

General Informations

All reagents commercially available were used without further purification. For the monomer synthesis, toluene and tetrahydrofuran (THF) both anhydrous (≥ 99.8%) grade were purchased from Sigma-Aldrich®. THF was distilled from sodium and benzophenone. The solvents for the polymerization were degassed with argon 10 minutes. Thin-layer chromatography (TLC) was carried out on MERCK TLC silica gel 60 F254 and the flash column chromatography was performed using MERCK silica gel 60 (0.040~0.063nm). ^{1}H-NMR and ^{13}C-NMR were recorded by NMR spectra were recorded by Varian/Oxford As-500 (500 MHz for ^{1}H/125 MHz for ^{13}C) spectrometer and Bruker DRX-300 (75 MHz for ^{13}C). The molar masses of macromonomers were measured by Bruker Daltonics

autoflex II TOF/TOF. Dithranol in THF was used as a matrix. The fractionation of denpols was done by preparative GPC (Japan Analytical Industry Co., Ltd. LC-9260 next recycling preparative HPLC).

Synthesis of Macromonomers

Synthesis of NB-G6

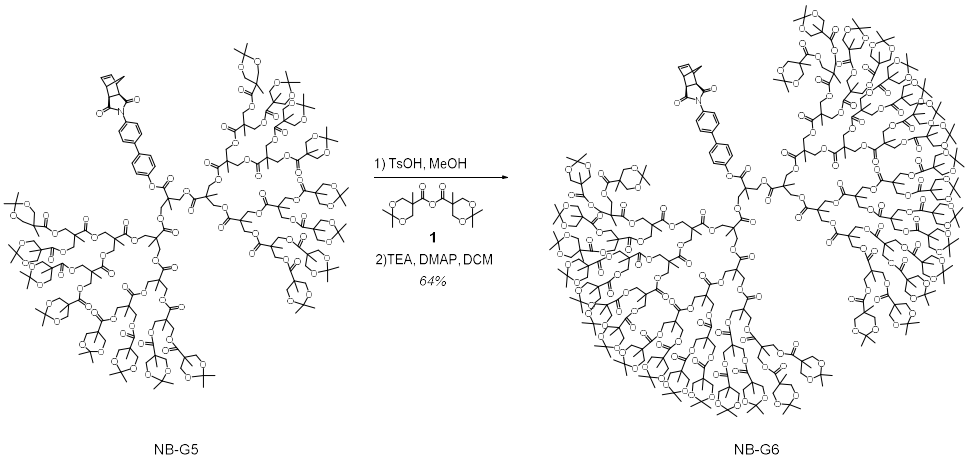

Scheme S2.1. Synthesis of the macromonomer NB-G6

NB-G5 and **1** were prepared according to the literature procedure[16]. 1.18g (0.26 mmol) of NBG5 was deprotected in excess methanol (6.5ml, 0.04M) with catalytic amount of *p*-toluenesulfonic acid (4.9mg, 10 mol%). After stirring 2 days, the reaction was quenched by excess amount of triethyl amine and the solvents were dried by rotary evaporator and high vacuum and used without further purification. To the mixture, dichloromethane (2.6mL, 0.1 M) and triethylamine (1.7 mL, 48 equiv) were added. Then isopropylidene-2,2-bis(oxymethyl)propionic anhydride(**1**) (4.12 g, 48 equiv) and 4-dimethylaminopyridine (DMAP) (3.1 mg, 10 mol %) were added at room

temperature, and the reaction mixture was stirred for 7 days. After completion of the reaction, saturated $NaHCO_3$ (10 mL) aqueous solution was added and the reaction stirred for 1 h. The mixture was washed with $NaHCO_3$ (10 mL) solution. The organic layer was extracted with ethyl acetate and dried with anhydrous $MgSO_4$ and the solvent was removed on a rotary evaporator. The product was purified by column chromatography with ethyl acetate–hexane mixture (5:1 in volumetric ratio). The separated product solutions were collected and concentrated to yield final product. 1.48g, 64%. ^{1}H NMR (500 MHz, CD_2Cl_2): δ 7.69 (dd, *J* = 10.8, 8.6 Hz, 4H), 7.37 (d, *J* = 8.5 Hz, 2H), 7.22 (d, *J* = 8.7 Hz, 2H), 6.37 (s, 2H), 4.58 (d, *J* = 10.7 Hz, 2H), 4.40 – 4.20 (m, 122H), 4.11 (d, *J* = 11.8 Hz, 64H), 3.60 (dd, *J* = 11.8, 2.0 Hz, 64H), 3.37 (s, 2H), 2.87 (s, 2H), 1.61 (s, 1H), 1.50 (m, 4H), 1.38 (s, 96H), 1.35 (s, 6H), 1.31 (s, 96H), 1.26 (s, 84H), 1.11 (s, 96H). ^{13}C NMR (75 MHz, CD_2Cl_2): δ δ 177.20, 173.86, 172.31, 171.91, 171.83, 138.39, 128.79, 128.00, 127.47, 98.32, 66.27, 66.24, 65.64, 65.12, 48.36, 47.15, 47.03, 46.26, 42.37, 25.68, 22.06, 18.69, 18.00, 17.85.MS (MALDI–TOF): m/z for $C_{432}H_{649}NO_{192}$: $[M]^+$ 8928.122 (calculated), 8928.531 (observed).

Synthesis of TD-G5

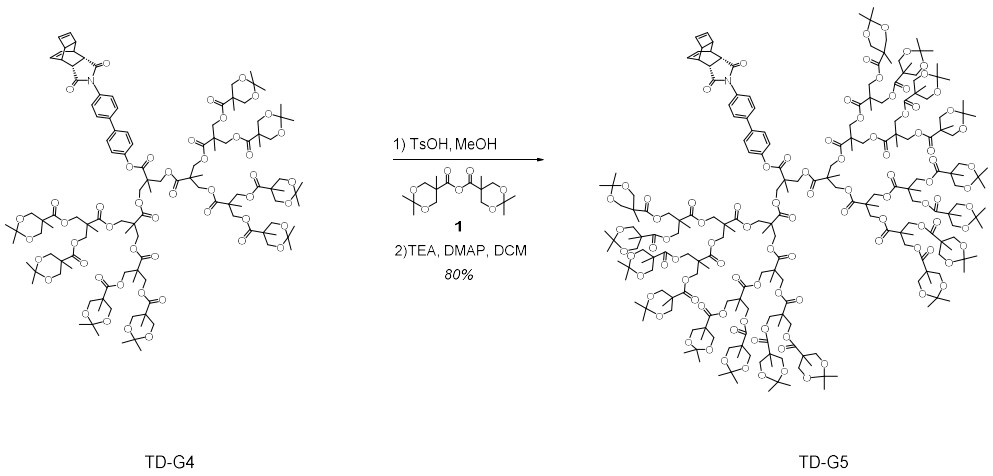

Scheme S2.2. Synthesis of the macromonomer TD-G5

TD-G4 was prepared according to the literature[17]. 1.02g (0.42 mmol) of TD-G4 was deprotected in excess methanol (10.5ml, 0.04M) with catalytic amount of *p*-toluenesulfonic acid (3.98mg, 5 mol%). After stirring 24 hours, the reaction was quenched by excess amount of triethyl amine and the solvents were dried by rotary evaporator and high vacuum and used without further purification. To the mixture, dichloromethane (4.2mL, 0.1 M) and triethylamine (1.4 mL, 24 equiv) were added. Then isopropylidene-2,2-bis(oxymethyl)propionic anhydride(ref) (3.33 g, 24 equiv) and 4-dimethylaminopyridine (DMAP) (5.1 mg, 10 mol %) were added at room temperature, and the reaction mixture was stirred for 2 days. After completion of the reaction, saturated $NaHCO_3$ (10 mL) aqueous solution was added and the reaction stirred for 1 h. The mixture was washed with $NaHCO_3$ (10 mL) solution. The organic layer was extracted with ethyl acetate and dried with anhydrous $MgSO_4$ and the solvent was removed on a rotary evaporator. The product was purified by column chromatography with ethyl acetate–hexane mixture (4:1 in volumetric ratio). The separated

product solutions were collected and concentrated to yield final product. 1.55g, 80%. ^{1}H NMR (500 MHz, CD_2Cl_2): ^{1}H NMR (500 MHz, CD_2Cl_2): δ 7.67 (m, 4H), 7.28 (d, *J* = 8.3 Hz, 1H), 7.22 (d, *J* = 8.4 Hz, 1H), 6.02 (m, 2H), 5.94 (s, 2H), 4.54 (d, *J* = 11.2 Hz, 2H), 4.39 (d, *J* = 11.3 Hz, 2H), 4.29 (m, 56H), 4.11 (d, *J* = 11.7 Hz, 32H), 3.60 (d, *J* = 11.8 Hz, 32H), 3.25 (s, 2H), 2.99 (s, 2H), 2.91 (s, 2H), 1.50 (s, 3H), 1.39 (s, 48H), 1.34 (s, 6H), 1.31 (s, 48H), 1.26 (m, 36H), 1.10 (s, 48H). ^{13}C NMR (125 MHz CD_2Cl_2): δ 178.08, 173.93, 172.35, 171.99, 171.94, 138.4, 128.92, 128.06, 127.55, 122.27, 98.42, 66.34, 66.30, 66.11, 65.91, 65.30, 47.29, 47.20, 43.97, 42.48, 37.63, 25.61, 22.26, 18.78, 18.03, 17.87. MS (MALDI−TOF): m/z for $C_{227}H_{331}NO_{96}Na$: $[M + Na]^+$ 4633.251 (calculated), 4634.080 (observed).

Synthesis of PNB-G6 and PTD-G5

General Procedure

2-mL sized screw-cap vial with septum was charged with monomer and a magnetic bar. The vial was purged with argon four times, and degassed THF was added purged with Ar, and then dissolved in dry and degassed solvent. The initiator solution was added at once to the monomer solution under vigorous stirring. After c.a. 12h, the polymerization was quenched with by excess ethyl vinyl ether. The concentrated reaction mixture was then precipitated and the polymer was collected and dried under reduced pressure.

PNB-G6: ^{1}H NMR (500 MHz, CD_2Cl_2): δ 7.68 (br, 4H), 7.40 (br, 2H), 7.22 (br, 2H), 4.29 (br, 122), 4.09 (d, *J* = 10.7 Hz, 64H), 3.59 (d, *J* = 10.9 Hz, 64H), 1.37 (br, 102H), 1.28 (b, 180H), 1.09 (br, 96H).

PTD-G5: ^{1}H NMR (500 MHz, CD_2Cl_2): δ 7.63 (br, 4H), 7.20 (br, 4H), 4.28 (s, 58H), 4.09 (d, *J* = 10.5 Hz, 32H), 3.58 (d, *J* = 10.4 Hz, 32H), 1.49 (br, 3H), 1.36 (br, 48H), 1.27 (br, *84*H), 1.08 (br, 48H).

Optimization for PNB-G6 and PTD-G5

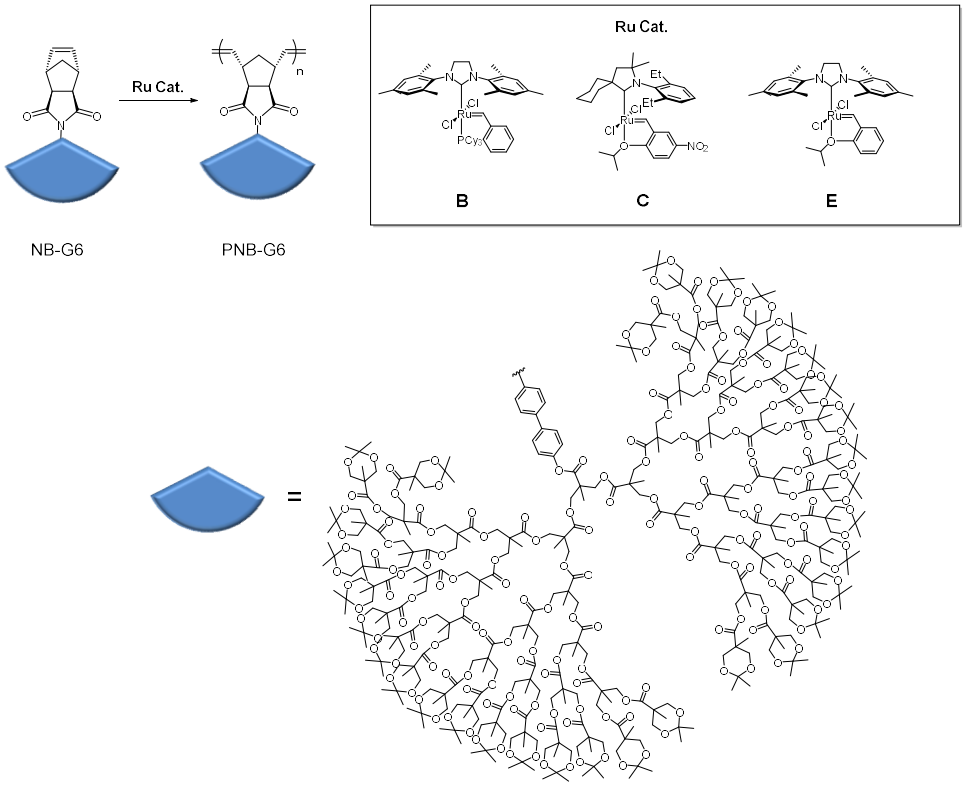

Scheme S2.3. Polymerization of NB-G6

Table S2.1. The optimization and fractionalization for PNB-G6

Entry	Solvent	Cat	[M]/[I]	Time(h)	Conc(M)	Temp(°C)	M_w[a]	Đ[a]	Conv(%)[b]
1[c]	Toluene	**2**	100	12	0.2	70	685	1.52	69
2[d]	THF	**2**	200	12	0.25	60	1199	1.84	78
3	DCE	**2**	200	12	0.25	60	878	1.60	80
4	Toluene	**2**	150	12	0.2	70	307	1.33	52
5	THF	**2**	200	12	0.3	60	850	2.66	84
6	DCE	**5**	200	12	0.3	70	894	1.98	72
7	Toluene	**3**	200	12	0.25	60	985	1.88	75
8	Toluene	**3**	200	12	0.25	70	894	1.98	75
9[e]	–	**–**	–	–	–	–	1956	1.32	–

[a]M_w and Đ were determined by SEC-MALLS in THF. [b]estimated by the relative integration of the denpol peak to the macromonomer peak. [c]corresponds to entry 11 in table 1 in the main text. [d]corresponds to entry 12 in table 1 in the main text. [e]high molecular weight fraction of the denpols obtained from entry 5-8 by preparative-SEC.

234 mg (Entry 5), 242 mg (Entry 6), 209 mg (Entry 7), 208 mg (Entry 8) of crude PNB-G6 were combined and fractionalized to afford 15 mg of high molecular weight PNB-G6 (Entry 9).

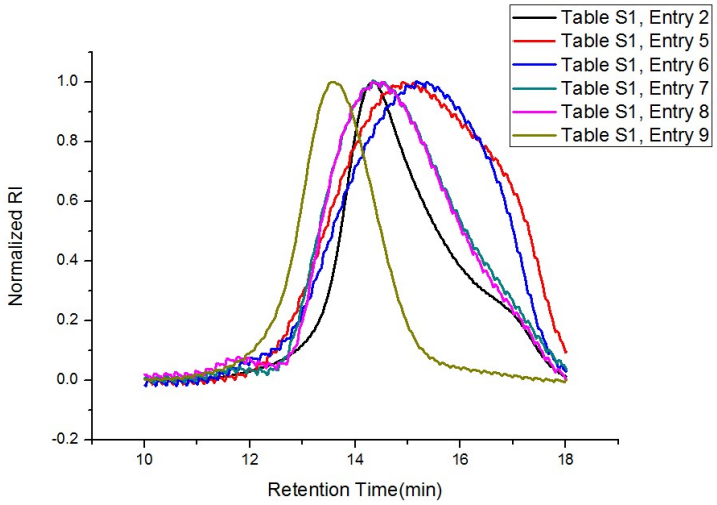

Figure S2.1. SEC trace of selected PNB-G6

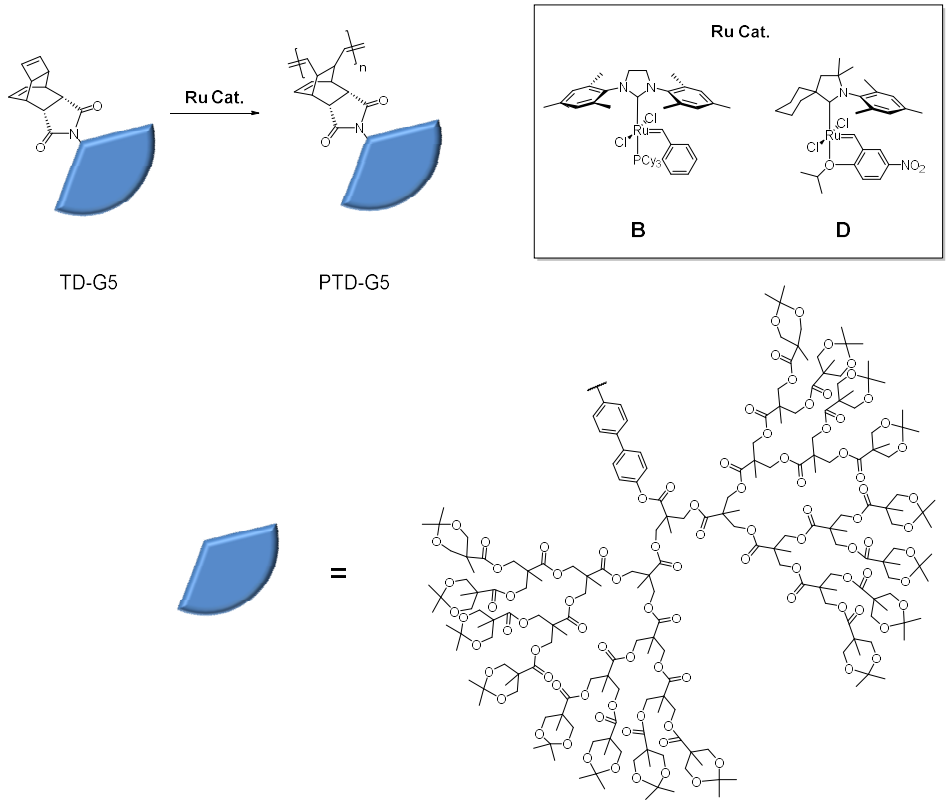

Scheme S2.4. Polymerization of TD-G5

Table S2.2. Synthesis and fractionalization for PTD-G5

Entry	Solvent	Cat	[M]/[I]	Time(h)	Conc(M)	Temp(°C)	M_w[a]	$Đ$[a]	Conv(%)[b]
1[c]	THF	**2**	200	16	0.2	70	807	1.45	64
2[d]	THF	**4**	200	12	0.25	60	1095	2.43	75
3[e]	-	-	-	-	-	-	1661	1.24	-

[a] M_w and Đ were determined by SEC-MALLS in THF. [b]estimated by the relative integration of the denpol peak to the macromonomer peak. [c]corresponds to entry 11 in table 1 in the main text. [d]corresponds to entry 12 in table 1 in the main text. [e]High molecular weight fraction of the denpols obtained from entry 2 by preparative-SEC.

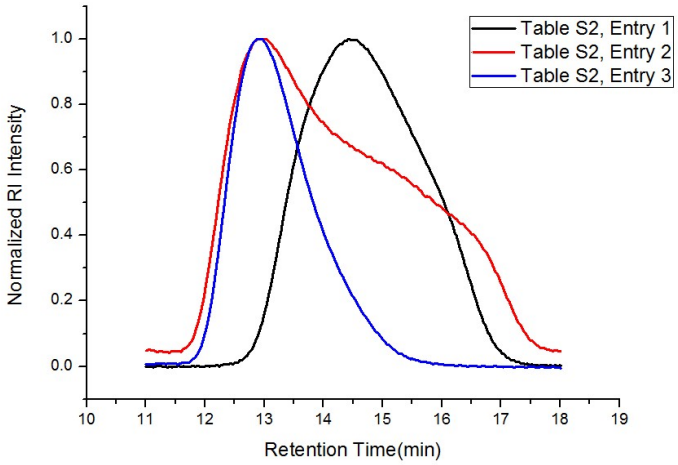

Figure S2.2. SEC trace of the PTD-G5

96 mg (Entry 2) of crude PTD-G5 were fractionalized to afford 22 mg of high molecular weight PTD-G5 (Entry 3).

Characterization with Scattering Techniques

General Information

We have used the following parameters to characterize the synthesized denpols: molecular weight M, contour length L, monomer size b_0 persistence length l_p, gyration radius R_g, cross-sectional radius R_{cs}, hydrodynamic radius R_h. We have used a combination of different experimental techniques to access these static and dynamic parameters in dilute denpol solutions, in THF and chloroform (CF). SEC-MALLS data were carefully analyzed in order to provide the radius of gyration R_g as a function of molecular weight M within individual fractions. Small Angle Neutron Scattering (SANS) was employed to measure the form factor over a broad wave vector range. The representation of the SANS patterns by the Kholodenko model[23] led to the estimation of L_K, $l_{p,K}$, and R_{cs}. Static light scattering (SLS)

was used to measure fraction solutions and obtained second virial coefficient A_2.

Size Exclusion Chromatography with Multi-Angles Laser Light Scattering (SEC-MALLS)

SEC-MALLS data provided independent measurements of both R_g and the corresponding M_w in real time during the elution process. The relationship between R_g vs M_w is utilized to evaluate the persistence length of the denpols, using the Benoit-Doty model as described in section II.2.5. THF-SEC-MALLS setup consisted of: Waters 1515 pump, manual injector with a loop volume of 50 µL, 2 Shodex GPC LF-804 size-exclusion columns maintained at 35 ºC, DAWN-HELEOS 8+ multi-angle laser light scatter and OptiLab T-rEx refractive index detectors (each from Wyatt Technologies Corporation). The mobile phase consisted of HPLC-grade THF (inhibitor free). CF-SEC-MALLS setup consisted of: Waters 515 pump, manual injector with a loop volume of 10 µL, Shodex GPC LF-804 size-exclusion columns maintained at 35 ºC, DAWN-HELEOS 8+ multi-angle laser light scatter and OptiLab T-rEx refractive index detectors (each from Wyatt Technologies Corporation). The mobile phase consisted of HPLC-grade CF(ethanol used as an inhibitor). Samples in 0.004-0.006 wt% THF or CF were filtered with a 0.2 µm PTFE filter before injection. Flow rate was 1.0 mL/min and temperature of column was maintained at 35 ℃. The 8-angle MALLS records the wave vector dependent intensity I(q) that leads to the radius of gyration R_g (typical data can be found in Figure S14. Values of I/c are then used to calculate the molecular weight M_w ("absolute" calibration of the GPC). The data was analyzed using the ASTRA software. Values of dn/dc

needed to obtain the molecular weight M_w were measured separately from batch mode measurements of polymer solutions at different concentrations and are provided in supporting information (Table S2.3).

Table S2.3. Refractive index increment

Polymer	$\partial n/\partial c$ (mL/g) (THF/CF)	
PNB-EH	0.118	0.112
PNB-G3	0.106	0.080
PNB-G4	0.079	0.06
PNB-G5	0.074	0.055
PNB-G6	0.069	0.048
PTD-EH	0.132	0.099
PTD-G3	0.107	0.084
PTD-G4	0.087	0.061
PTD-G5	0.085	0.055

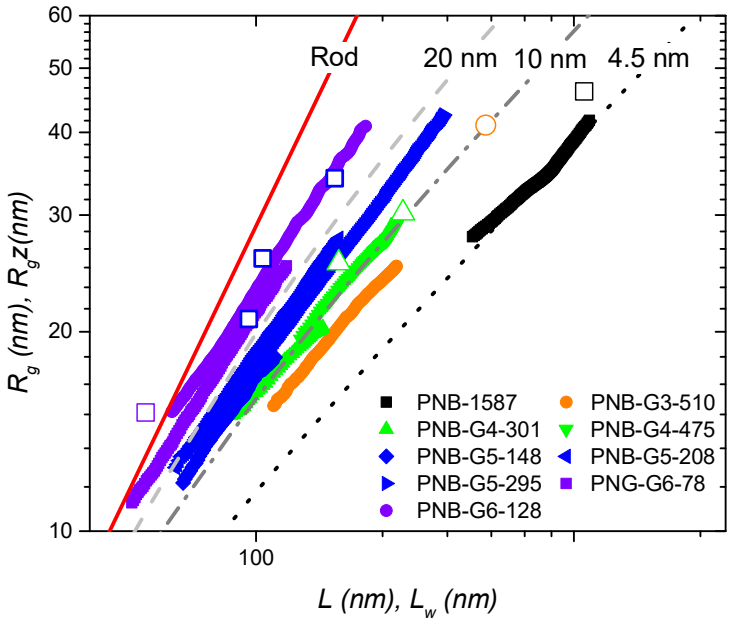

Figure S2.3. MALLS-GPC PNB-Gn in CF

In Figure S2.11 open symbols correspond to the measurement of non-fractionated sample.

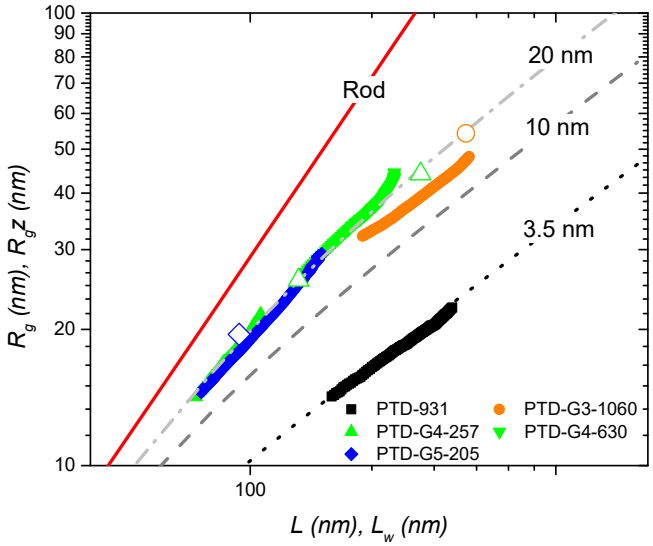

Figure S2.4. MALLS-GPC PTD-Gn in CF

In Figure S2.12 the open symbols correspond to the measurement of the non-fractionated samples

Table S2.4. Persistence length (lp) of selected polymers estimated by Benoit-Doty expression.

Name	l_p (nm) (THF/CF)	
PNB-EH-1587	3.6	4.6
PNB-G3-1257	9.9	10.6
PNB-G4-301	8.0	9.6
PNB-G5-295	13.5	14.5
PNB-G6-128	27.3	36.3
PNB-G6-220	26.0	26.2
PTD-G3-1376	11.3	17.4
PTD-G4-630	20.1	21.7
PTD-G5-205	20.2	18.9
PTD-G5-369	22.1	23.8

Excluding the anomalous value (red colored in Table S2.4), the values of the persistence length in the two solvents are very similar.

Table S2.5. Polymer characteristics measured by GPC-MALLS in THF and CF

Samples Name	MALLS results (THF | CF)					
	M_w (kg/mol)		$Đ$		R_g (nm)	
PNB-EH-287	102	79	1.07	1.06	-[a]	-[a]
PNB-EH-1587	545	437	1.33	1.19	36.5	36.1
PNB-G3-510	-	666	-	1.26	-	25.6
PNB-G3-750	940	978	1.52	1.55	33	36.1
PNB-G3-1257	1542	1640	1.6	1.48	52.1	56
PNB-G4-301	750	720	1.18	1.25	19.5	20.5
PNB-G4-475	1179	1136	1.28	1.37	26.7	27.7
PNB-G5-148	657	678	1.51	1.28	14.4	14.9
PNB-G5-208	879	949	1.8	1.45	20	21.1
PNB-G5-295	1237	1350	2.28	1.76	26.8	28.5
PNB-G6-78	685	698	1.52	1.45	14	14.5
PNB-G6-128	1199	1145	1.56	1.77	24.9	26.5
PNB-G6-220	1956	1960	1.32	1.33	27.7	24.5
PTD-EH-931	272	292	1.24	1.16	20.5	20.7
PTD-G3-1060	1469	1424	1.4	1.25	39.5	46.1
PTD-G3-1376	1938	1847	1.3	1.20	47.5	56.9
PTD-G4-257	606	626	1.11	1.17	18.4	18.8
PTD-G4-630	1459	1532	1.18	1.15	35.6	38.3
PTD-G5-205	807	938	1.45	1.39	18.1	19.3
PTD-G5-369	1661	1699	1.24	1.41	28.3	30.4

[a]Rg range (<10 nm) is too small to be measured by MALLS detector.

Small Angle Neutron Scattering (SANS)

SANS experiments were performed on the PA20 spectrometer of the LLB, CEA Saclay. We used wavelengths ranging from 0.5 to 12 nm (dispersion of 10%) with 3 sample–detector configurations, to provide broad wave vector coverage from 0.02 to 4 nm^{-1}. For the SANS experiments, denpol solutions were prepared in deuterated d8–THF. Standard procedure for signal treatment and normalization were done using. Care was taken to subtract the incoherent background coming from the hydrogenated denpols. The data analysis was done using SASfit software[28]. In particular, the intensity patterns were represented by the Kholodenko form factor[23].

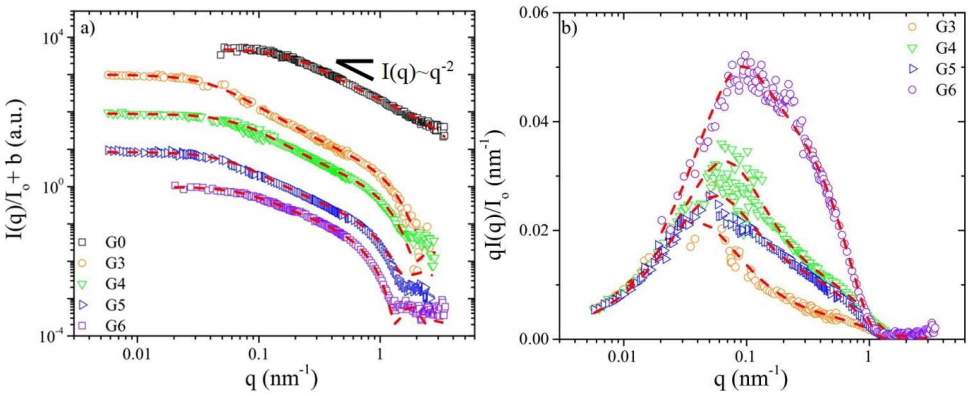

Figure S2.5. a) Scattering intensities from the combined SANS and SLS experiments on PNB–Gn denpols in dilute d_8–THF solution (c=5 g/l) as a function of wave-vector q . The data along with their representation (dashed lines) have been shifted vertically for clarity. b) Representation (red dashed lines) of the scattering intensity, normalized by the forward scattering intensity and the wave-vector (for rods) by the Kholodenko's form factor[23-25]

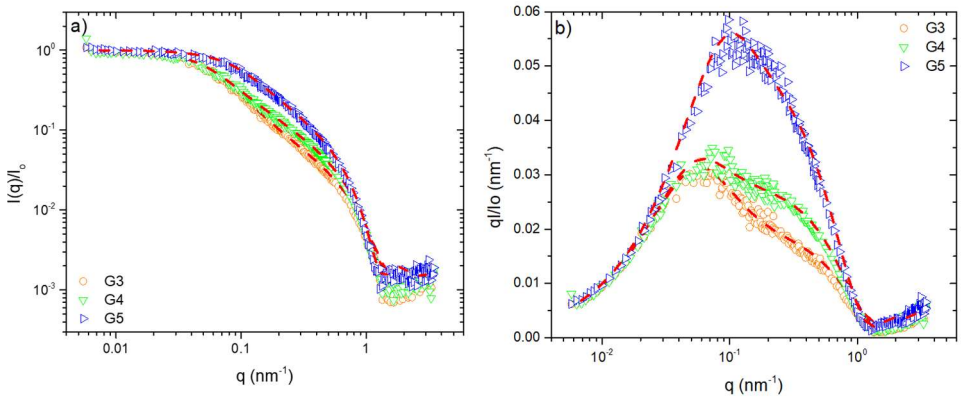

Figure S2.6. a) Scattering intensities from the combined SANS and SLS experiments on PTD-Gn denpols in dilute d_8-THF solution (c=5 g/l) as a function of wave-vector q . The data along with their representation (dashed lines) have been shifted vertically for clarity. b) Representation (red dashed lines) of the scattering intensity, normalized by the forward scattering intensity and the wave-vector (for rods) by the Kholodenko's form factor[23-25]

Worm like chain models

The denpols conformation was represented by a wormlike chain (WLC) model also known as Kratky-Porod. The semi-flexible chain is characterized by persistence length l_p and its contour length L. The WLC model can be retrieved from the freely jointed chain of N monomers with length b_0 and a fixed angle θ between consequent monomers. Then $l_p = \frac{b}{2} = \frac{b_0}{2}\frac{1-\cos}{1+\cos\theta}$, b is known as the Kuhn segment length.

Gyration radius and Benoit-Doty relation

In the SEC-MALLS experiments, the scattered intensity is measured as a function of elution time and an instantaneous molecular weight M is obtained. Then, the chemical contour length $L=(M/M_0)\ b_0$ is computed from the monomer molar mass, M_0, calculated from the macromonomer chemical formula (values available in Table S3). The

monomer size b_0 is obtained from the chemical structure. As in our previous work, we employed b_0=0.49±0.04 nm for pNB and b_0=0.37± 0.01 nm for pTD chains.

The mean-square-radius of gyration of monodisperse worm like chains is a function of the persistence length l_p (values available in Table S5) and the contour length L, as given by the Benoit-Doty relation:

$$R_g^2(L) = \frac{L.l_p}{3} - l_p^2 + \frac{2}{L}l_p^3 - \frac{2}{L^2}\left(1 - e^{-L/l_p}\right)l_p^4 \qquad (1)$$

Retrieving the Gaussian coil limit at L/l_p>>1 and R_g^2=$L.l_p$/3, and the rod limit at L/l_p<<1 and R_g^2= L^2/12. In the case of thick polymer a cross section radius is needed for a better descrption. In the simple case of a rigid sphero-cylinder of length L and cross section radius R_{cs}:

$$R_g^2(L) = \frac{L^2}{12} + \frac{R_{cs}^2}{2} \approx \frac{L^2}{12} \qquad (2)$$

Form factor and Kholodenko model[23]

The wide q-range of the SANS experiments allow access to the full form-factor P_0 (q) of the polymer chain. The WLC model does not result into a simple P_0 (q) expression. Instead, Kholodenko has introduced an empirical form factor model that is correct in both the flexible chain and the rod limits[23], and is now well accepted for semi-flexible chains[29].

$$P_0(q, l_{p,K}, L_K) = \frac{2}{x}\left[I_1(x,q) - \frac{1}{x}I_2(x,q)\right] \qquad (3)$$

where $I_1(x,q)$ and $I_2(x,q)$ are 1st kind of modified Bessel function,

x=3L_K/(2$l_{p,K}$), L_K and $l_{p,K}$ parameters are the contour length and persistence length, respectively, with K subscript being used to denote the values obtained from fitting the SANS spectra to the Kholodenko form factor with the ones.

In the case of a thick WLC a term corresponding to the cylindrical cross-section form factor is included to the overall form factor with the form:

$$P_{cs}(q, R_{cs}) = \left(2\frac{J_1(qR_{cs})}{q.R_{cs}}\right)^2 \quad (4)$$

where R_{cs} is the cross-section radius and $J_1(qR_{cs})$ is 1st kind of Bessel function.

The overall thick WLC Kholodenko form factor is:

$$P_K(q, L_K, l_k, R_{cs}) = P_o(q, l_K, L_K).P_{cs}(q, R_{cs}) \quad (5)$$

By construction it recovers the Gaussian coil form factor in the limit $L>>l_p$ and $R_{cs}<<1$ and the rod or cylinder limit in the case $l_p>>L$.

Atomic Force Microscopy (AFM)

The AFM images were collected on a Bruker NanoScope V Multimode 8 device at ambient temperature in tapping mode using non-contact mode silicon tips from Nanoworld (Pointprobe ® tip, NCHR type) with spring constant of 42 N m^{-1} and tip radius of ≤ 8 nm. 10 μL of the sample solution (0.01 mg/mL in chloroform) was used and then was place on freshly cleaved mica. Then the mica substrate was spin-coated using Spin Coater ACE-200 at a speed 3000 rpm during 15 s. The scanning speed was at a line frequency of 1.0 Hz, and the original

images were sampled at a resolution of 512 x 512 pixels.

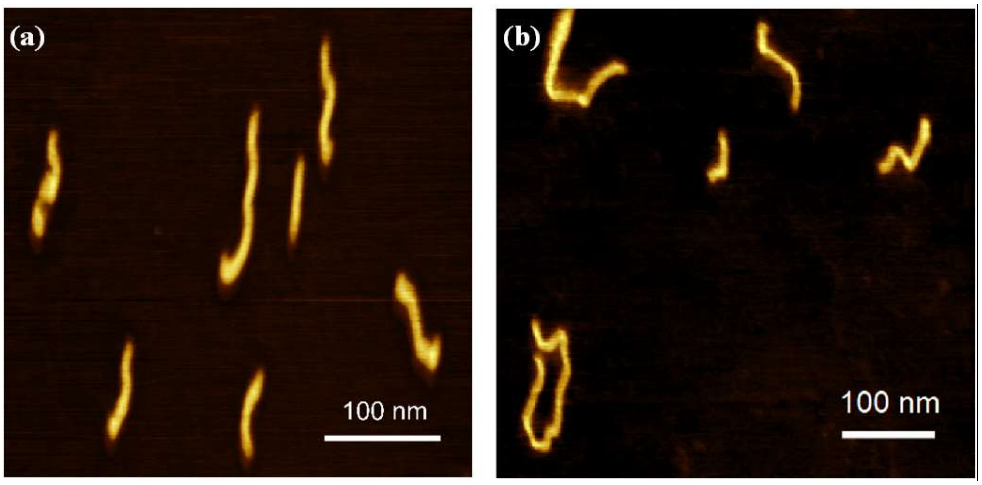

Figure S2.7: AFM images of high generation denpols: (a) PNB-G6-220 (b) PTD-G5-369.

NMR and MALDI-TOF Spectroscopy for New Compounds

^{1}H: NB-G6

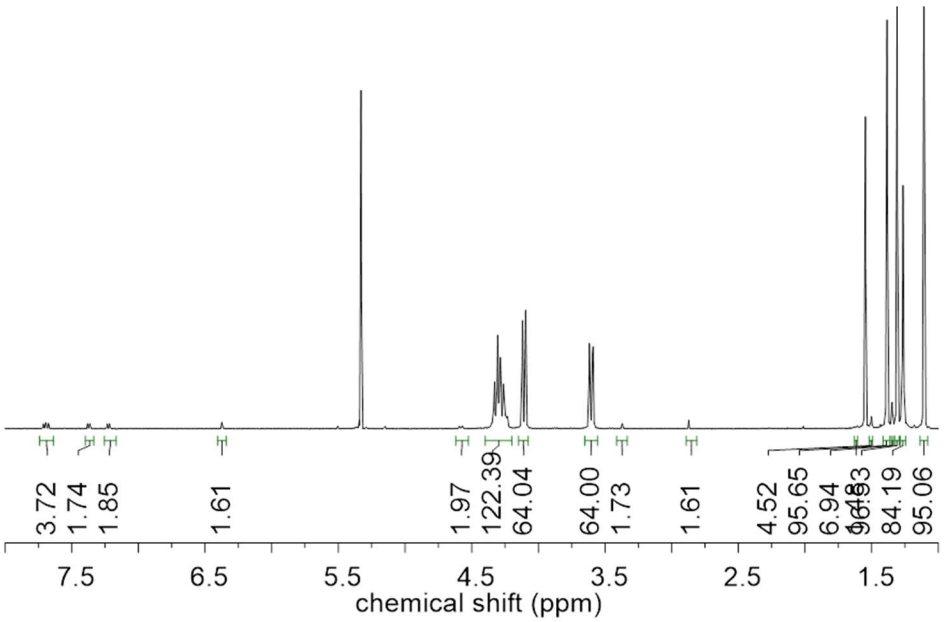

^{13}C: NB-G6

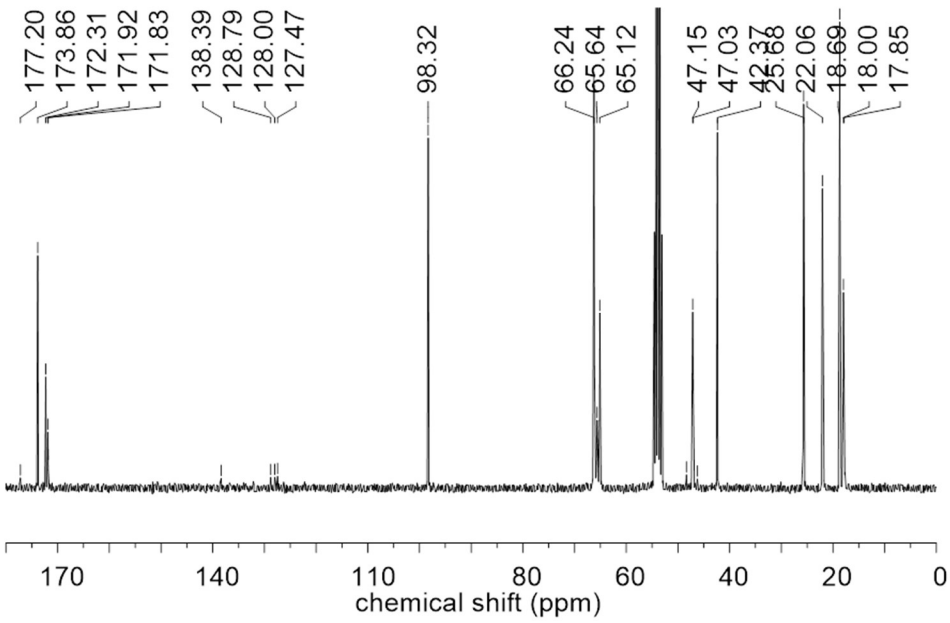

MALDI-TOF Spectra of NB-G6

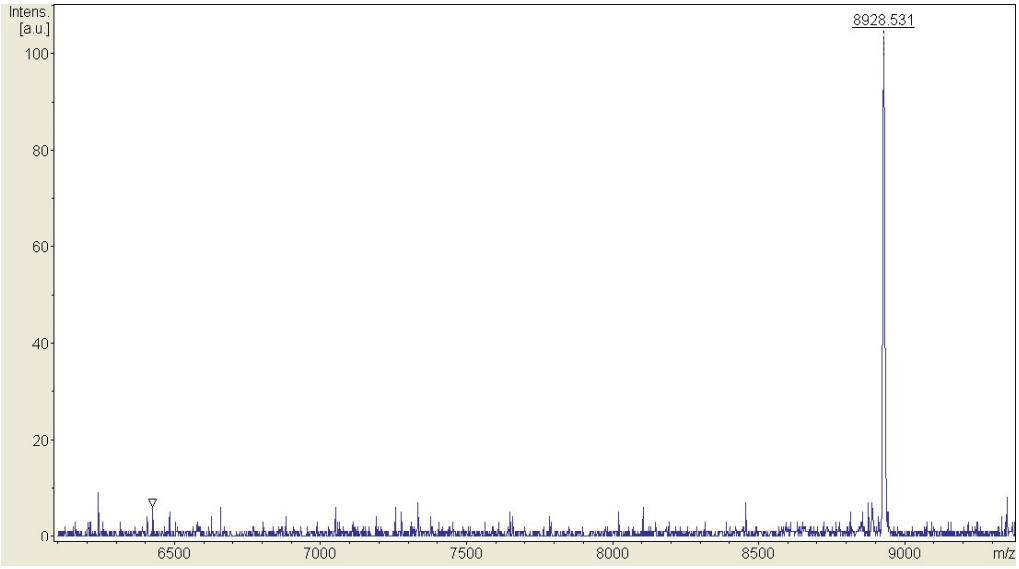

Figure S2.5. MALDI-TOF Spectra of NB-G6

^{1}H: **TD-G5**

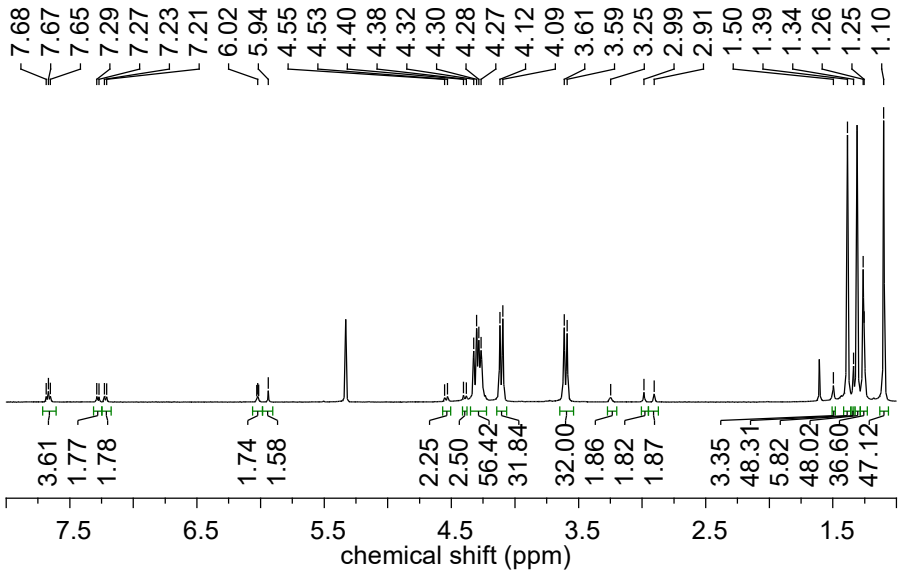

^{13}C: TD-G5

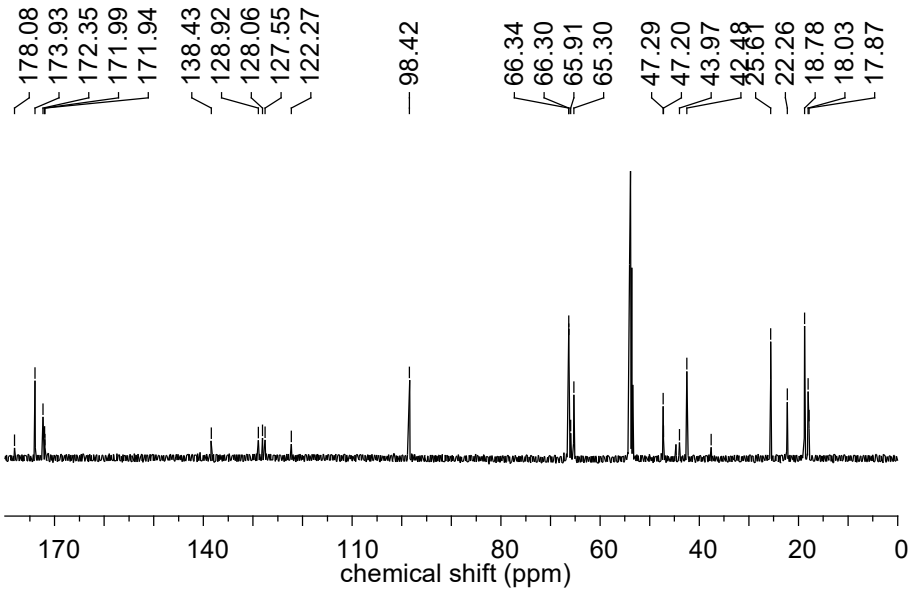

MALDI-TOF Spectra of TD-G5

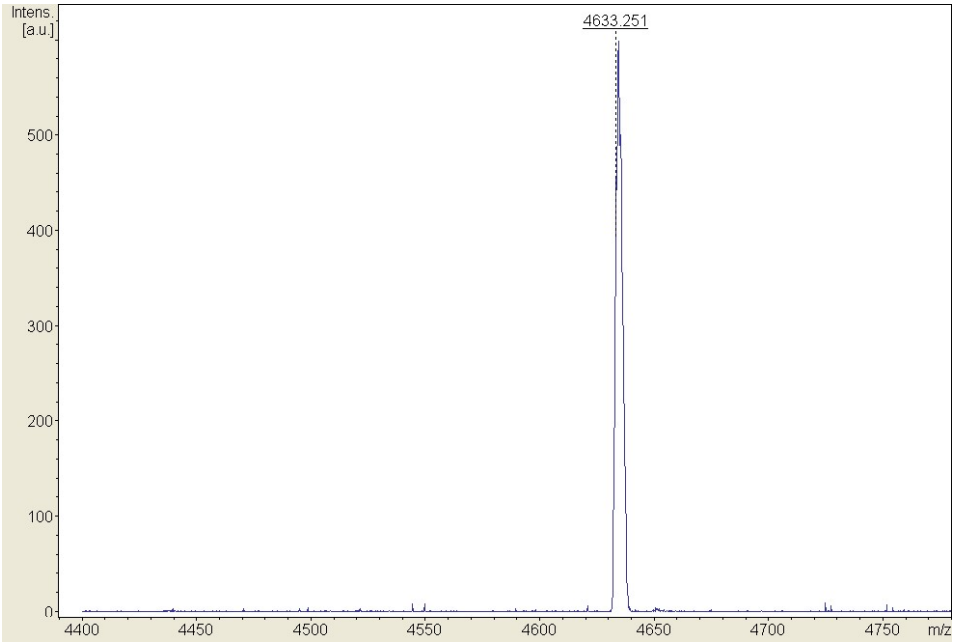

^{1}H: PNB-G6

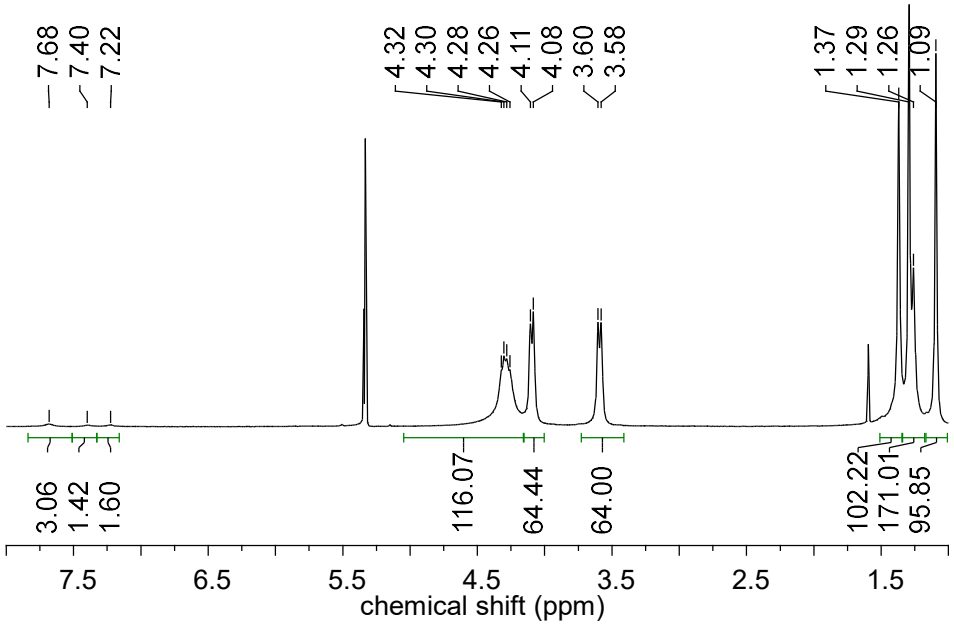

^{1}H: PTD-G5

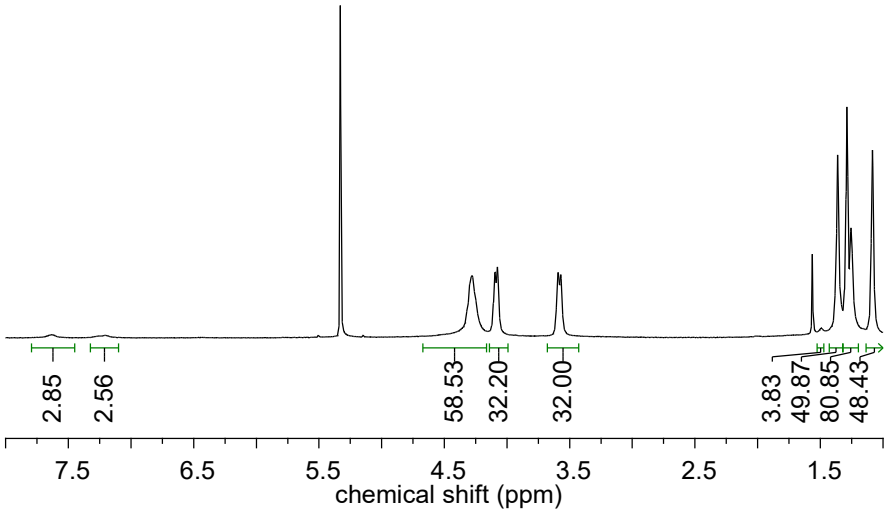

2.6 References

(1) ecommandoux, S.; Chécot, F.; Borsali, R.; Schappacher, M.; Deffieux, A.; Brûlet, A.; Cotton, J. P. *Macromolecules* 2002, *35*, 8878.

(2) underlich, K.; Müllen, K.; Fytas, G. In *Conjugated Polymers and Oligomers*, p 1.

(3) Parshad, B.; Kumari, M.; Achazi, K.; Böttcher, C.; Haag, R.; Sharma, S. K. *Polymers* 2016, *8*, 311.

(4) Küchler, A.; Adamcik, J.; Mezzenga, R.; Schlüter, A. D.; Walde, P. *RSC Advances* 2015, *5*, 44530.

(5) Piunova, V. A.; Miyake, G. M.; Daeffler, C. S.; Weitekamp, R. A.; Grubbs, R. H. *Journal of the American Chemical Society* 2013, *135*, 15609.

(6) Feng, S.; Xiong, X.; Zhang, G.; Xia, N.; Chen, Y.; Wang, W. *Macromolecules* 2009, *42*, 281.

(7) Das, J.; Yoshida, M.; Fresco, Z. M.; Choi, T.-L.; Fréchet, J. M. J.; Chakraborty, A. K. *The Journal of Physical Chemistry B* 2005, *109*, 6535.

(8) Förster, S.; Neubert, I.; Schlüter, A. D.; Lindner, P. *Macromolecules* 1999, *32*, 4043.

(9) Zhang, B.; Wepf, R.; Fischer, K.; Schmidt, M.; Besse, S.; Lindner, P.; King, B. T.; Sigel, R.; Schurtenberger, P.; Talmon, Y.; Ding, Y.; Kröger, M.; Halperin, A.; Schlüter, A. D. *Angewandte Chemie International Edition* 2011, *50*, 737.

(10) Mikhailov, I. V.; Darinskii, A. A.; Zhulina, E. B.; Borisov, O. V.; Leermakers, F. A. M. *Soft Matter* 2015, *11*, 9367.

(11) Chang, A. B.; Lin, T.-P.; Thompson, N. B.; Luo, S.-X.; Liberman-Martin, A. L.; Chen, H.-Y.; Lee, B.; Grubbs, R. H. *Journal of the American Chemical Society* **2017**, *139*, 17683.

(12) Guo, Y.; van Beek, J. D.; Zhang, B.; Colussi, M.; Walde, P.; Zhang, A.; Kröger, M.; Halperin, A.; Dieter Schlüter, A. *Journal of the American Chemical Society* **2009**, *131*, 11841.

(13) Grebikova, L.; Kozhuharov, S.; Maroni, P.; Mikhaylov, A.; Dietler, G.; Schluter, A. D.; Ullner, M.; Borkovec, M. *Nanoscale* **2016**, *8*, 13498.

(14) Ouali, N.; Méry, S.; Skoulios, A.; Noirez, L. *Macromolecules* **2000**, *33*, 6185.

(15) Dutertre, F.; Bang, K.-T.; Loppinet, B.; Choi, I.; Choi, T.-L.; Fytas, G. *Macromolecules* **2016**, *49*, 2731.

(16) Kim, K. O.; Choi, T.-L. *ACS Macro Letters* **2012**, *1*, 445.

(17) Kim, K. O.; Choi, T.-L. *Macromolecules* **2013**, *46*, 5905.

(18) Ki-Young, Y.; Suyong, S.; Yong-Jae, K.; Inhye, K.; Eunji, L.; Tae-Lim, C. *Macromolecular Rapid Communications* **2015**, *36*, 1069.

(19) Christian, S. *Macromolecular Rapid Communications* **2004**, *25*, 1283.

(20) R., A. D.; Vincent, L.; J., O. L. D.; Guy, B.; H., G. R. *Angewandte Chemie International Edition* **2007**, *46*, 7262.

(21) Gawin, R.; Tracz, A.; Chwalba, M.; Kozakiewicz, A.; Trzaskowski, B.; Skowerski, K. *ACS Catalysis* **2017**, *7*, 5443.

(22) Cotton, J. P.; Decker, D.; Benoit, H.; Farnoux, B.; Higgins, J.; Jannink, G.; Ober, R.; Picot, C.; des Cloizeaux, J. *Macromolecules* **1974**, *7*, 863.

(23) Kholodenko, A. L. *Macromolecules* **1993**, *26*, 4179.

(24) Kholodenko, A. L. *The Journal of Chemical Physics* **1992**, *96*, 700.

(25) Cho, H.; Chung, I.-J. *Macromolecular Theory and Simulations* 1999, *8*, 279.
(26) Paturej, J.; Sheiko, S. S.; Panyukov, S.; Rubinstein, M. *Science Advances* 2016, *2*, e1601478.
(27) Feuz, L.; Leermakers, F. A. M.; Textor, M.; Borisov, O. *Macromolecules* 2005, *38*, 8891.
(28) Ingo, B.; Joachim, K.; F., T. A. *Journal of Applied Crystallography* 2015, *48*, 1587.
(29) Hsu, H.-P.; Paul, W.; Binder, K. *Polymer Science Series C* 2013, *55*, 39.

Chapter 3. Synthesis and Ultrasound-Induced Degradation of the Polyphenylene-Based Dendronized Polymers: The Effect of Side Groups on Mechanochemical Chain Scission

3.1 Abstract

We synthesized dendronized polymers (denpols) bearing polyphenylene dendron via ring-opening metathesis polymerization (ROMP). Their Ultrasonic degradation behavior revealed that the size of the larger side chains led to increased degradation rates. Importantly, we found that the rate enhancement was proportional to the natural log of persistence length (Ln(l_p)) or the square root of monomer molecular weight ($M_{mon}^{0.5}$). It was discovered that those trends could be extended to the related polymers having short or long alkyl chains and ester dendrons.

3.2 Introduction

In chapter 2, we prepared denpols having ester dendrons up to 6th generation and thoroughly investigated their conformation by the scattering techniques. The successful preparation of such high generation denpols led us to synthesize the denpols having the polyphenylene denrdrimers developed by Müllen and coworkers[1]. They have rarely been used in denpols[2,3], because the rigid and bulky characteristics of these dendrons make their polymerization difficult. However, we envisioned that our ROMP technique[4,5] would be capable of overcoming this challenge. Furthermore, we were intrigued by the novelty of these types of polymers and the potential to reach high molecular weight side chains even at low dendron generations. Notably, we wonder about the relationship between the chain rigidity of the denpols and their properties.

Polymer mechanochemistry has attracted much attention since the

mechanical force can induce the chemical reaction to the polymer which cannot be initiated by heat, light, electrics and chemical reagents[6]. It allows the researchers to develop unique functional materials such as force sensors[7], self-reinforcing materials[8] and conducting polymers[9]. However, there is still a lack of understanding of the fundamentals that determine the mechanochemical reactivity of a polymer chain. One of the most important questions in the field is how the side chain affects the mechanochemical behaviors of a polymer.

Several studies have been devoted to exploring the effect of the side groups on the mechanochemical reactions. Ultrasound-induced degradation of a polymer in a solution is commonly used for the kinetic and mechanistic studies because of the high reproducibility, compatibility with the common techniques such as SEC and use of small quantities of the analyte. Early studies compared the degradation of the poly(alkyl methacrylates) with different alkyl chains[10-12]. Their kinetic analysis revealed that the polymers having larger alkyl chains degrade faster although the exact rate constant trend was unclear. However, recent studies contrast to those works. For instance, Moore and coworkers compared the degradation rate of poly(acrylates) having methyl, ethyl, and butyl isomers side groups[13]. It was found that the alkyl side chains did not affect the degradation rate.

The degradation trend of polymers with much longer side groups has been much less studied. Sheiko and coworkers investigated the degradation of poly (alkyl methacrylate)s having poly(butyl acrylate)s as a side group[14]. Their observation was that the degradation rate

increased as the length of the side group increased. However, an exact relationship between the side chain and the rate enhancement was not established. Overall, those studies suggested that there is a lack of systematic research providing the role of the side chain quantitatively, comprising small to large side chains.

We envisioned that dendronized polymers (denpols) are well-suited for the systematic study because one can tune the size and structure of the side unit at the molecular level without the defect issue while maintaining a constant grafting density. In this chapter, we report the synthesis of a new class of polyphenylene-based denpols via living ROMP. The comparison of their ultrasonic degradation to other PTDs with different side chains revealed the role of side group size on the kinetics of mechanochemical chain scission.

3.3 Result and Discussion

3.3.1 Synthesis of the Macromonomers and Polymers

Scheme 1. Synthetic Route for the Synthesis of Macromonomers.[a]

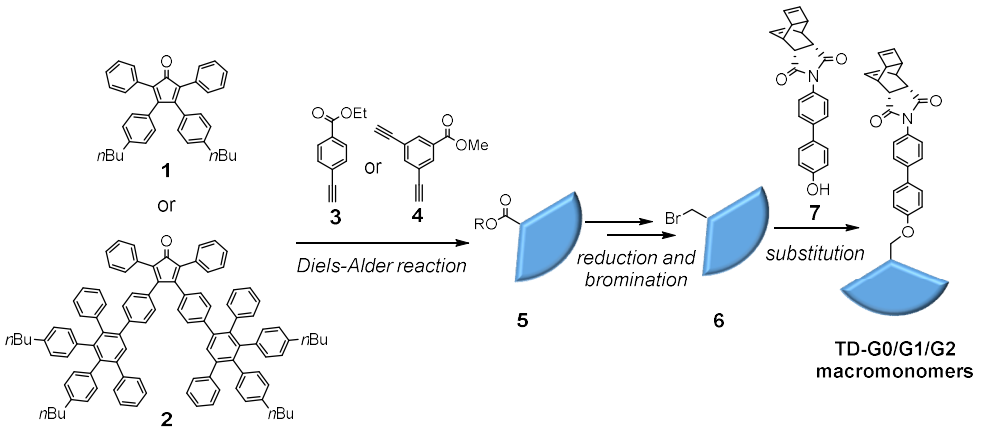

a) Reactions were conducted with the following general conditions: Diels–Alder: o-xylene, 120 ºC or 150 ºC, 12 h; ester reduction: $LiAlH_4$, tetrahydrofuran (THF), room temperature (RT), 1 h; bromination: CBr_4, PPh_3, THF or CH_2Cl_2, RT, 1 h; and substitution: triethylamine, *N*,*N*–dimethylformamide, 55 ºC, 12 h.

To synthesize denpols with Müllen's polyphenylene dendrons, we prepared macromonomers containing small to large dendrons (Scheme 3.1). In general, these macromonomers were prepared by a convergent approach, specifically using a Diels–Alder reaction between cyclopentadienone derivatives (**1** and **2**) electron poor alkynes (**3** and **4**). The Diels–Alder reaction between building blocks **1** and **3**, **1** and **4**, and **2** and **4** yielded generation–zero (G0), first–generation (G1), and second–generation (G2) dendrons, respectively, which each contained an ester moiety (**5**) as a handle for further modification. Subsequently, reduction and bromination (**6**) followed by a simple substitution reaction with **7**, yielded the final TD macromonomers (TD–G0, TD–G1,

and TD-G2). Notably, macromonomers, along with all precursors, were purified by flash column chromatography and characterized by NMR spectroscopy and matrix-assisted laser desorption/ionization mass spectrometry (MALDI) to ensure the production of defect-free dendrons.

Scheme 3.2. Synthesis of Polyphenylene-Based Denpols[a]

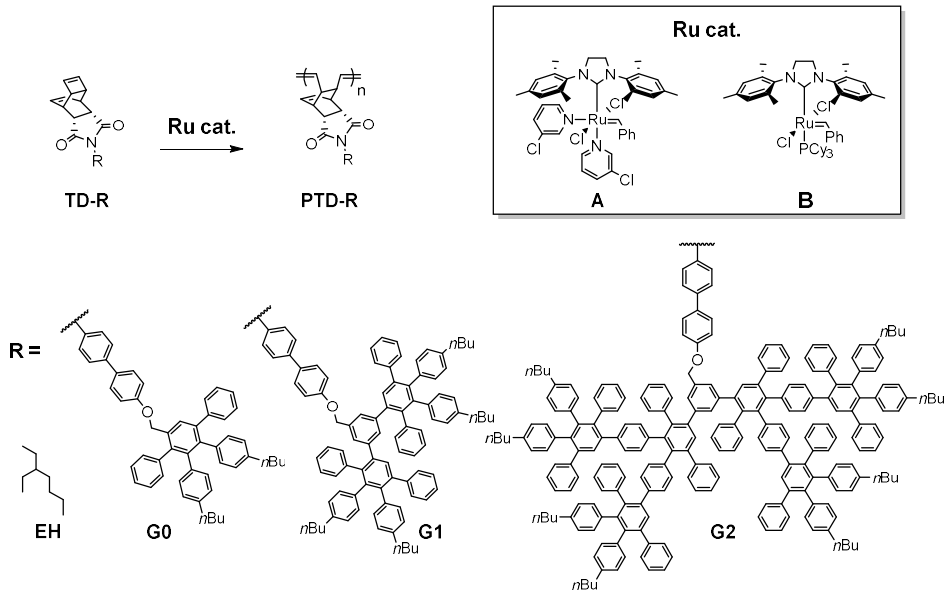

a) PTD-G0/G1 was obtained by using Grubbs 3rd-generation catalyst in dichloromthane at RT. PTD-G2 was obtained by using Grubbs 2nd-generation catalyst in dichloroethane at 50 °C.

ROMP of TD-G0 and TD-G1 (Scheme 3.2) was carried out using the fast-initiating Grubbs 3rd-generation catalyst (**A**) at room temperature in CH_2Cl_2. We observed controlled polymerizations in which we could target specific *DP*s by varying the monomer to initiator ratio. The resulting PTD-G0 and PTD-G1 polymers were prepared with a wide range of DP_ws (90 – 564, determined by dividing the M_w by the monomer molecular weight, M_{mon}) and with narrow dispersity (1.02 –

1.15). Having successfully polymerized TD-G0/G1, we sought to polymerize the much bulkier TD-G2. However, initial attempts using A at room temperature only gave low molecular weight polymer, presumably due to low reactivity and stability of the propagating species[15-19], limiting efficient propagation of this challenging macromonomer. Fortunately, by switching to Grubbs 2nd-generation catalyst(B) and increasing the temperature to 50 ºC, we successfully obtained high molecular weight PTD-G2 with DP_ws in the range of 91 – 465, and with acceptable dispersity (1.18 – 1.29). In addition, we prepared a linear polymer series (PTD-EH) having relatively small 2-ethyl-1-hexyl side chains, according to literature protocols,[20] for comparison. These four series of polymers (summarized in Table 3.1) represented the core polymers for investigating the mechanochemical degradation kinetics.

Table 3.1 Polymer Series Molecular Weight Characterization and Mechanochemical Degradation Rate Constants.

Polymer	M_w[a](kDa)	DP_w[b]	$Đ_M$[a]	k_{RI}[c]($\times10^{-2}$ min^{-1})	k_{res}[d]($\times10^{-2}$ min^{-1})
PTD-EH	39	124	1.01	0.09 ± 0.01	0.07
	71	227	1.01	0.66 ± 0.02	0.67
	118	378	1.01	3.02 ± 0.03	3.01
	151	482	1.07	5.82 ± 0.20	5.86
	202	646	1.03	11.62 ± 0.41	11.85
PTD-G0	101	116	1.03	0.21 ± 0.01	0.21
	187	213	1.02	1.09 ± 0.12	1.09

	316	361	1.04	4.54 ± 0.04	4.62
	391	447	1.08	8.29 ± 0.23	8.65
	494	564	1.10	14.53 ± 0.96	14.87
PTD-G1	130	90	1.02	0.15 ± 0.01	0.15
	274	189	1.05	1.45 ± 0.07	1.42
	468	324	1.04	5.42 ± 0.21	5.72
	643	445	1.15	12.53 ± 0.55	13.16
PTD-G2	290	91	1.29	0.29 ± 0.03	0.31
	645	202	1.21	2.11 ± 0.01	2.29 ± 0.02
	1088	341	1.28	8.29 ± 0.07	9.20 ± 0.07
	1484	465	1.18	16.91 ± 0.33	18.65 ± 0.55

a) Determined by SEC with MALLS. b) Determined by dividing the M_w by M_{mon} (313, 876, 1444, and 3191 Da for PTD-EH, PTD-G0, PTD-G1, and PTD-G2, respectively). c) Rate constants calculated from linear regression of the Ln(RI signal intensity) at the P_{max} retention time of the parent polymer versus sonication time. Values are an average of three runs ± one standard deviation. d) Rate constants calculated in the same manner as k_{RI} except using chromatograms that were resolved using non-linear regression to remove overlap of the daughter fragments at P_{max}. Values are for a single run unless the single run value fell outside of 3 standard deviations from k_{RI}, in which case the average and standard deviation of three runs were calculated.

3.3.2 Ultrasonication and Kinetic Analysis.

To investigate the degradation of denpols, dilute solutions of each polymer were subjected to ultrasonication in tetrahydrofuran (THF), and aliquots were removed at various time points over the course of the experiment for analysis by size exclusion chromatography (SEC)

with multi-angle laser light scattering (MALLS). Kinetic analyses were conducted using the method initially described by Florea,[21] which has been used to determine degradation rate constants for linear and star polymers.[22,23] In short, first order rate constants (k_{RI}) were obtained by monitoring the refractive index (RI) signal at a single retention time (P_{max}) corresponding to the peak maximum of the parent polymer (pre-sonication) over the course of the sonication experiment (Experimental Section for more details). With narrow dispersities and adequate SEC column separation, this method is more effective at distinguishing the degradation of the parent polymer from daughter fragments than molecular weight-based kinetics analyses.[22] To confirm that the daughter fragments were not significantly contributing to the RI signal at P_{max}, nonlinear regression analysis was used to resolve each SEC trace. Using the resolved peaks, we calculated rate constants for scission of the parent polymer based upon the resolved P_{max} RI intensity (k_{res}, Table 3.1) and total peak area (k_{area}) (Table S3.1). Good agreement between k_{RI}, $k_{res,\ and}$ k_{area} values support that the concentration of parent polymer determined by a single retention time is a good representation of the total parent concentration. In all cases, except for PTD-G2-202, PTD-G2-341, and PTD-G2-465 where the numbers indicate the DP_w, the k_{res} value fell within 3 standard deviation of the average k_{RI} value (determined from three independent sonication experiments), indicating minimal influence of the daughter fragments overall. For the three polymers in which that wasn't the case, we calculated the average and standard deviation using the resolved SEC traces and have used those values for subsequent analysis (and hence the use of just k to denote the rate constant in discussions below).

The rate constants for mechanochemical scission were plotted as a function of the weight average molecular weight (M_w) and DP_w. First, examination of the M_w plot (Figure 3.1A) shows a substantially different dependence on molecular weight for each polymer type. As the side chain size increases, the degradation rate constant decreases. For instance, PTD-EH-646 and PTD-G2-91 have comparable M_ws of 202 and 290 kDa, respectively; however, PTD-EH-646 has a ca. 40 times larger degradation rate. This result is consistent with the rate constant trends observed by Moore and coworkers for polymers bearing small side chains,[13] and can be explained by the contour length, rather than the molecular weight, being a more important kinetic parameter for polymer degradation.[24] For polymers with consistent molecular weight, a polymer with larger side chains will have a shorter contour length and thus slower degradation. Next, examination of the DP_w plot (Figure 3.1B) shows that the data for each polymer type does not converge in the same manner that Moore and coworkers observed with polymers having smaller side chains.[13] Instead we see that the rate constant increases with increasing side chain size for a given DP_w, which is consistent with the brush polymer trend observed by Sheiko and coworkers.[14] By comparing polymers with similar DP_ws from each series, we see that in comparison to PTD-EH-482, PTD-G0-446, PTD-G1-445, PTD-G2-465 have ca. 1.4, 2.2, and 2.9 times larger rate constants, respectively. Overall, these results suggest that the side chains, not just the contour length, play an important role in influencing the degradation rate as we anticipated.

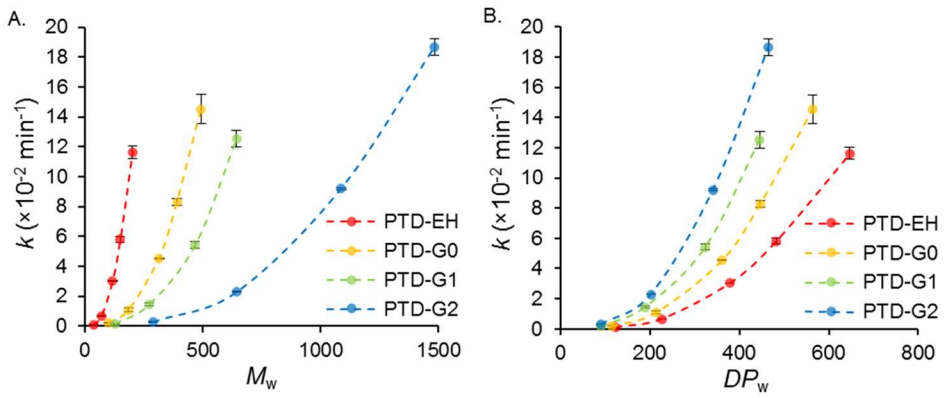

Figure 3.1. Rate constants (k) for the mechanochemical degradation of linear and dendronized polymers as a function of M_w (A), and DP_w (B). Dashed lines are for visual aid only. Each data point is the average rate constant determined from three independent experiments and error bars represent ± one standard deviation.

We predicted that elongated conformation would closely relate to the degradation rate. In order to examine the effect of the chain extension to the degradation rate, we estimated the flory exponent (v) from log-log plots of R_g vs M_w (Figure S3.2) obtained from the SEC-MALLS data. The parameter v is related to the conformation of the polymer, with a value of 0.5 indicating a random coil and 1.0 indicating a rigid rod.[25] To further characterize the chain rigidity of each polymer, we estimated the persistence length (l_p) for each series using the Benoit-Doty law.[26] Estimated v and l_p of each polymer are summarized in table 3.2, indicating a significant increase in polymer rigidity with increasing side group size.

Table 3.2 The shape factors of PTD polymers

Factor	PTD-EH	PTD-G0	PTD-G1	PTD-G2
ν^a	0.47	0.57	0.79	0.81
l_p^b	3.3 ± 0.2	6.2 ± 0.1	11.1 ± 0.3	38.5 ± 0.3

[a]Estimated by SEC-MALLS[b] Obtained from SEC-MALLS data using Benoit Doty equation.

Interestingly, we found that for each polymer, the natural log of the l_p value was almost exactly equal to the degradation rate enhancement (how many times greater the rate constant trend was than PTD-EH, Figure S3.3), such that if k was divided by Ln(l_p), the rate constant trends for each polymer converged onto the PTD-EH trend line (Figure 3.2A). This result suggested that we could accurately determine the ultrasonic degradation rate of any PTD polymer using only two factors, its contour length and rigidity (when all other factors are constant, such as ultrasonic power intensity, solvent, temperature, etc.). Despite how well this trend fits the data, we sought to find another parameter that could be exactly measured and was proportional to the rate enhancement. We found that to be the square root of M_{mon} (Figure 3.2B), such that plotting $k/M_{mon}^{0.5}$ versus the DP_w leads to convergence of our rate constant trend lines. While we do not have an explanation for the exponent in this relationship, M_{mon} itself is a useful estimation of side group size as it eliminates the need for the somewhat arbitrary assignment of where a side group starts and where the backbone ends. Therefore, we would expect the rate enhancement to increase with increasing M_{mon}.

3.3.3 Testing the Generality of the Trends

As we were able to find relationships that led to convergence of our rate constant trends, we envisioned using these plots as "master curves" from which we would be able to predict the degradation rate constants of other polymers. In order to test the generality of any observed kinetic trends, we also synthesized three PTDs, again by following reported protocols,[5,20] bearing an octadecyl side chain (PTD-OD), a third-generation ester dendron (PTD-eG3), or a fourth-generation ester dendron (PTD-eG4) (Scheme 3.3). We expected that these polymers might have different properties than the polyphenylene-based denpols and would provide a good assessment of the generality of our master curve. Using the DP_w and I_p or M_{mon} as input variables, we predicted rate constants (k_{p1}, based on the relationship with I_p and k_{p2}, based on the relationship with M_{mon}) for each polymer (Table 3.3), and then sonicated each polymer and determined experimental rate constants for comparison.

Scheme 3.3 Other Polymers for Testing the Generality

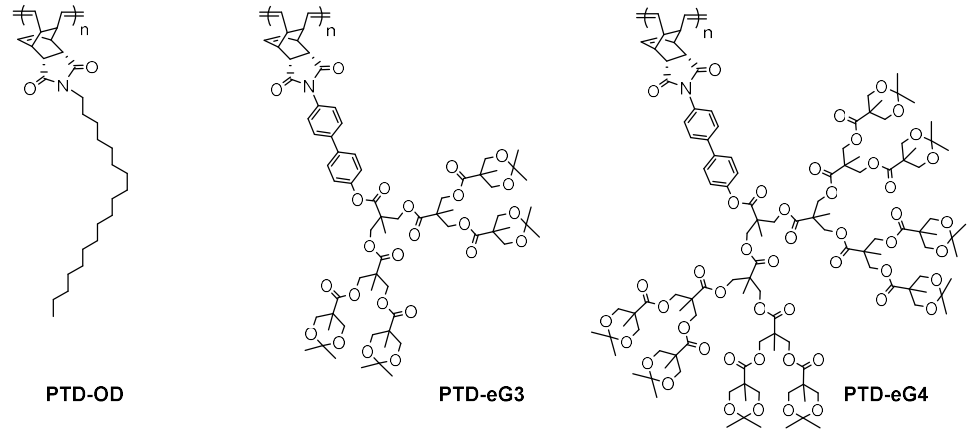

Table 3.3 Predicted vs Experimental Mechanochemical Degradation Rate Constants.

Polymer	M_w[a] (kDa)	DP_w[b]	$Đ$[a]	k_{p1}[c] ($\times10^{-2}$ in^{-1})	k_{p2}[d] ($\times10^{-2}$ min^{-1})	k ($\times10^{-2}$ min^{-1})
PTD-OD	114	251	1.02	1.3	1.4	1.19 ± 0.05[e]
PTD-eG3	603	450	1.03	10.0	10.8	9.94 ± 0.09[f]
PTD-eG4	1124	462	1.17	15.2	15.5	15.96 ± 0.86[e]

a) Determined by SEC with MALLS. b) Determined by dividing the M_w by the monomer molecular weight (453, 1342, and 2430 Da for PTD-OD, PTD-eG3, and PTD-eG4, respectively). c) Rate constants predicted from the Ln(I_p) master curve. The DP_w was used to determine the expected k/Ln(I_p) value from the polynomial fit of the master curve data, which was then multiplied by Ln(I_p) to obtain k_{p1} d) Rate constants predicted from the $M_{mon}^{0.5}$ master curve. The DP_w was used to determine the expected $k/M_{mon}^{0.5}$ value from the polynomial fit of the master curve data, which was then multiplied by $M_{mon}^{0.5}$ to obtain k_{p2}. e) k_{RI} value. f) k_{res} value.

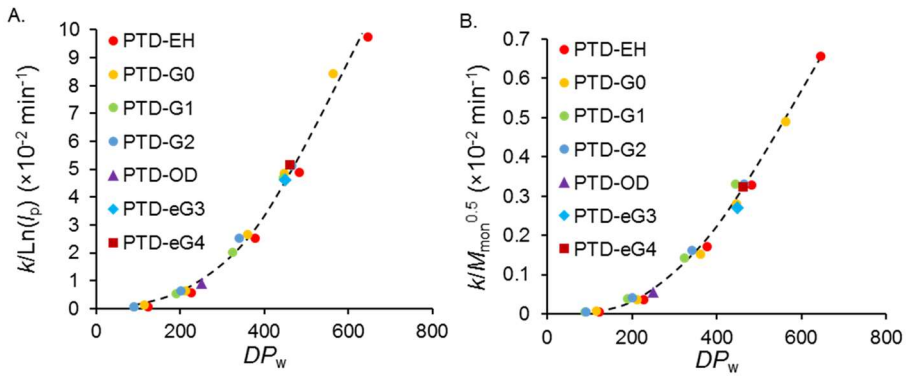

Figure 3.2 Plots of $k/\mathrm{Ln}(l_p)$ (degradation rate constant divided by the natural log of the persistence length) as a function of DP_w (A), and $k/M_{mon}^{0.5}$ (degradation rate constant divided by the square root of the monomer molecular weight) as a function of DP_w (B), showing convergence of the rate constant trends for all denpols and linear polymers studied. Dashed lines are for visual aid only.

The predicted rate constants, in both cases, were in good agreement with the experimentally determined rate constants, and the experimentally determined $k/\mathrm{Ln}(l_p)$ or $k/M_{mon}^{0.5}$ values fell on the same trend as their respective master curves (see Figure 3.2). Given the diversity of the side chains in this study (short and long alkyl chains, polyphenylene dendrons, and flexible ester dendrons), it appears that our master curve is quite general and would likely be able to predict the degradation rate of other PTD-based polymers over the same *DP* range. Furthermore, we believe these findings will be useful in the development of new theoretical models pertaining to the ultrasonic degradation of polymers.

3.4 Conclusions

In this study we have synthesized a series of well-defined denpols based on polyphenylene dendrons, for the first time, and systematically studied their ultrasonic degradation kinetics to further elucidate the role of side chain size in polymer mechanochemistry. We found that as the size of the side group increased, the degradation rate constant also increased, in agreement with the majority of studies thus far (the studies that did not see a difference in side group size were likely looking at too small of differences between their comparisons). More importantly, we found that the rate enhancement was proportional to Ln(I_p) and $M_{mon}^{0.5}$, and that these relationships could be used to generate master curves that describe the reaction rate trends of polymers bearing alkyl chains and rigid and flexible dendrons of various generations. These results are consistent with polymers having elongated and rigid conformations degrading more rapidly. We expect that these results will be helpful in the development of new theoretical models that describe the ultrasonic degradation of polymers.

3.5 Experimental section

Materials

Dry THF was obtained from a Glass Contour solvent purification system. DCM and DCE were used as polymerization solvents and were distilled after drying over CaH_2 overnight, then was degassed by three freeze-pump-thaw cycles. THF that was used as polymerization solvent was distilled from sodium and benzophenone and was

degassed via bubbling Ar gas through the solvent. All other reagents and solvents were used as obtained from commercial sources.

Characterization

^{1}H and ^{13}C NMR spectra were recorded on a Varian/Oxford As-500 (500 MHz for ^{1}H and 125 MHz for ^{13}C), Agilent 400-MR (400 MHz for ^{1}H and 100 MHz for ^{13}C) and Bruker DRX-300 (300 MHz for ^{1}H, 75 MHz for ^{13}C) spectrometers. Chemical shifts are reported in delta (δ) units, expressed in parts per million (ppm) downfield from tetramethylsilane using the residual protio-solvent as an internal standard ($CDCl_3$, ^{1}H: 7.26 ppm and ^{13}C: 77.16 ppm; CD_2Cl_2, ^{1}H: 5.33 ppm and ^{13}C 53.84 ppm). Abbreviations associated with the peak assignment are as follows: s, singlet; d, doublet; t, triplet; q, quartet; m, multiplet, br, broad peak. The number of hydrogens assigned for polymer spectra correspond to a single repeat unit. The molar masses of each precursor were measured by Bruker Microflex TOF and Bruker UltrafleXtreme TOF/TOF. 7,7,8,8-Tetracyanoquinodimethanel (TCNQ) was used as a matrix. SEC setup consisted of: Waters 1515 pump, manual injector with a loop volume of 50 μL, 2 Shodex GPC LF-804 size-exclusion columns maintained at 35 ºC, DAWN-HELEOS 8+ multi-angle laser light scatter and OptiLab T-rEx refractive index detectors (each from Wyatt Technologies Corporation). The mobile phase consisted of HPLC-grade THF (inhibitor free). Molecular weights were determined from light scattering using dn/dc values calculated from batch mode measurements of polymer solutions at different concentrations. The fractionation of PTD-G2-465 was done by using Japan Analytical Industry Co., Ltd. LC-9260 next recycling preparative HPLC.

Table S3.1. Mechanochemical Degradation Rate Constant Summary

Polymer	DP_w[a]	k_{RI}[b] ($\times 10^{-2}$ min^{-1})	k_{res}[c] ($\times 10^{-2}$ min^{-1})	k_{area}[d] ($\times 10^{-2}$ min^{-1})
PTD-EH	124	0.09 ± 0.01	0.07	0.19
	227	0.66 ± 0.02	0.67	0.67
	378	3.02 ± 0.03	3.01	3.01
	482	5.82 ± 0.20	5.86	5.91
	646	11.62 ± 0.41	11.85	12.09
PTD-G0	116	0.21 ± 0.01	0.21	0.20
	213	1.09 ± 0.12	1.09	1.07
	361	4.54 ± 0.04	4.62	4.64
	447	8.29 ± 0.23	8.65	8.99
	564	14.53 ± 0.96	14.87	14.97
PTD-G1	90	0.15 ± 0.01	0.15	0.17
	189	1.45 ± 0.07	1.42	1.30
	324	5.42 ± 0.21	5.72	5.77
	445	12.53 ± 0.55	13.16	13.24
PTD-G2	91	0.29 ± 0.03	0.31	0.25
	202	2.11 ± 0.01	2.29 ± 0.02	2.28
	341	8.29 ± 0.07	9.20 ± 0.07	9.18
	465	16.91 ± 0.33	18.65 ± 0.55	18.05
PTD-OD	251	1.19 ± 0.05	1.30	1.28
PTD-eG3	450	9.68 ± 0.05	9.94 ± 0.09	9.99

PTD-eG4	462	15.96 ± 0.86	16.77	16.17

[a)] Determined by dividing the M_w (from SEC/MALLS analysis) by the monomer molecular weight. [b)] Rate constants calculated from linear regression of the Ln(RI signal intensity) at the P_{max} retention time of the parent polymer versus sonication time. Values are an average of three runs ± one standard deviation. [c)] Rate constants calculated in the same manner as k_{RI} except using chromatograms that were resolved using non-linear regression to remove overlap of the daughter fragments at P_{max}. Values are for a single run unless the single run value fell outside of 3 standard deviations from k_{RI}, in which case the average and standard deviation of three runs were calculated. d) Rate constants calculated from linear regression of Ln(peak area), using the area of the parent polymer obtained from the resolved chromatograms, versus sonication time.

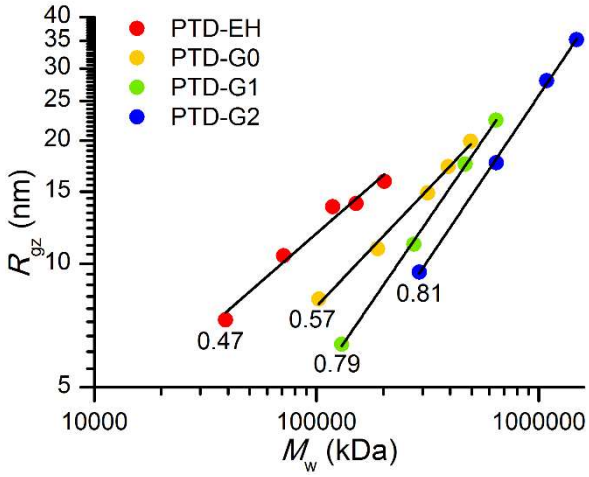

Figure S3.2 Log-log plot of the z-average radius of gyration (R_{gz}) versus M_w for each polymer in the series. The value for the slope of the apparent linear fit is reported below the fit curve. This data shows an increase in polymer rigidity with increasing side chain size.

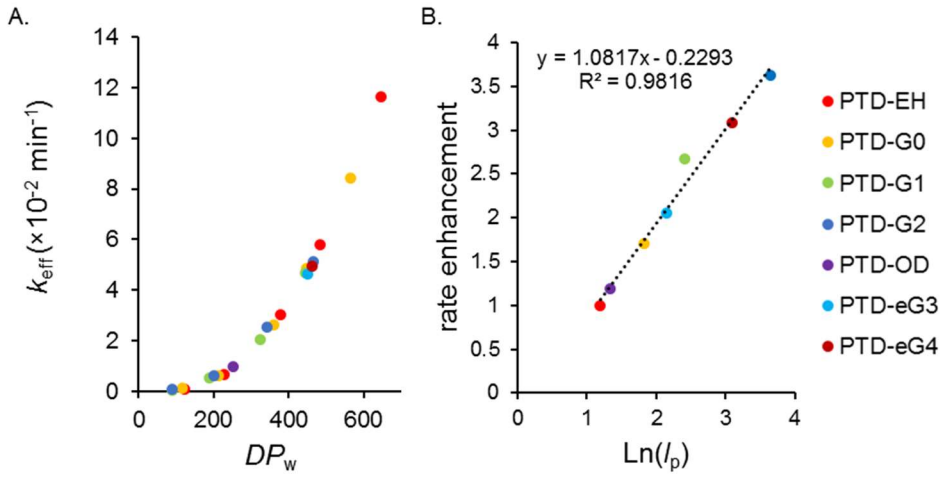

Figure S3.3 Plots of effective rate constant (k_{eff}) for each polymer type vs DP_w (A), rate enhancement for each polymer type vs Ln(I_p) (B).The rate k_{eff} is equal to the experimental rate constants k divided by the "rate enhancement" (or the number of times larger the rate constant trend is compared to PTD-EH) for a given polymer type. The rate enhancement values were calculated as single values for each polymer type such that all of the k_{eff} trends would overlap with the PTD-EH polymer trend line (thus the rate enhancement for PTD-EH is equal to 1.0). The rate enhancement was found to be almost exactly equal to Ln(I_p) such that plotting k/Ln(I_p) vs DP_w yields convergence of all of the rate constant trends (see main text Figure 3.2).

Synthesis of Monomers

Synthesis of TD-G0

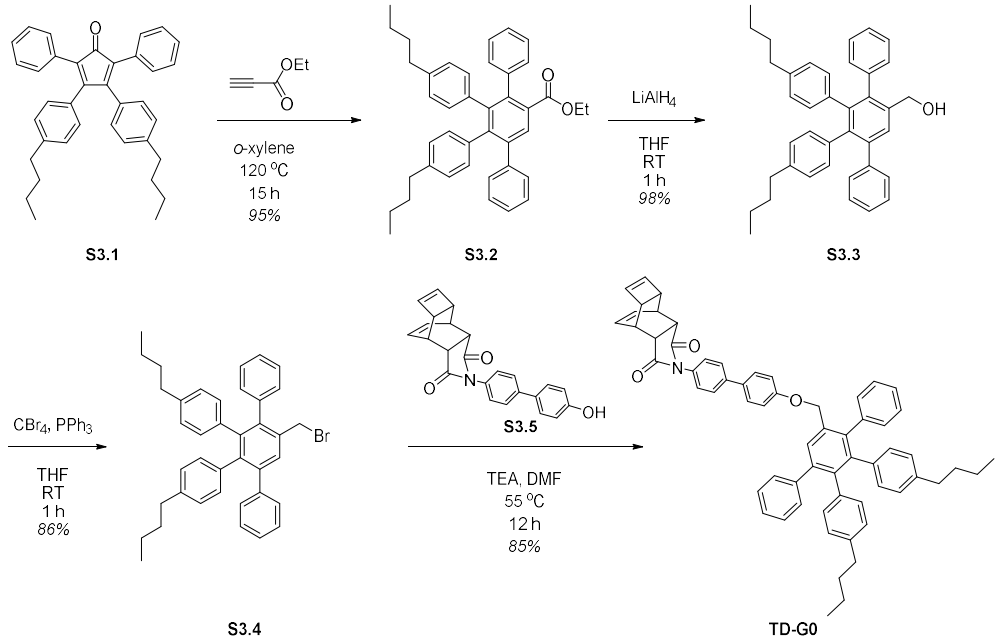

Scheme S3.1 Synthesis of the monomer TD-G0.

Synthesis of S3.2

S3.1 (2 mmol, 1.0 mol. eq., prepared as previously described[27]) and ethyl propiolate (6 mmol, 3.0 mol. eq.) were dissolved in 20 mL of *o*-xylene and stirred for 15 h at 120 ºC under an Ar atmosphere. After, the solvent was removed under reduced pressure and the crude product was purified by flash column chromatograph on silica gel (hexanes/DCM = 1/1). The product was obtained in 95% yield. ^{1}H NMR (500 MHz, CD_2Cl_2, δ): 7.80 (s, 1H), 7.25 – 7.07 (m, 8H), 7.03 (dd, *J* = 6.8, 2.9 Hz, 2H), 6.83 – 6.58 (m, 8H), 4.00 (q, *J* = 7.1 Hz, 2H), 2.48 – 2.30 (m, 4H), 1.46 – 1.33 (m, 4H), 1.23 – 1.05 (m, 4H), 0.95 (t, *J* = 7.1 Hz, 3H), 0.84 (m, *J* = 7.3, 4.0 Hz, 6H). ^{13}C NMR (75 MHz, CD_2Cl_2, δ): ^{13}C NMR (75 MHz, CD_2Cl_2) δ 168.96, 143.62, 142.93, 141.74, 141.23, 140.86, 140.70, 140.49, 140.42, 137.21, 137.12, 132.39, 131.54, 131.37, 130.36, 130.27, 129.90, 127.97, 127.40, 127.33, 127.08,

126.80, 126.51, 61.26, 35.40, 33.79, 22.31, 22.23, 14.09, 13.92. MS (MALDI-TOF) m/z for $C_{41}H_{42}O_2$: $[M]^+$: 566.318 (calculated), 566.330 (observed).

Synthesis of S3.3

To a stirred solution of S3.2 (1.92 mmol, 1.0 mol. eq.) in THF (19 mL), $LiAlH_4$ (2.88 mmol, 1.5 mol. eq.) was slowly added at 0 ºC, then stirred at RT for 1 h. The reaction was quenched with a 10 wt% NaOH solution at 0 ºC. The resulting mixture was filtered through a celite pad and the solvent was removed under reduced pressure. The crude product was purified by silica gel column chromatography (hexanes/DCM = 1/3). The product was obtained in 98% yield. ^{1}H NMR (500 MHz, CD_2Cl_2, δ): 7.65 (s, 1H), 7.17 (d, *J* = 33.2 Hz, 10H), 6.74 (d, *J* = 26.9 Hz, 8H), 4.52 (s, 2H), 2.44 (d, *J* = 14.3 Hz, 4H), 1.80 (s, 1H), 1.44 (d, *J* = 11.7 Hz, 4H), 1.20 (d, *J* = 15.8 Hz, 4H), 0.89 (s, 6H). ^{13}C NMR (75 MHz, CD_2Cl_2, δ): ^{13}C NMR (75 MHz, CD_2Cl_2) δ 142.58, 142.31, 141.33, 140.48, 140.16, 140.08, 140.01, 139.85, 138.41, 137.85, 137.76, 131.74, 131.50, 130.64, 130.33, 128.91, 127.92, 127.28, 127.00, 126.74, 126.52, 63.81, 35.41, 35.35, 33.84, 33.78, 22.35, 22.24, 14.13. MS (MALDI-TOF) m/z for $C_{39}H_{40}O$: $[M]^+$: 524.308 (calculated), 524.394 (observed).

Synthesis of S3.4

To a stirred solution of S3.3 (1.88 mmol, 1.0 mol. eq.) and carbon tetrabromide (2.44 mmol, 1.3 mol. eq.) in THF (19 mL), triphenylphosphine (2.35 mmol, 1.25 mol. eq.) was added at 0 ºC, then stirred at RT for 1 h. The solvent was removed from the resulting mixture under reduced pressure. The crude product was purified by silica gel column chromatography (hexanes/DCM = 3/1). The product

was obtained in 86% yield. ^{1}H NMR (500 MHz, CD_2Cl_2, δ): 7.63 (s, 1H), 7.19 (s, 10H), 6.75 (s, 4H), 6.69 (s, 4H), 4.43 (s, 2H), 2.41 (d, *J* = 21.6 Hz, 4H), 1.42 (d, *J* = 19.1 Hz, 4H), 1.17 (s, 4H), 0.86 (d, *J* = 7.5 Hz, 6H). ^{13}C NMR (75 MHz, CD_2Cl_2, δ): 142.90, 142.00, 141.75, 141.31, 141.24, 140.70, 140.30, 139.27, 137.62, 137.39, 135.29, 131.59, 131.40, 130.70, 130.25, 127.97, 127.80, 127.31, 127.03, 126.95, 126.72, 35.40, 35.33, 33.81, 33.76, 33.31, 22.33, 22.22, 14.10. MS (MALDI-TOF) m/z for $C_{39}H_{40}O$: $[M]^+$: 586.224 (calculated), 586.320 (observed).

Synthesis of TD-G0

To a stirred solution of S3.5 (1.78 mmol, 1.1 mol. eq., prepared as previously described) and TEA (1.78 mmol, 1.1 mol. eq.) in DMF (8 mL), S3.4 (1.62 mmol, 1.0 eq) was added at RT, then the reaction mixture was stirred at 55 ºC for 12 h. After extraction with DCM twice, the combined organic layer was dried over $MgSO_4$ and the solvent was removed under reduced pressure. The crude residue was purified by flash column chromatograph on silica gel (hexanes/DCM = 1/3). The product was obtained in 85% yield. ^{1}H NMR (500 MHz, CD_2Cl_2, δ): 7.70 (s, 1H), 7.66 – 7.55 (m, 2H), 7.55 – 7.46 (m, 2H), 7.24 – 7.19 (m, 2H), 7.19 – 7.06 (m, 10H), 6.97 – 6.87 (m, 2H), 6.73 (d, *J* = 11.1 Hz, 4H), 6.69 (t, *J* = 6.2 Hz, 4H), 6.10 – 5.99 (m, 2H), 5.94 (s, 2H), 4.90 (s, 2H), 3.24 (d, *J* = 1.2 Hz, 2H), 2.98 (t, *J* = 1.5 Hz, 2H), 2.90 (s, 2H), 2.39 (m, 4H), 1.49 – 1.33 (m, 4H), 1.15 (m, 4H), 0.85 (q, 6H). ^{13}C NMR (75 MHz, CD_2Cl_2, δ): 178.08, 158.79, 142.19, 142.01, 141.39, 141.12, 140.37, 140.34, 139.98, 139.67, 139.19, 138.15, 137.30, 137.16, 133.78, 133.06, 131.40, 131.20, 130.52, 130.38, 130.11, 129.44, 128.59, 128.31, 127.64, 127.53, 127.08, 126.83, 126.80, 126.53, 126.25, 115.38, 68.82, 44.25, 43.54, 37.18, 35.18, 35.12, 33.46, 33.43, 22.00,

21.89, 14.06. MS (MALDI-TOF) m/z for $C_{63}H_{57}NO_3Na$: $[M+Na]^+$: 898.424 (calculated), 899.011 (observed).

Synthesis of TD-G1

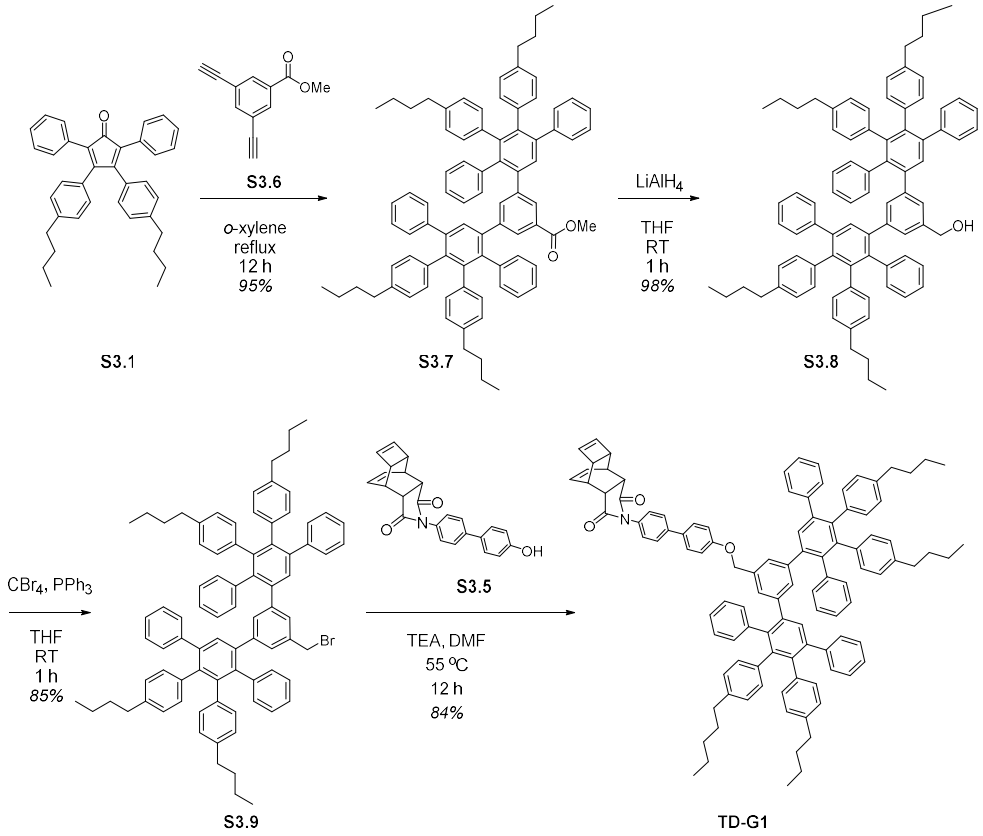

Scheme S3.2 Synthesis of the monomer TD-G1.

Synthesis of S3.7

S3.1 (4.72 mmol, 2.3 mol. eq.) and S3.6 (2.05 mmol, 1 mol. eq., prepared as previously described[28]) were dissolved in 20 mL of *o*-xylene and stirred for 12 h at 150 ºC under an Ar atmosphere. After, the solvent was removed under reduced pressure and the crude product was purified by flash column chromatograph on silica gel (hexanes/DCM = 1/1). The product was obtained in 95% yield. ^{1}H NMR (500 MHz, CD_2Cl_2, δ): 7.61 (s, 2H), 7.26 (s, 1H), 7.23 – 7.12 (m, 10H), 6.90 (m, 6H), 6.83 (m, 6H), 6.76 (s, 8H), 6.69 (s, 8H), 3.73 (s, 3H), 2.42 (m, 4H), 1.43 (m, 4H), 1.19 (m, 4H), 0.87 (m, 12H). ^{13}C NMR (75 MHz, CD_2Cl_2, δ): 166.92, 142.44, 142.24, 142.01, 141.24, 140.54, 140.34, 140.29, 140.20, 139.68, 139.63, 137.98, 137.68, 136.37, 132.00, 131.68, 131.63, 131.41, 130.41, 129.48, 129.30, 127.85, 127.38, 127.28, 127.00, 126.59, 126.16, 52.11, 35.41, 35.35, 33.83, 22.34, 22.24, 14.11. MS (MALDI-TOF) m/z for $C_{84}H_{80}O_2$: $[M]^+$: 1120.616 (calculated), 1121.640 (observed).

Synthesis of S3.8

To a stirred solution of S3.7 (1.95 mmol, 1.0 mol. eq.) in THF (20 mL), $LiAlH_4$ was added slowly at 0 ºC, then stirred at RT for 1 h. The reaction was quenched with a 10 wt% NaOH solution at 0 ºC. The resulting mixture was filtered through a celite pad and the solvent was removed under reduced pressure. The crude product was purified by silica gel column chromatography (hexanes/DCM = 1/3). The product was obtained in 98% yield. ^{1}H NMR (500 MHz, CD_2Cl_2, δ): 7.22 – 7.10 (m, 12H), 7.01 (s, 1H), 6.89 (m, 4H), 6.85 (m, 4H), 6.81 (m, 4H), 6.74

(s, 8H), 6.67 (s, 8H), 4.27 (s, 3H), 2.40 (m, 8H), 1.41 (m, 8H), 1.17 (m, 8H), 0.85 (m, 12H). ^{13}C NMR (75 MHz, CD_2Cl_2, δ): 142.36, 141.90, 141.21, 140.81, 140.49, 140.35, 140.17, 140.01, 139.63, 138.13, 137.81, 132.12, 131.74, 131.71, 131.43, 130.45, 127.86, 127.30, 127.02, 126.57, 126.00, 65.25, 35.45, 35.39, 33.86, 22.37, 22.27, 14.16. MS (MALDI-TOF) m/z for $C_{83}H_{80}ONa$: $[M]^+$: 1115.611 (calculated), 1116.555 (observed).

Synthesis of S3.9

To a stirred solution of **S3.8** (1.91 mmol, 1.0 mol. eq.) and carbon tetrabromide(2.48 mmol, 1.3 mol. eq.) in THF (19 mL), triphenyl phosphine (2.3 mmol, 1.25 mol. eq.) was added at 0 ºC and stirred at RT for 1 h. The solvent was removed from the resulting mixture under reduced pressure. The crude product was purified by silica gel column chromatography (hexanes/DCM = 3/1). The product was obtained in 85% yield. ^{1}H NMR (500 MHz, CD_2Cl_2, δ): 7.26 (s, 2H), 7.21 (m, 10H), 7.09 (s, 1H), 6.96 (m, 6H), 6.90 (m, 2H), 6.86 (m, 4H), 6.79 (s, 8H), 6.72 (s, 8H), 4.17 (s, 2H), 2.45 (m, 8H), 1.47 (m, 8H), 1.23 (m, 8H), 0.91 (m, 12H). ^{13}C NMR (75 MHz, CD_2Cl_2, δ): 142.43, 142.31, 142.22, 141.25, 140.51, 140.18, 140.01, 139.65, 138.09, 137.77, 136.93, 132.17, 132.02, 131.73, 131.39, 130.46, 129.10, 127.88, 127.43, 127.31, 127.04, 126.60, 126.17, 35.46, 35.40, 33.86, 22.37, 22.28, 14.17. MS (MALDI-TOF) m/z for $C_{83}H_{79}Br$: $[M]^+$: 1154.537 (calculated), 1154.578 (observed).

Synthesis of TD-G1

To a stirred solution of **S3.5** (1.78 mmol, 1.1 mol. eq.) and TEA (1.78

mmol, 1.1 mol. eq.) in DMF (8 mL), **S3.9** (1.62 mmol, 1.0 mol. eq.) was added at RT, and the reaction mixture was stirred at 55 ºC for 12 h. After extraction with DCM twice, the combined organic layer was dried over $MgSO_4$ and the solvent was removed under reduced pressure. The crude residue was purified by flash column chromatograph on silica gel (hexanes/DCM = 1/3). The product was obtained in 84% yield. ^{1}H NMR (500 MHz, CD_2Cl_2, δ): 7.66 (d, *J* = 8.1 Hz, 2H), 7.53 (d, *J* = 8.2 Hz, 2H), 7.34 – 7.14 (m, 14H), 7.07 (s, 1H), 6.99 (s, 2H), 6.96 – 6.80 (m, 12H), 6.77 (s, 8H), 6.70 (s, 8H), 6.06 (s, 2H), 5.97 (s, 2H), 4.80 (s, 2H), 3.29 (s, 2H), 3.01 (s, 2H), 2.93 (s, 2H), 2.43 (m, 8H), 1.51 – 1.35 (m, 8H), 1.27 – 1.06 (m, 8H), 1.04 – 0.77 (m, 12H). ^{13}C NMR (125 MHz, $CDCl_3$, δ): 178.02, 158.73, 142.00, 141.83, 141.51, 140.77, 140.23, 140.17, 139.87, 139.68, 139.56, 139.34, 138.15, 137.71, 137.40, 135.70, 132.93, 131.78, 131.49, 131.42, 131.38, 131.24, 130.61, 130.21, 128.62, 128.23, 127.53, 127.02, 126.90, 126.86, 126.74, 126.19, 125.62, 115.55, 70.02, 44.34, 43.61, 37.25, 35.21, 35.15, 33.48, 22.02, 21.94, 14.05. MS (MALDI-TOF) m/z for $C_{107}H_{97}NO_3$: $[M]^+$: 1444.750 (calculated), 1443.974 (observed).

Synthesis of TD-G2

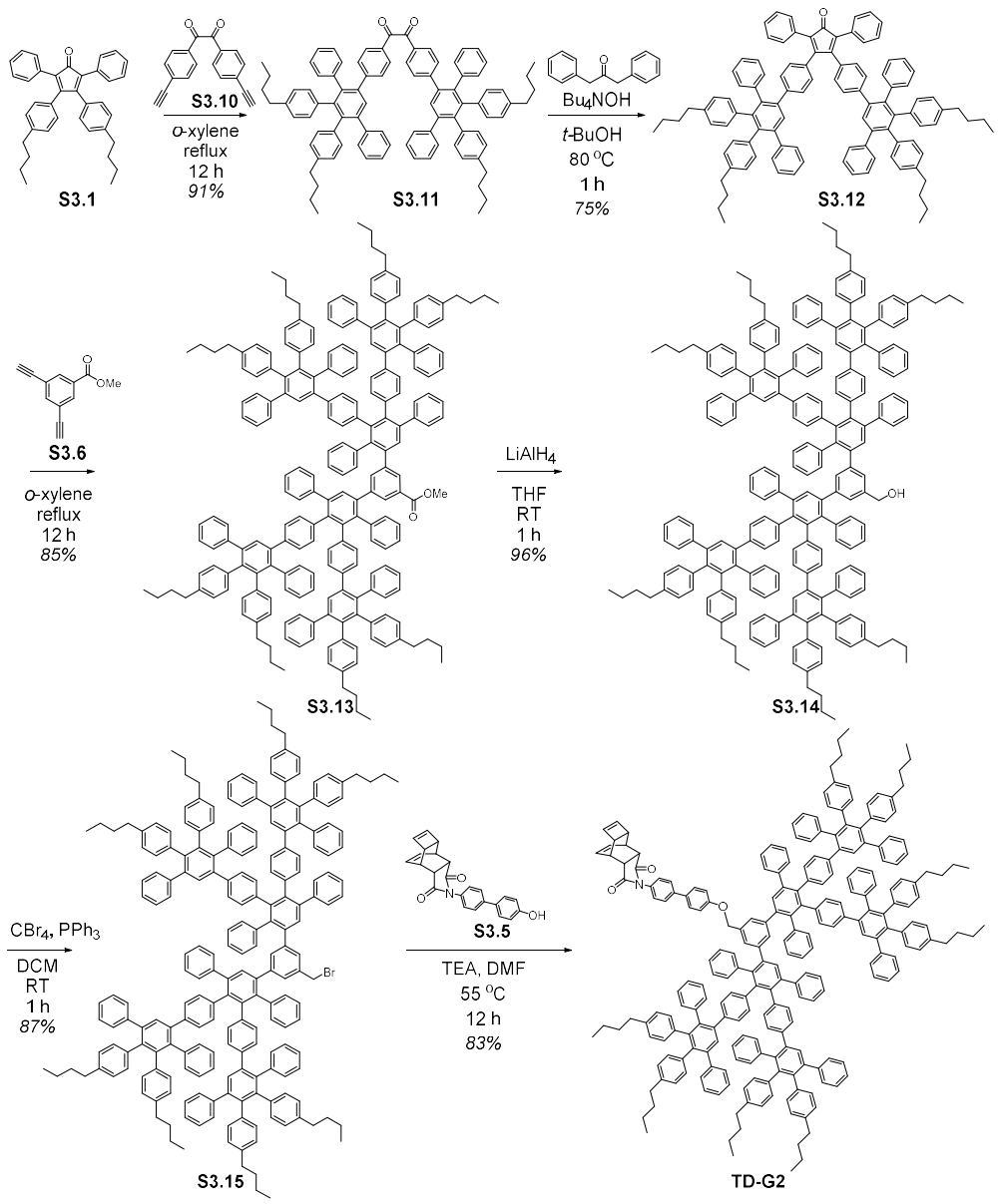

Scheme S3.3. Synthesis of the monomer TD-G2.

Synthesis of S3.11

S3.1 (29.3 mmol, 2.5 mol. eq.) and **S3.10** (11.6 mmol, 1.0 mol. eq., prepared as previously described[29]) were dissolved in 60 mL of *o*-

xylene and stirred for 12 h at 150 ºC under an Ar atmosphere. After, the solvent was removed under reduced pressure and the crude product was purified by flash column chromatograph on silica gel (hexanes/DCM = 1/1). The product was obtained in 91% yield. ^{1}H NMR (500 MHz, CD_2Cl_2, δ): 7.73 (d, *J* = 8.4 Hz, 4H), 7.51 (2, 1H), 7.32 (d, *J* = 8.4 Hz, 4H), 7.17 (10, 3H), 6.97 (m, 6H), 6.89 (m, 4H), 6.76 (s, 8H), 6.70 (s, 8H), 2.41 (m, 8H), 1.42 (m, 8H), 1.17 (m, 8H), 0.86 (m, 12H). ^{13}C NMR (125 MHz, CD_2Cl_2, δ): 194.49, 149.39, 142.78, 142.10, 141.38, 141.99, 140.69, 140.35, 140.12, 139.68, 139.48, 137.73, 137.51, 131.90, 131.60, 131.19, 131.12, 130.97, 130.29, 129.52, 127.96, 127.45, 127.33, 127.07, 126.68, 126.28, 35.41, 35.35, 33.82 , 22.32, 22.22, 14.09. MS (MALDI-TOF) m/z for $C_{90}H_{82}O_2$: $[M]^+$: 1194.631 (calculated), 1194.775 (observed).

Synthesis of S3.12

S3.12 was prepared using a modified literature procedure.[30] S3.11 (9.86 mmol, 1.0 mol. eq.) and diphenylacetone (10.85 mmol, 1.1 mol. eq.) were dissolved in 20 mL of 1,4-dioxane and heated to 80 ºC for 30 min. Then, tetrabutylammonium hydroxide in methanol (0.1M, 19.7 mL, 2.0 mol. eq.) was added dropwise. After 1 h, the reaction solution was cooled to RT. The solvent was removed under reduced pressure and the crude product was purified by flash column chromatograph on silica gel (hexanes/toluene = 1/1). The product was obtained in 75% yield. ^{1}H NMR (500 MHz, CD_2Cl_2, δ): 7.49 (s, 2H), 7.24 (m, 6H), 7.21 – 7.11 (m, 13H), 7.02 – 6.78 (m, 15H), 6.73 (s, 8H), 6.71 – 6.60 (m, 12H), 2.41 (m, 8H), 1.42 (m, 8H), 1.18 (m, 8H), 0.87 (m, 12H). ^{13}C NMR (75 MHz, CD_2Cl_2, δ): 200.44, 154.57, 142.80, 142.41, 141.21, 140.52, 140.24, 139.71, 138.05, 137.75, 132.02, 131.70, 131.47, 131.12,

130.56, 130.37, 129.86, 129.30, 128.38, 127.94, 127.72, 127.30, 127.18, 127.05, 126.61, 126.11, 125.66, 35.43, 33.85, 22.35, 22.24, 14.14. MS (MALDI-TOF) m/z for $C_{105}H_{92}O$: $[M]^+$: 1369.718 (calculated), 1370.740 (observed).

Synthesis of S3.13

S3.12 (1.23 mmol, 2.5 mol. eq.) and S3.6 (0.49 mmol, 1.0 mol. eq.) were dissolved in 5 mL of *o*-xylene and stirred for 12 h at 150 ºC under an Ar atmosphere. After, the solvent was removed under reduced pressure and the crude product was purified by flash column chromatograph on silica gel hexanes/DCM = 2/3). The product was obtained in 85% yield. ^{1}H NMR (500 MHz CD_2Cl_2, δ): 7.58 (s, 2H), 7.45 (s, 2H), 7.41 (s, 2H), 7.22 (m, 28H), 7.15 – 7.07 (m, 4H), 6.91 (m, 20H), 6.86 – 6.65 (m, 51H), 6.58 (d, *J* = 8.0 Hz, 4H), 6.51 (d, *J* = 8.0 Hz, 4H), 3.74 (s, 3H), 2.61 – 2.25 (m, 16H), 1.62 – 1.33 (m, 16H), 1.29 – 1.05 (m, 16H), 1.03 – 0.74 (m, 24H). ^{13}C NMR (75 MHz, CD_2Cl_2, δ): 166.90, 142.52, 142.42, 142.09, 141.99, 141.73, 141.30, 141.09, 140.67, 140.59, 140.46, 140.11, 139.92, 139.60, 139.08, 138.40, 138.30, 138.12, 137.92, 136.46, 132.04, 131.77, 131.39, 130.39, 129.07, 128.80, 127.90, 127.50, 127.27, 127.20, 126.99, 126.52, 125.88, 52.13, 35.45, 35.39, 33.86, 22.37, 22.25, 14.16. MS (MALDI-TOF) m/z for $C_{220}H_{192}O_2$: $[M]^+$: 2867.499 (calculated), 2867.417 (observed).

Synthesis of S3.14

To a stirred solution of S3.13 (0.39 mmol, 1.0 mol. eq.) in THF (4 mL), $LiAlH_4$ (0.59 mmol, 1.5 mol. eq.) was added slowly at 0 ºC, then stirred for 1 h. The reaction was quenched with a 10 wt% NaOH solution at 0 ºC. The resulting mixture was filtered through a celite pad and then the solvent was removed under reduced pressure. The

crude product was purified by silica gel column chromatography (hexanes/DCM = 1/3). The product was obtained in 96% yield. ^{1}H NMR (500 MHz, CD_2Cl_2, δ): 7.43 (s, 2H), 7.36 (s, 2H), 7.29 – 7.02 (m, 31H), 7.02 – 6.86 (m, 20H), 6.86 – 6.61 (m, 50H), 6.61 – 6.53 (m, 6H), 6.50 (m, 6H), 4.28 (s, 2H), 2.55 – 2.25 (m, 16H), 1.51 – 1.31 (m, 16H), 1.20 (m,16H), 0.97 – 0.68 (m, 24H). ^{13}C NMR (75 MHz, CD_2Cl_2): δ 142.52, 142.41, 142.18, 141.83, 141.61, 141.23, 141.08, 140.68, 140.60, 140.57, 140.45, 140.33, 140.09, 139.90, 139.86, 139.60, 139.52, 139.42, 139.24, 139.03, 138.52, 138.30, 138.20, 137.92, 132.17, 132.03, 131.76, 131.37, 130.47, 130.38, 129.05, 128.77, 127.89, 127.40, 127.27, 127.19, 126.98, 126.68, 126.51, 126.14, 125.87, 65.23, 35.45, 35.38, 33.86, 22.36, 22.24, 14.16. MS (MALDI-TOF) m/z for $C_{219}H_{192}O$: $[M]^+$: 2839.504 (calculated), 2839.484 (observed).

Synthesis of S3.15

To a stirred solution of **S3.14** (0.38 mmol, 1.0 mol. eq.) and carbon tetrabromide (0.49 mmol, 1.3 mol. eq.) in DCM (4 mL), triphenyl phosphine (0.47 mmol, 1.25 mol. eq.) was added at 0 ºC, then and stirred at RT for 1 h. The solvent was removed from the resulting mixture under reduced pressure. The crude product was purified by silica gel column chromatography (hexanes/DCM = 3/1). The product was obtained in 87% yield. ^{1}H NMR (500 MHz, CD_2Cl_2, δ): 7.41 (s, 2H), 7.38 (s, 2H), 7.21 (m, 6H), 7.17 (m, 21H), 7.11 – 7.03 (m,6 6H), 6.97 – 6.85 (m, 22H), 6.81 – 6.71 (m, 27H), 6.71 – 6.61 (m, 23H), 6.55 (d, J = 8.2 Hz, 4H), 6.47 (d, J = 8.2 Hz, 4H), 4.12 (s, 2H), 2.57 – 2.22 (m, 16H), 1.44 – 1.33 (m, 16H), 1.17 (m, 16H), 1.00 – 0.72 (m, 24H). ^{13}C NMR (75 MHz, CD_2Cl_2, δ): 142.50, 142.38, 142.11, 141.65, 141.23, 141.04, 140.64, 140.44, 140.17, 140.08, 139.88, 139.60, 139.41,

139.02, 138.44, 138.27, 138.13, 137.88, 132.00, 131.73, 131.35, 130.35, 129.01, 128.74, 127.86, 127.46, 127.23, 127.15, 126.94, 126.48, 125.84, 35.41, 35.35, 33.83, 22.34, 22.22, 14.12. MS (MALDI-TOF) m/z for $C_{219}H_{191}Br$: $[M]^+$ 2901.420 (calculated), 2901.511 (observed).

Synthesis of TD-G2

To a stirred solution of S3.5 (0.36 mmol, 1.1 mol. eq.) and TEA (0.36 mmol, 1.1 mol. eq.) in DMF (3mL), S3.15 (0.33 mmol, 1.0 mol. eq.) was added at RT, and the reaction mixture was stirred at 55 ºC for 12 h. After extraction with DCM twice, the combined organic layer was dried over $MgSO_4$ and the solvent was removed under reduced pressure. The crude residue was purified by flash column chromatograph on silica gel (hexanes/DCM = 1/3). The product was obtained in 83% yield. ^{1}H NMR (500 MHz, CD_2Cl_2, δ): δ 7.66 (d, *J* = 8.1 Hz, 2H), 7.52 (d, *J* = 8.2 Hz, 2H), 7.44 (s, 2H), 7.39 (s, 2H), 7.30 – 7.14 (m, 30H), 7.10 (m, *J* = 6.2 Hz, 4H), 7.00 (s, 1H), 6.93 (m, 20H), 6.88 – 6.65 (m, 53H), 6.58 (d, *J* = 7.8 Hz, 4H), 6.50 (d, *J* = 7.8 Hz, 4H), 6.06 (s, 2H), 5.97 (s, 2H), 4.77 (s, 2H), 3.29 (s, 2H), 3.01 (s, 2H), 2.94 (s, 2H), 2.63 – 2.21 (m, 16H), 1.45 (m, 16H), 1.20 (m, 16H), 0.89 (m, 24H). ^{13}C NMR (75 MHz, CD_2Cl_2, δ): 178.25, 158.98, 142.50, 142.39, 142.14, 142.00, 141.63, 141.51, 141.18, 141.05, 140.66, 140.59, 140.43, 140.35, 140.08, 139.88, 139.83, 139.62, 139.57, 139.50, 139.40, 139.27, 139.00, 138.47, 138.41, 138.28, 138.17, 137.90, 136.18, 133.05, 132.01, 131.75, 131.36, 130.45, 130.36, 129.02, 128.88, 128.74, 128.51, 127.87, 127.56, 127.39, 127.24, 127.17, 126.95, 126.67, 126.49, 126.21, 125.85, 115.66, 70.10, 44.66, 43.90, 37.56, 33.84, 22.34, 22.22,

14.13. MS (MALDI-TOF) m/z for $C_{243}H_{209}NO_3Na$: $[M^+Na]^+$ 3213.620 (calculated), 3214.915 (observed).

Synthesis of TD-OD

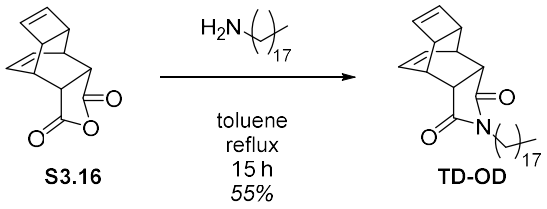

Scheme 3.4. Synthesis of the monomer TD-OD.

Synthesis of TD-OD

S16 (0.49 mmol, 1.0 mol. eq., prepared as previously described[3]) and 1-octadecylamine (0.59 mmol, 1.2 mol. eq.) were dissolved in toluene (2 mL) in a round bottom flask fit with a Dean-Stark trap and a reflux condenser. The solution was refluxed for 15 h, then cooled to RT. The solvent was removed under reduced pressure and the crude solids were re-dissolved in a 2:1 mixture of DCM and hexanes. This solution was put on a plug of silica gel and flushed through with ca. 200 mL of eluent (hexanes/DCM = 1/2). The solvent was removed under reduced pressure to give the desired product. The product was obtained in 55% yield. ^{1}H NMR (300 MHz, $CDCl_3$): δ 5.88 (m, 4H), 3.40 (t, J = 9.6 Hz, 2H), 3.16 (s, 2H), 2.81 (s, 2H), 2.71 (s, 2H), 1.47 (m, 2H), 1.25 (s, 30H), 0.88 (t, J = 6.6 Hz, 3H). ^{13}C NMR (126 MHz, $cdcl_3$) δ 178.88, 138.06, 128.34, 44.31, 43.36, 38.76, 36.79, 32.03, 29.81, 29.77, 29.73, 29.66, 29.61, 29.47, 29.26, 27.77, 26.91, 22.80, 14.23. MS (MALDI-TOF) m/z for $C_{30}H_{47}NO_2$: $[M]^+$ 453.36 (calculated), 451.78 (observed).

Synthesis of Polymers

PTD-EH,[31] PTD-eG3,[5] and PTD-eG4,[5] and their monomers, were prepared as previously described.

PTD-G0/G1/G2/OD were each prepared using the following general procedure: monomer and initiator/catalyst were each added to separate vials, purged with Ar, and then dissolved in dry and degassed solvent. The initiator solution was added at once to the monomer solution under vigorous stirring. After a given time, the polymerization was quenched with by excess ethyl vinyl ether. The concentrated reaction mixture was then precipitated and the polymer was collected and dried under reduced pressure. For specific details see below.

PTD-G0

Prepared on a 70 mg scale, at 0.1 M monomer concentration, using G3 catalyst (1.1 mM initiator concentration), at RT for 12 h, and precipitation into acetone. The polymers were obtained in 87 – 94% yield. Representative NMR characterization: ^{1}H NMR (500MHz, $CDCl_3$, δ): 7.72 (s, 1H), 7.53 – 7.20 (br, 6H), 7.06 (br, 10H), 6.76 (br, 2H), 6.67 (s, 4H), 6.61 (s, 4H), 6.55 – 6.27 (br, 2H), 5.19 (br, 2H), 4.80 (br, 2H), 3.52 – 2.65 (s, 6H), 2.35 (m, 4H), 1.37 (m, 4H), 1.12 (m, 4H), 0.82 (m 6H).

PTD-G1

Prepared on a 70 mg scale, at 0.1 M monomer concentration, using G3 catalyst (0.7 mM initiator concentration), at RT for 12 h, and precipitation into acetone. The polymers were obtained in 91 – 96% yield. Representative NMR characterization: ^{1}H NMR (300 MHz, $CDCl_3$, δ): 7.82 – 6.90 (br, 21H), 6.90 – 6.03 (br, 30H), 5.29(br, 2H), 4.49 (br, 2H), 3.11 (br, 6H), 2.32 (br, 8H), 1.36 (br, 8H), 1.12 (br, 8H), 0.80 (br, 12H).

PTD-G2

Prepared on a 70 mg scale, at 0.15 M monomer concentration, using G2 catalyst (0.3 mM initiator concentration), at 50 ºC for 12 h, and precipitation into acetone. PTD-$G2_{465}$ was also subjected to fractionation to remove some low molecular weight oligomers and narrow the $Đ_M$ (decrease of ca. 0.04). The polymers were obtained in 93 – 97% yield. Representative NMR characterization: ^{1}H NMR (300 MHz, $CDCl_3$, δ): 7.90 – 5.80 (br, 127H), 2.36 (br, 16H), 1.37 (br, 16H), 1.12 (br, 16H), 0.80 (br, 24H).

PTD-OD

Prepared on a 95 mg scale, at 0.1 M monomer concentration, using G3 catalyst (2.5 mM initiator concentration), at RT for 5.5 h, and precipitation into methanol. The polymer was obtained in 79% yield. ^{1}H NMR (300 MHz, $CDCl_3$) δ 6.35 (s, 2H), 5.15 (s, 2H), 3.33 (s, 2H), 3.09 (s, 1H), 2.95 (s, 2H), 2.67 (s, 0H), 1.43 (s, 1H), 1.25 (s, 14H), 0.87 (t, J = 6.5 Hz, 2H).

Ultrasonication Protocol

Polymer (15 mg) was added to a two-arm Suslick flask (one arm fit with a rubber septum, the other a glass stopper). The flask was sealed to the sonication horn and purged with Ar for 15 min. In a separate sealed flask, Ar was bubbled through THF (same quality as the GPC mobile phase) for 15 min. The polymer was then dissolved at 1 mg/mL with the THF. An Ar filled balloon was attached to the flask via a needle through the rubber septum. The Suslick flask was then submerged in a cold bath for the remainder of the experiment. The cold bath consisted of a jacketed beaker filled with isopropanol attached to a recirculating chiller, maintaining a bath temperature of ca. 1 ºC, and an internal solution temperature during sonication of ca.

10 ºC. Polymer solutions were sonicated using a 20 kHz Sonics VCX-500 series sonication probe with an extender tip (1.25 cm tip diameter), calibrated according to literature procedures,[32] at 19.3 W/cm^2 (40% amplitude setting on sonicator) using pulse sequence of 1s on, 9s off. Aliquots of 0.5 mL were withdrawn from the reaction periodically and analyzed by GPC. Sonication experiments were conducted in triplicate.

Determination of Rate Constants

Modification of the raw RI traces included: aligning traces via the solvent peak, correcting the baselines, and normalizing the polymer peaks to constant area. The purpose of alignment was to account for minor delays between sample injection and data collection. Peak normalization was used to account for any minor changes in sample concentration (e.g. solvent evaporation prior to analysis, variability in injected volume, etc.). The P_{max} retention time for the time zero RI trace was recorded. The RI intensity at that retention time from each RI trace in the series was then used to generate a first-order kinetic plot and determine k_{RI} for the degradation of the parent polymer. The rate constants k_{res} and k_{area} were determined by resolving overlapped peaks using a non-linear regression analysis. GPC peaks after time zero were assumed to be the sum of two polynomial modified Gaussian functions,[33] and were fit using the nonlinear curve fit tool in Origin Pro 8.

Persistence Length Calculation

The persistence length (l_p) values were calculated from R_{gz} data obtained by MALLS by solving the following equation derived from

Benoit-Doty's Law[26]:

$$F(x) = -\frac{1}{2}\frac{{R_{gz}}^2}{L^2}x^4 + \frac{1}{6}x^3 - \frac{1}{2}x^2 + x + e^{-x} - 1 = 0 \qquad (1)$$

with $x = L/l_p$ and $L = DP \times b$, where b is the length of the monomer unit, which was estimated to be 0.37 nm.[4] With this calculation, l_p is dependent on L and requires x to be significantly larger than unity. Furthermore, the calculated l_p is most accurate at its asymptotic value at sufficiently large values of L.[11] The l_p vales (averages ± one standard deviation calculated from three GPC runs) for PTD-EH, PTD-G0, PTD-G1, PTD-G2, PTD-OD, PTD-eG3, and PTD-eG4 were determined to be 3.3 ± 0.2, 6.2 ± 0.1, 11.1 ± 0.3, 38.5 ± 0.3, 3.8 ± 0.2, 8.6 ± 0.1, and 22.0 ± 0.2 nm, respectively.

Overlap concentration

The overlap concentration (c^*) of each polymer was estimated with equations 2, 3, and 4.[34]

$$c^* = \frac{3M_w}{4\pi N_A (R_g)^3} \qquad (2)$$

$$c^* = \frac{8M_w}{N_A (h_0)^3} \qquad (3)$$

$$c^* = \frac{2^{1.5} M_w}{N_A (L \times l_p)^{1.5}} \qquad (4)$$

Where h_0 is the root-mean-square end-to-end distance of the polymer chain [which is equal to $(6{R_{gz}}^2)^{0.5}$],[35] N_A is the Avogadro's number, and L is the contour length. Equation 2 and 3 represent c* for a random coil (more consistent with PTD-EH and PTD-G0), and equation 4 represents c* for a worm-like chain (more consistent with

PTD-G1 and PTD-G2). The calculated c* values for all polymers using each equation are shown in Table S3.2.

None of c^* is below 1mg/ml, indicating that there is no chain overlapping during the ultrasonication analysis.

Table S3.2. Overlap concentration Summary

polymer	M_w (kDa)[a]	R_{gz} (nm)[a]	c*(g/L)[b]	c*(g/L)[c]	c*(g/L)[d]
PTD-EH	39	8.6	24.18	55.15	97.85
	71	10.5	24.60	56.11	72.25
	118	13.8	17.85	40.71	56.03
	151	14.0	21.64	49.36	49.61
	202	15.9	19.94	45.48	42.86
	680	33.8	6.98	15.92	23.37
PTD-G0	101	8.6	63.80	145.51	110.16
	187	10.7	59.81	136.40	81.13
	316	14.9	37.89	86.42	62.31
	391	17.2	30.13	68.72	56.02
	494	19.9	24.71	56.36	49.87
PTD-G1	130	6.4	199.80	455.68	85.84
	274	11.1	78.030	177.95	59.14
	468	17.5	34.42	78.49	45.25
	643	22.4	22.58	51.50	38.60
PTD-G2	290	9.7	127.11	289.89	29.25
	645	17.7	46.33	105.68	19.61

	1088	28.0	19.64	44.79	15.09
	1484	35.3	13.40	30.58	12.92
PTD-OD	114	10.4	39.63	90.38	80.60
PTD-eG3	603	20.3	28.73	65.52	52.36
PTD-eG4	1124	29.6	17.11	39.03	22.85

[a)] Determined by SEC/MALLS analysis. [b)] Calculated using equation 2.

[c)] Calculated from equation 3. [d)] Calculated using equation 4.

NMR Spectra for New Compounds

^{1}H: S3.2

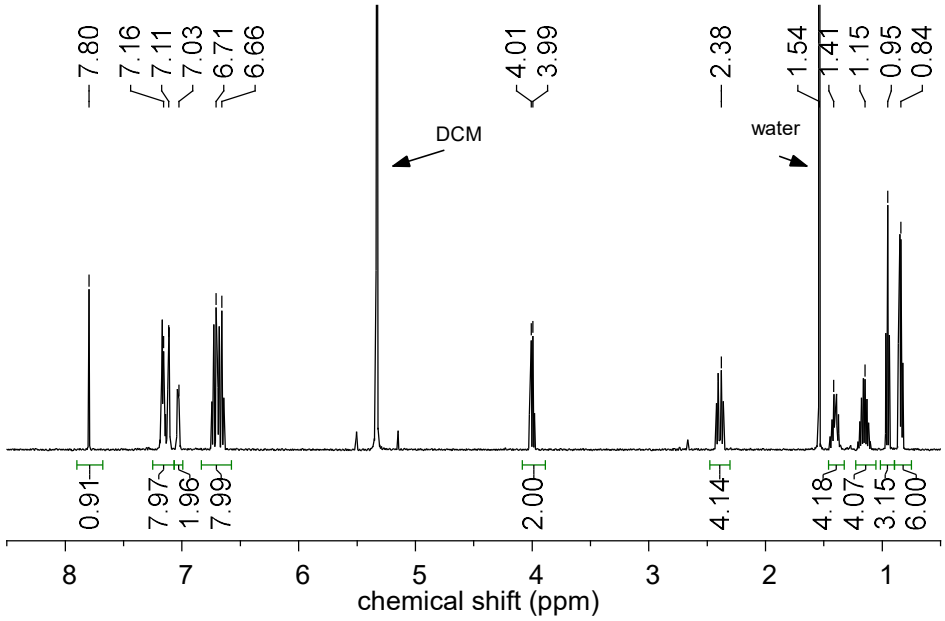

^{13}C: S3.2

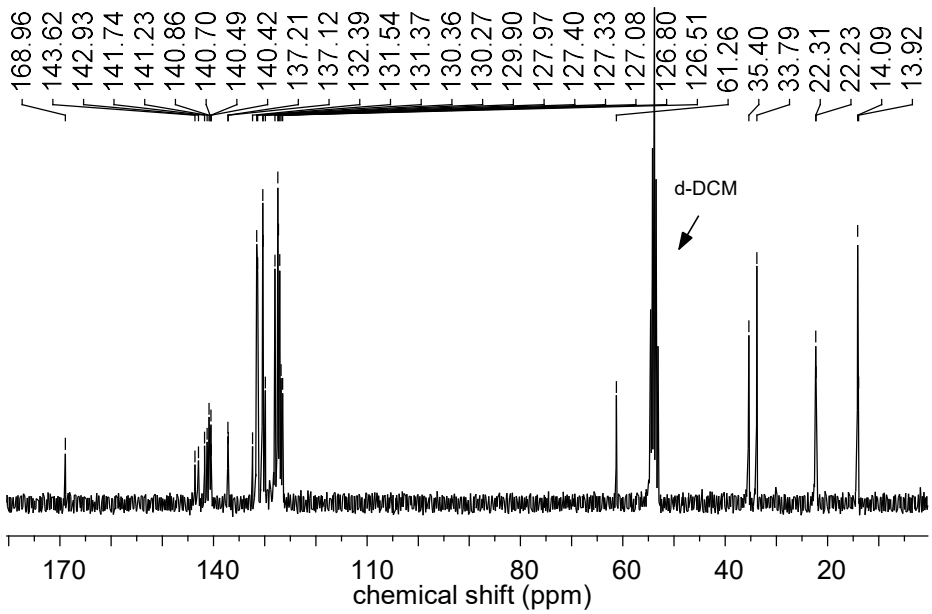

^{1}H: S3.3

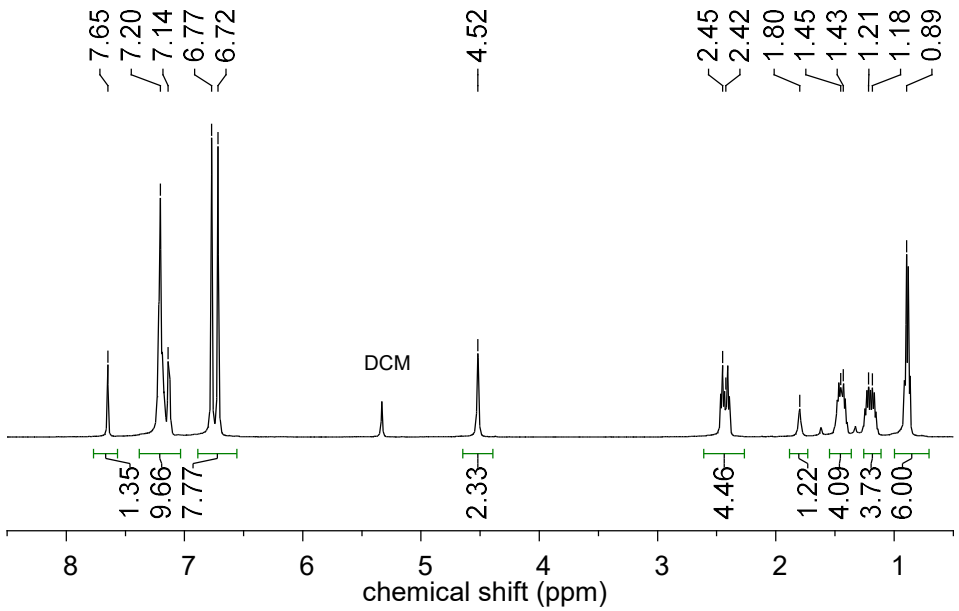

^{13}C: S3.3

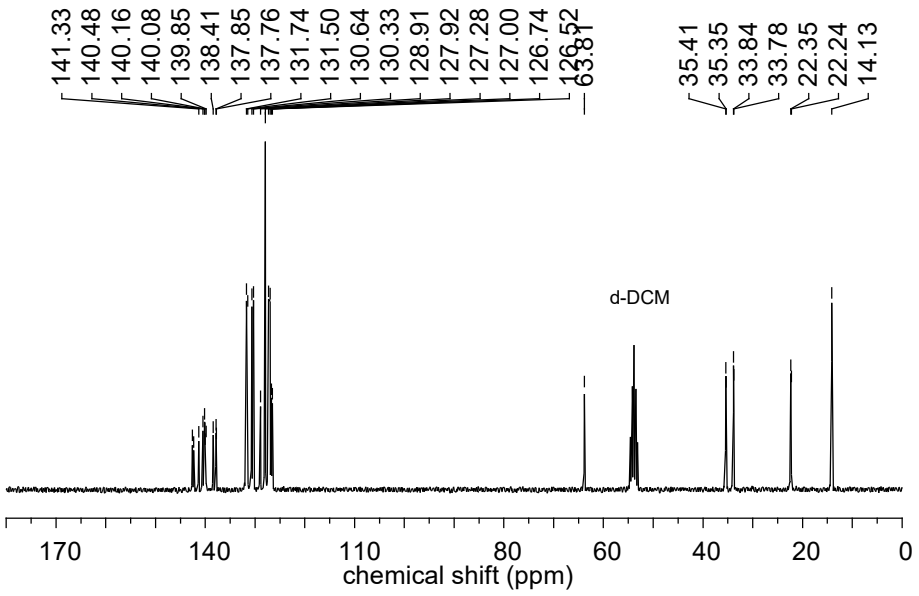

^{1}H: S3.4

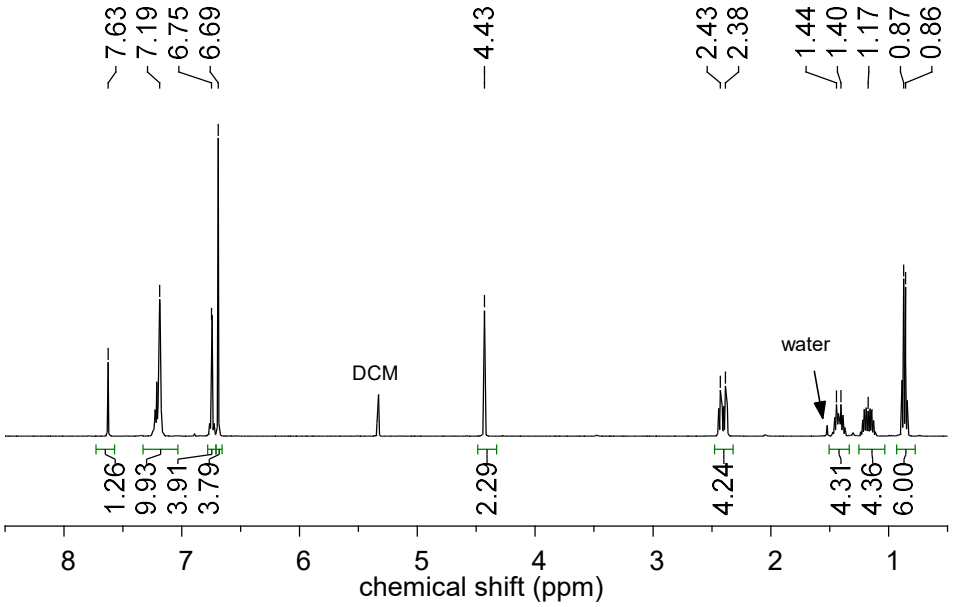

^{13}C: S3.4

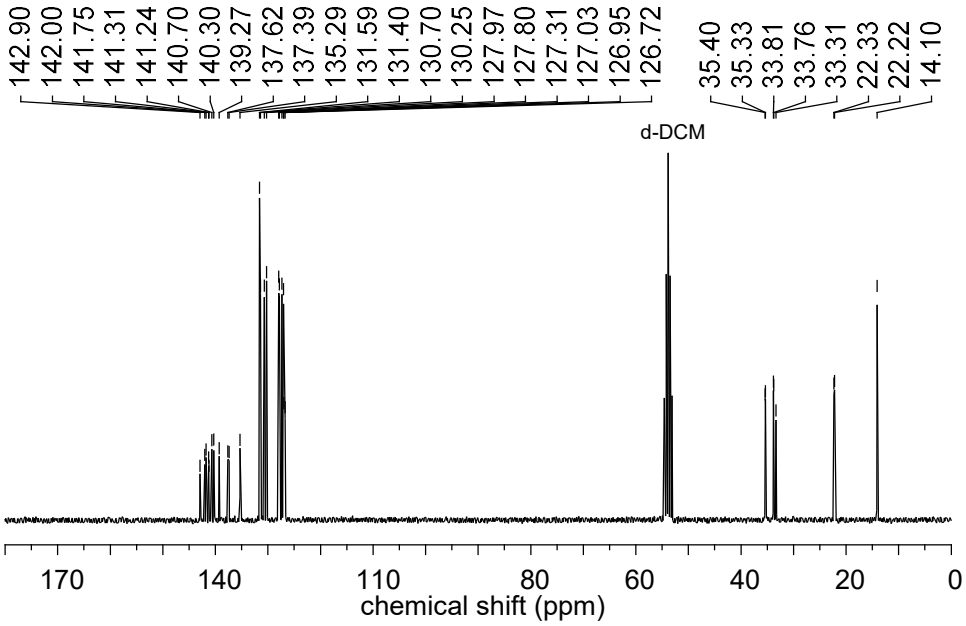

^{1}H: TD-G0

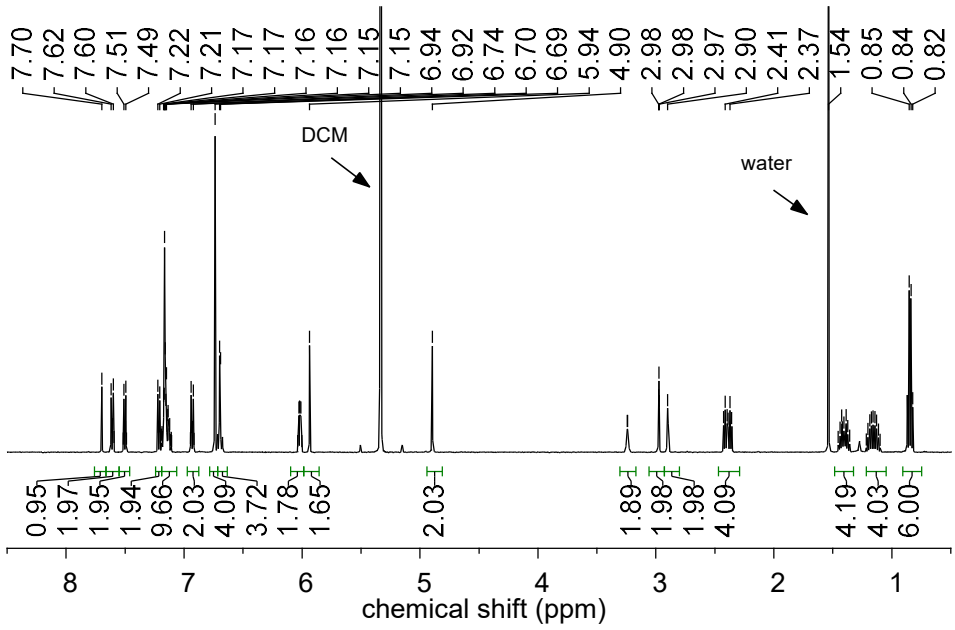

^{13}C: TD-G0

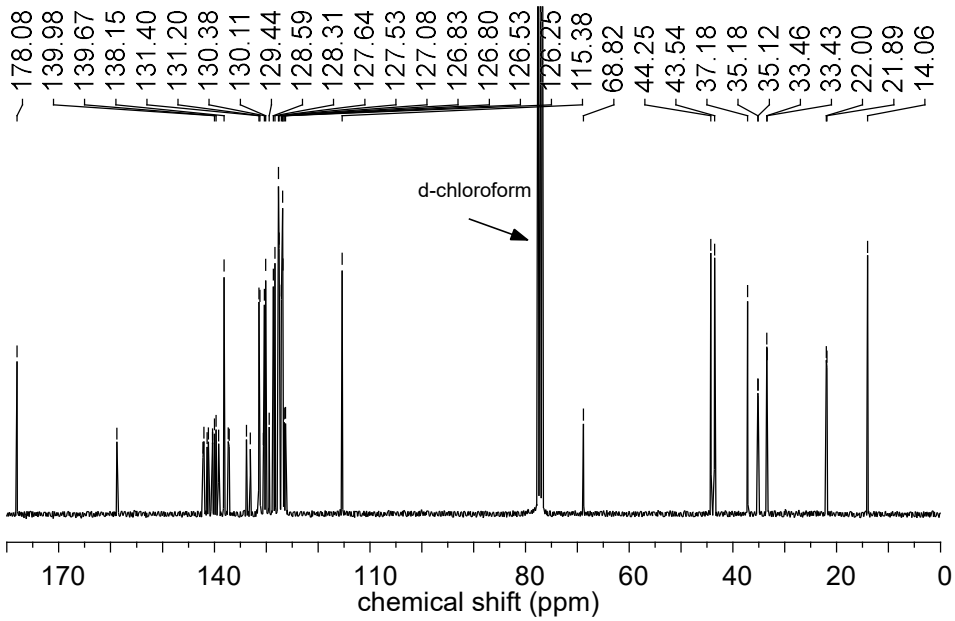

^{1}H: S3.7

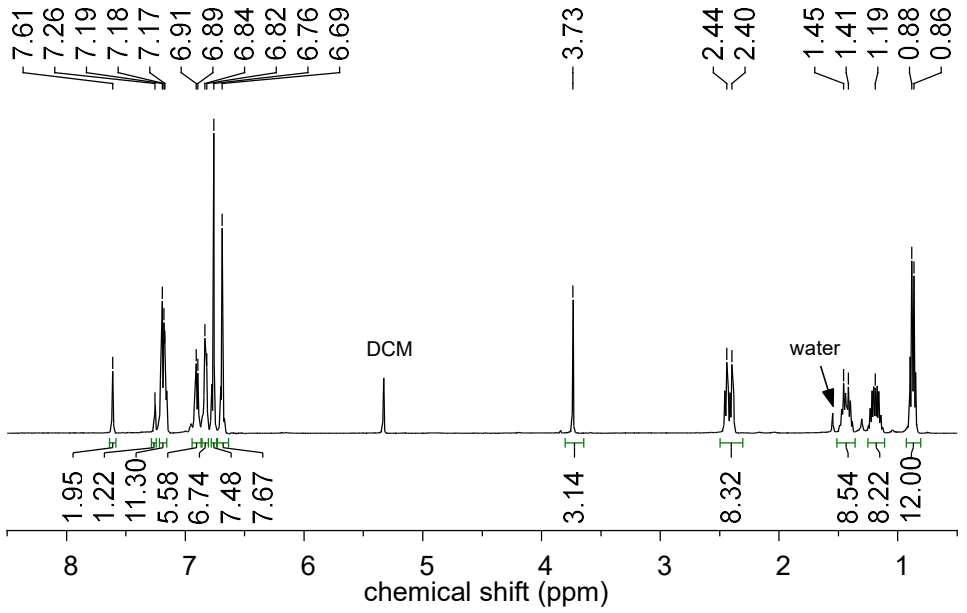

^{13}C: S3.7

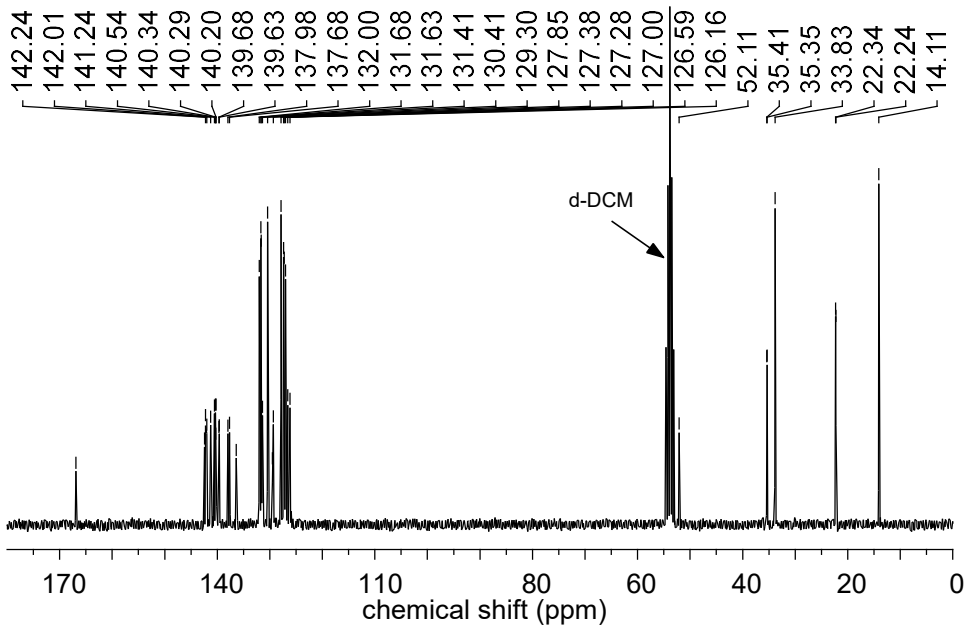

^{1}H: S3.8

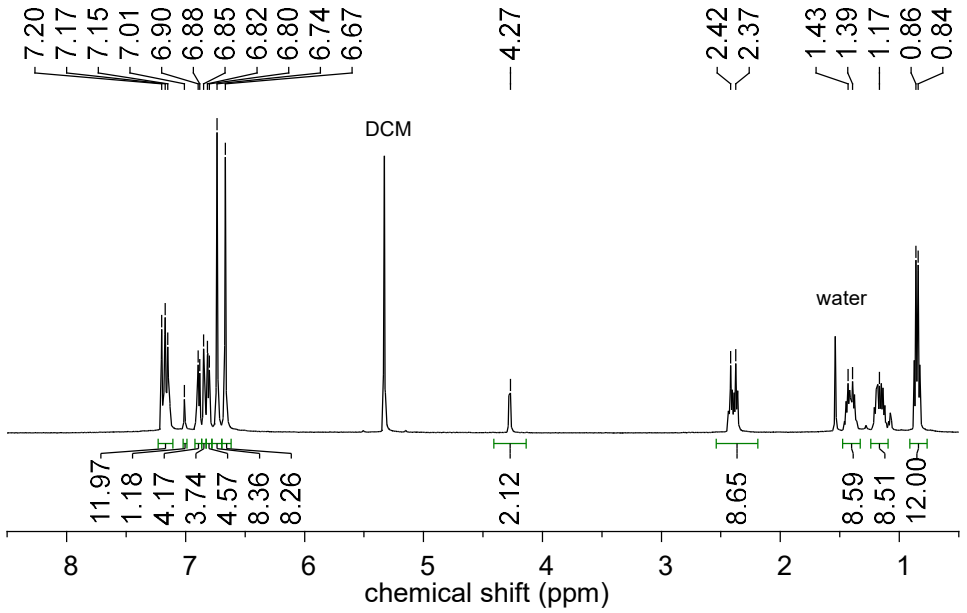

^{13}C: S3.8

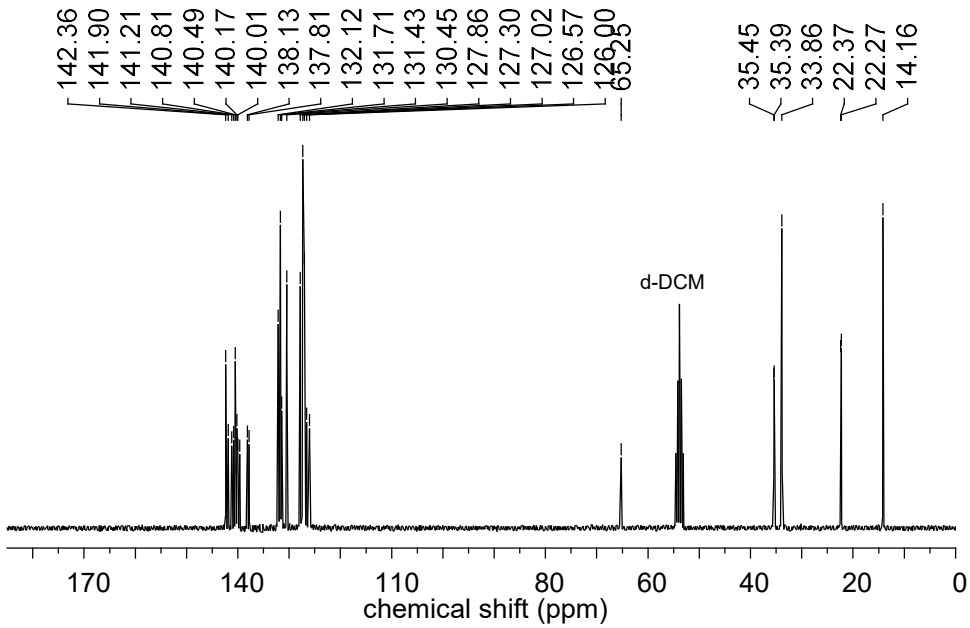

^{1}H: S3.9

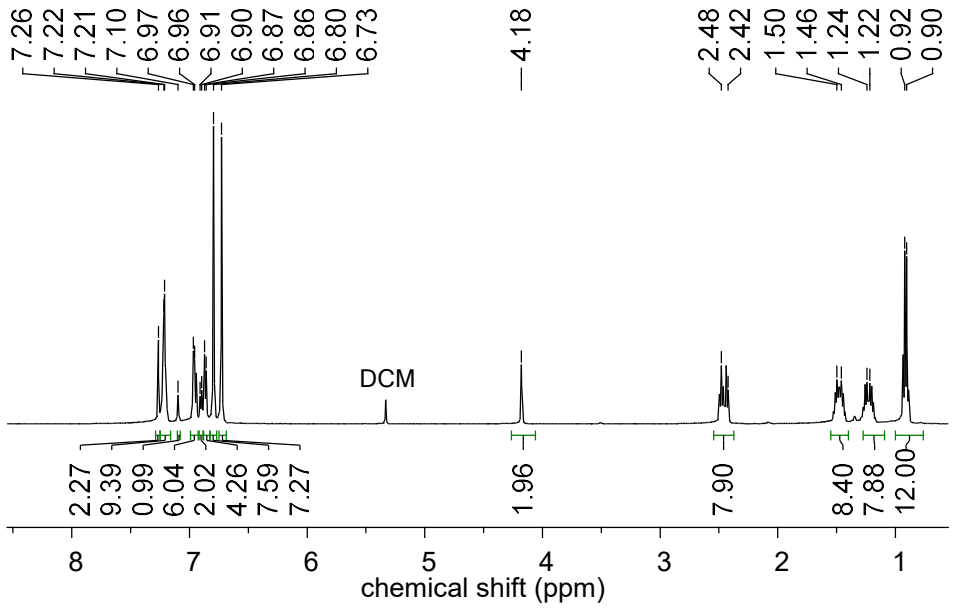

^{13}C: S3.9

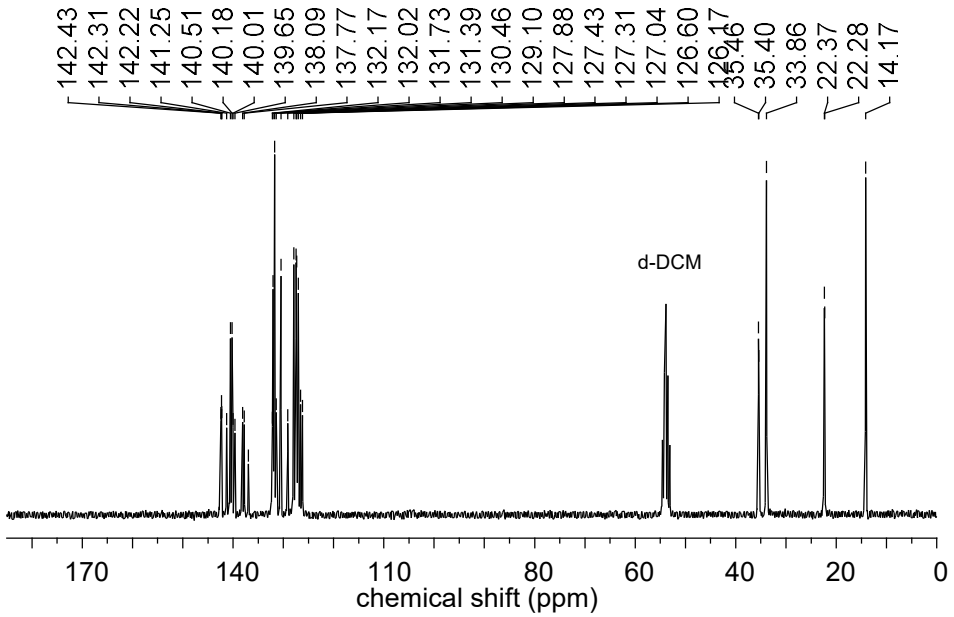

^{1}H: TD-G1

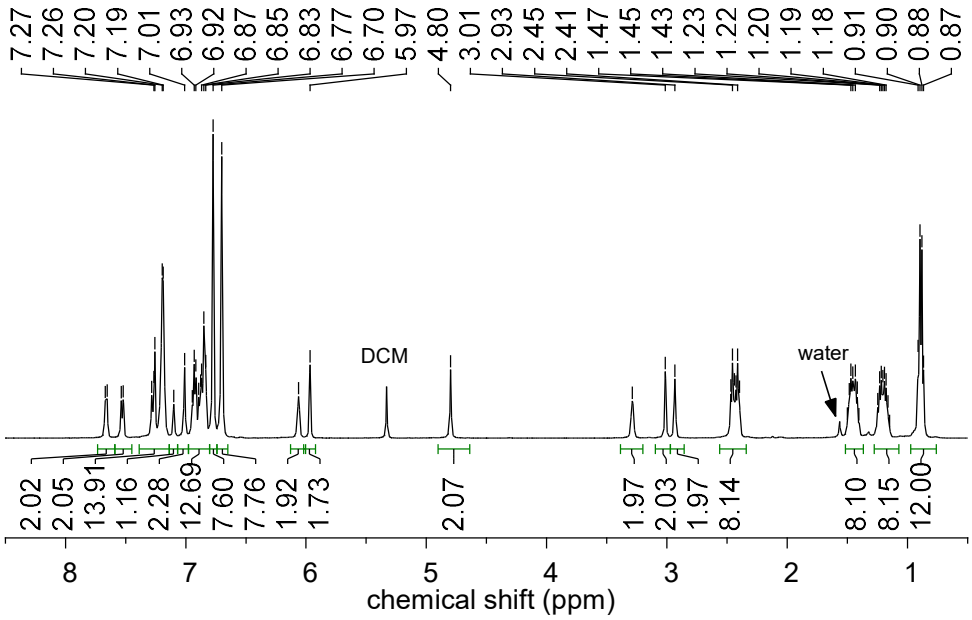

^{13}C: TD-G1

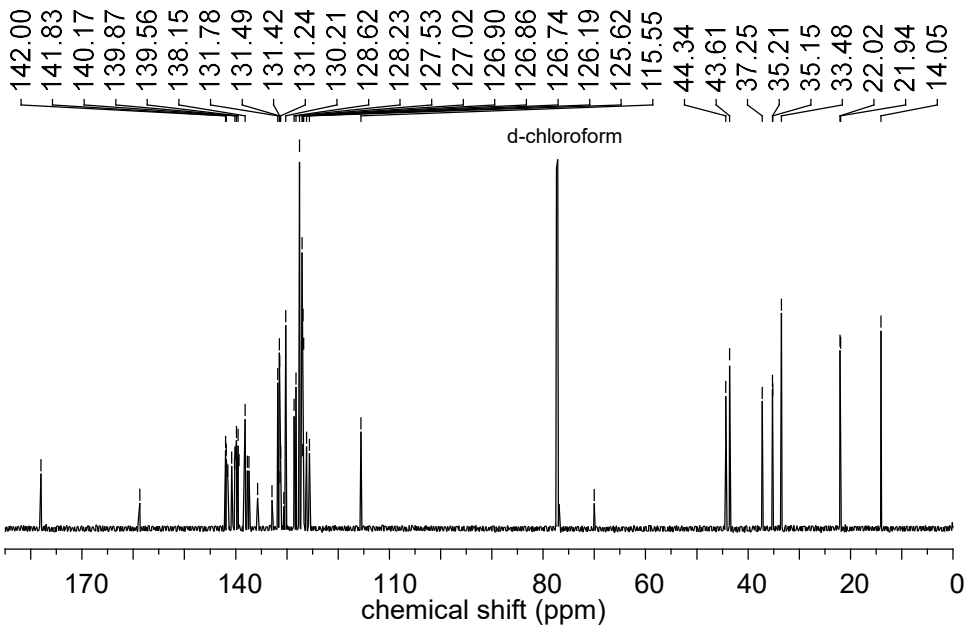

^{1}H: S3.11

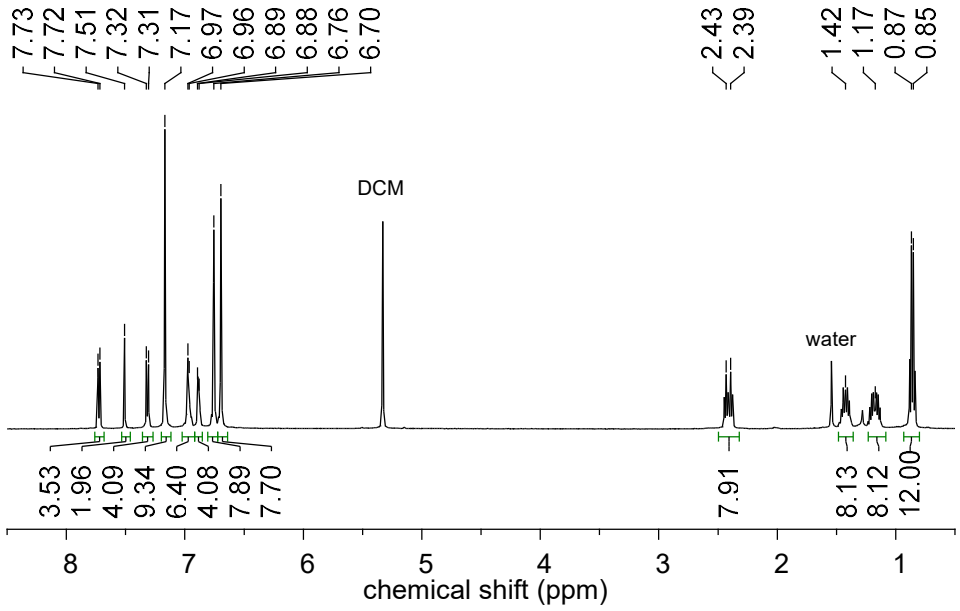

^{13}C: S3.11

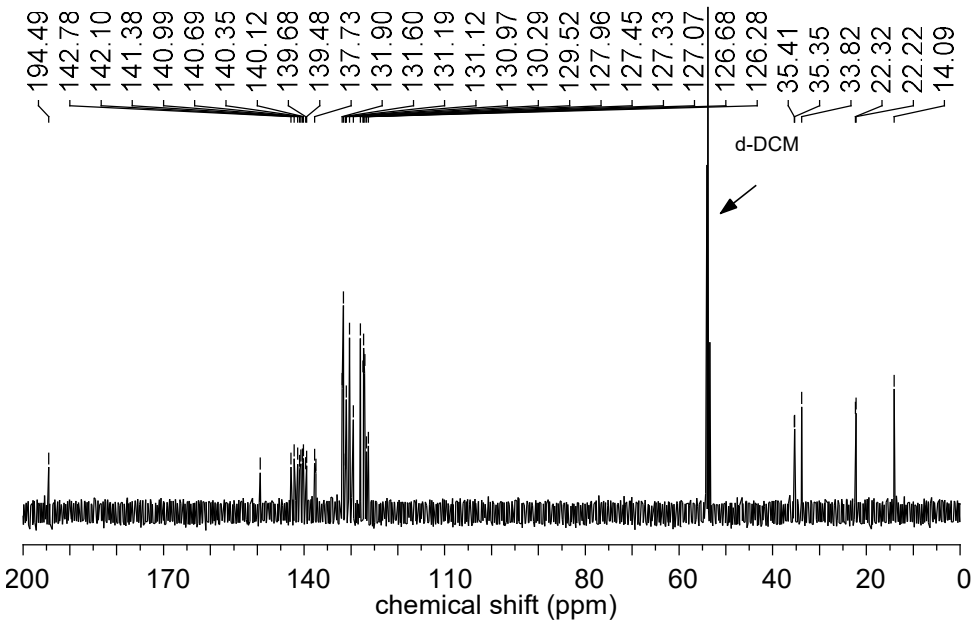

^{1}H: S3.12

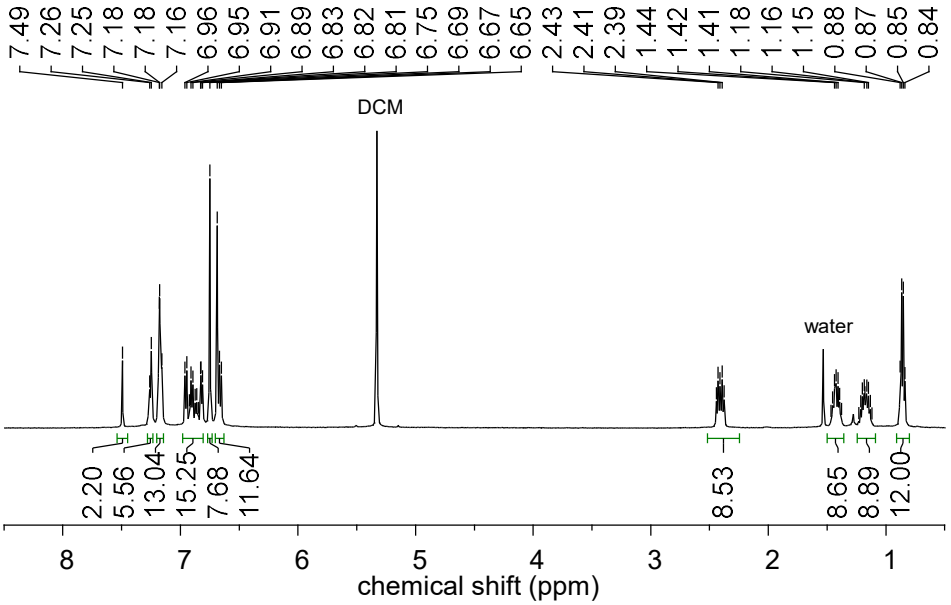

^{13}C: S3.12

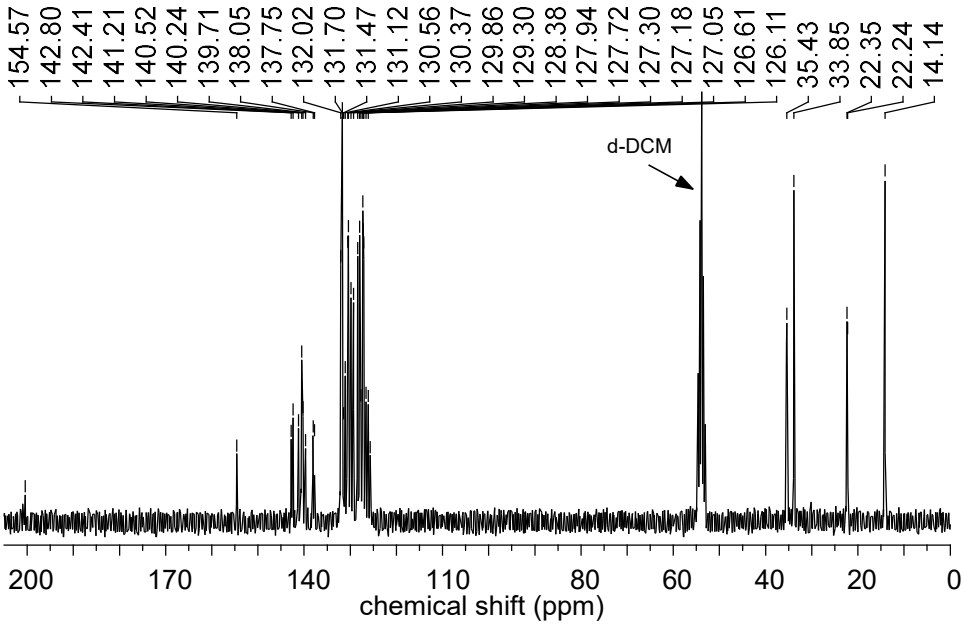

^{1}H: S3.13

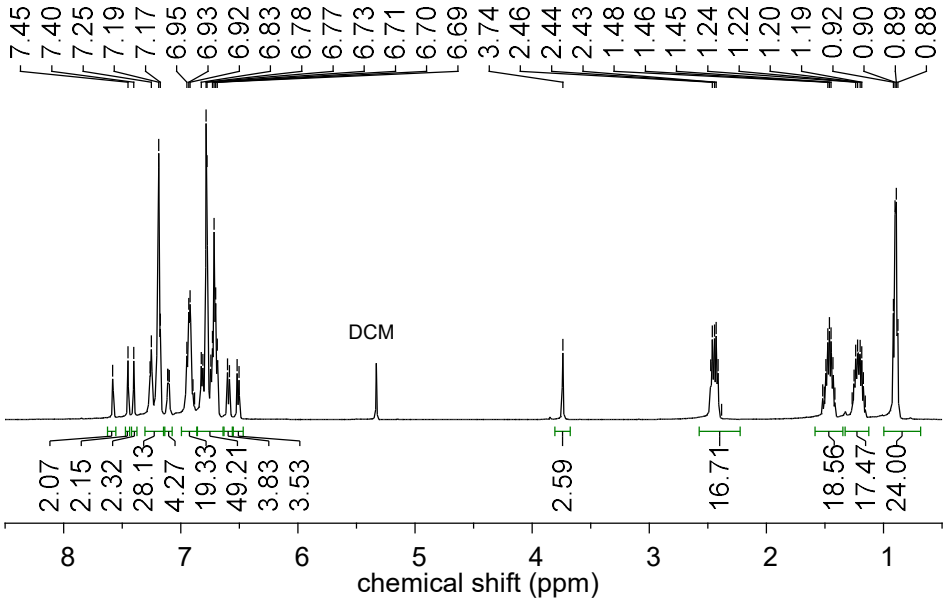

^{13}C: S3.13

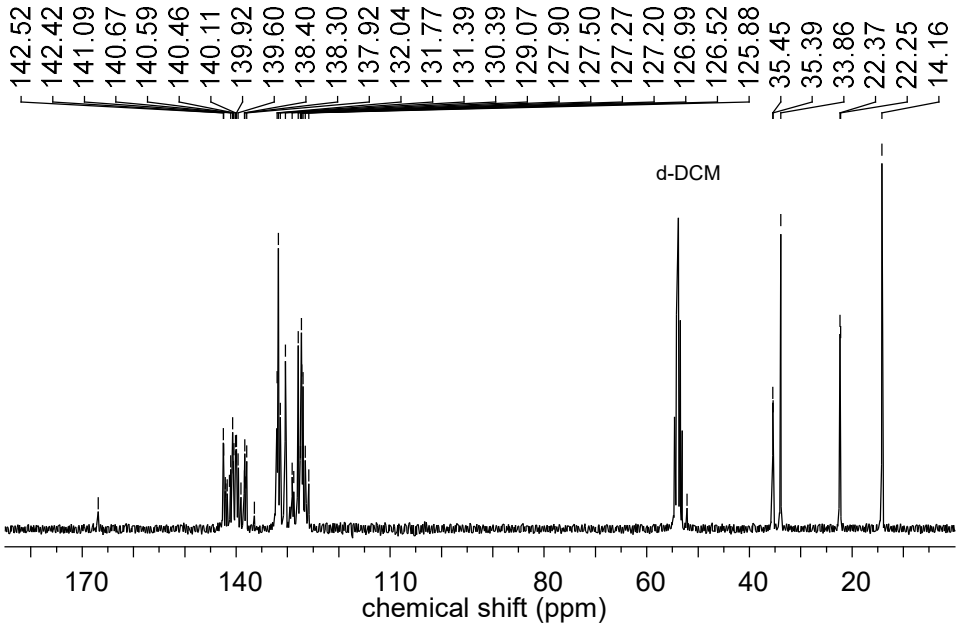

^{1}H: S3.14

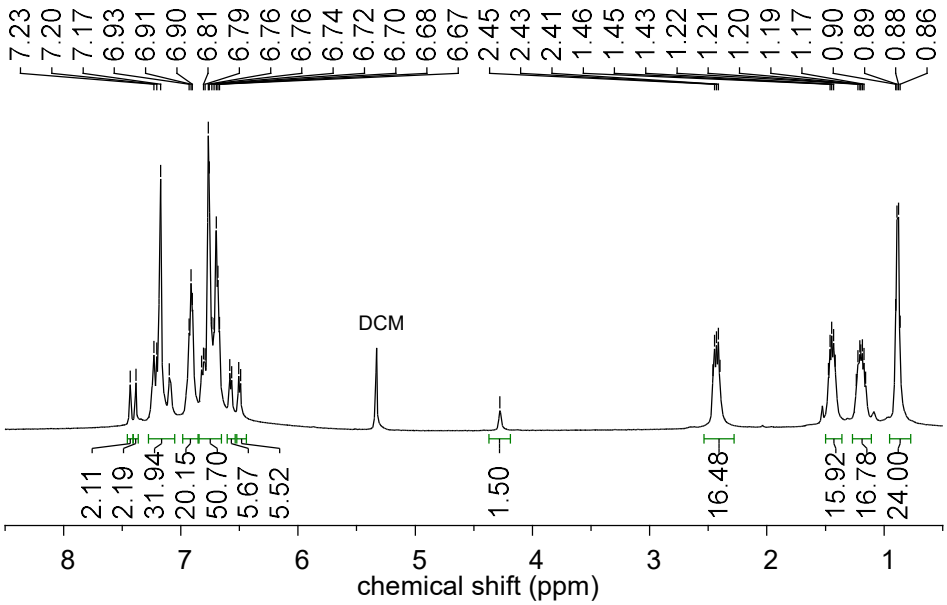

^{13}C: S3.14

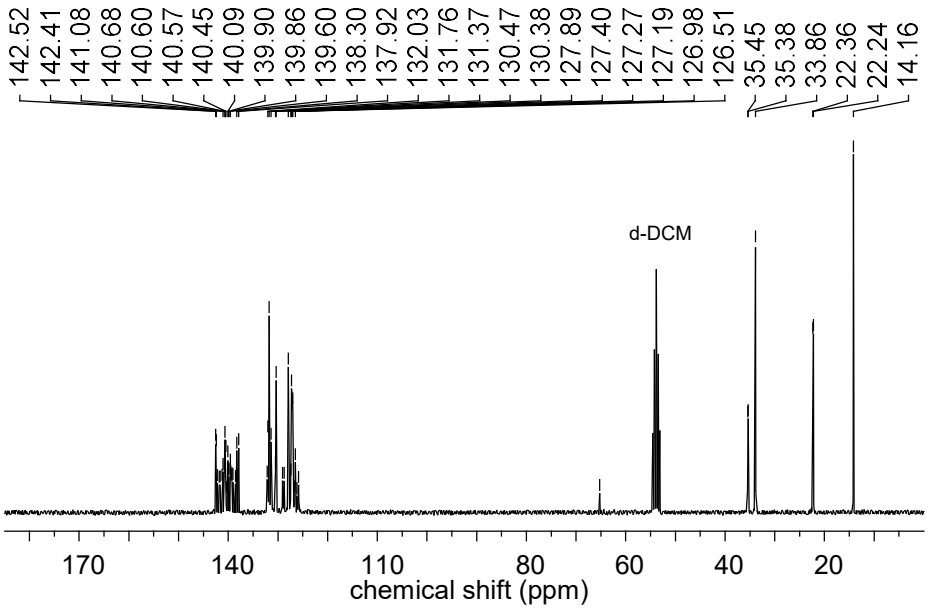

^{1}H: S3.15

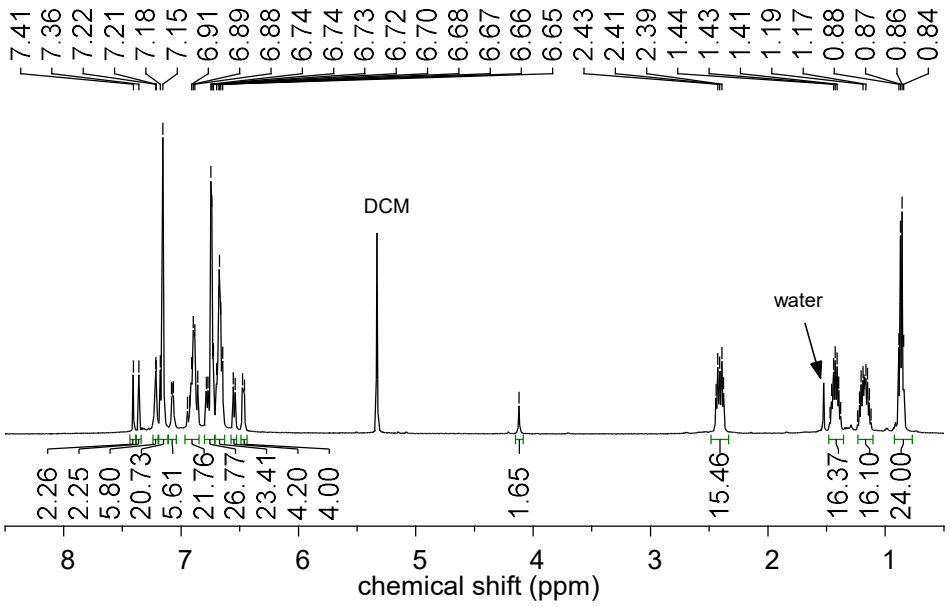

^{13}C: S3.15

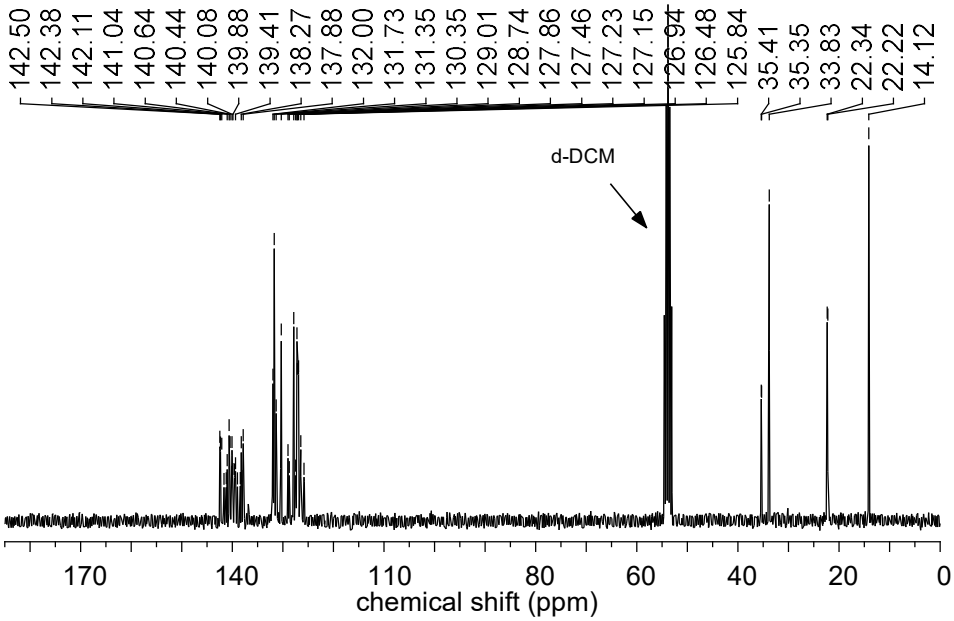

^{1}H: TD-G2

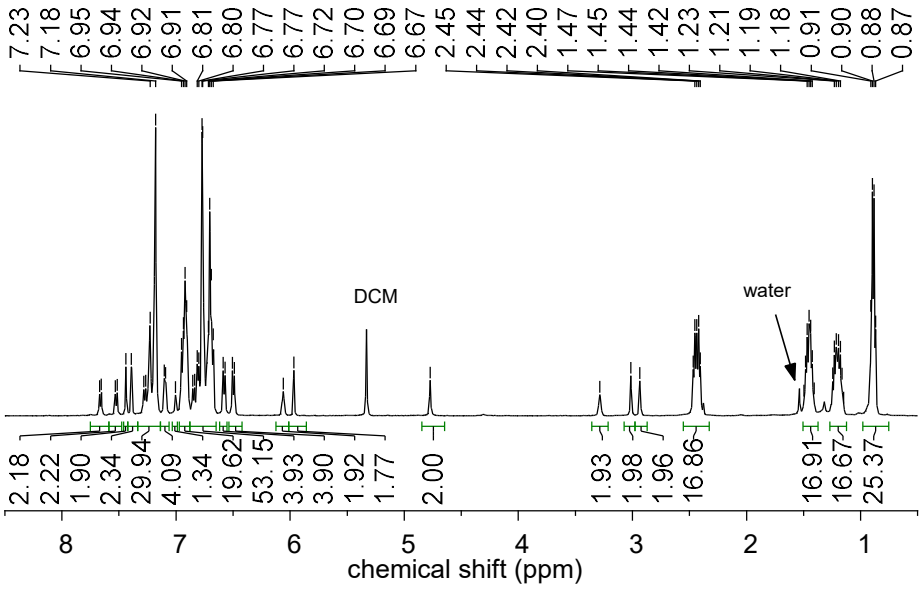

^{13}C: TD-G2

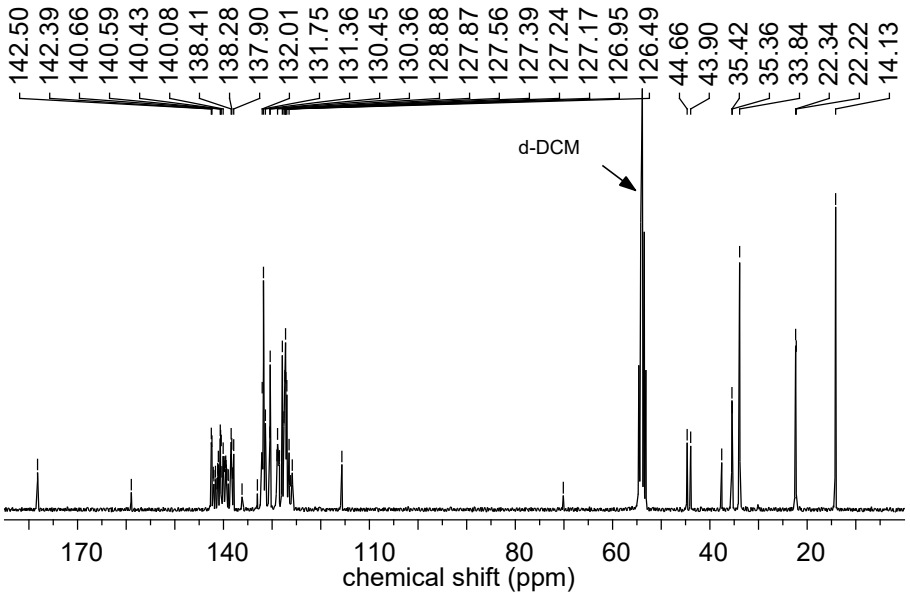

^{1}H: TD-OD

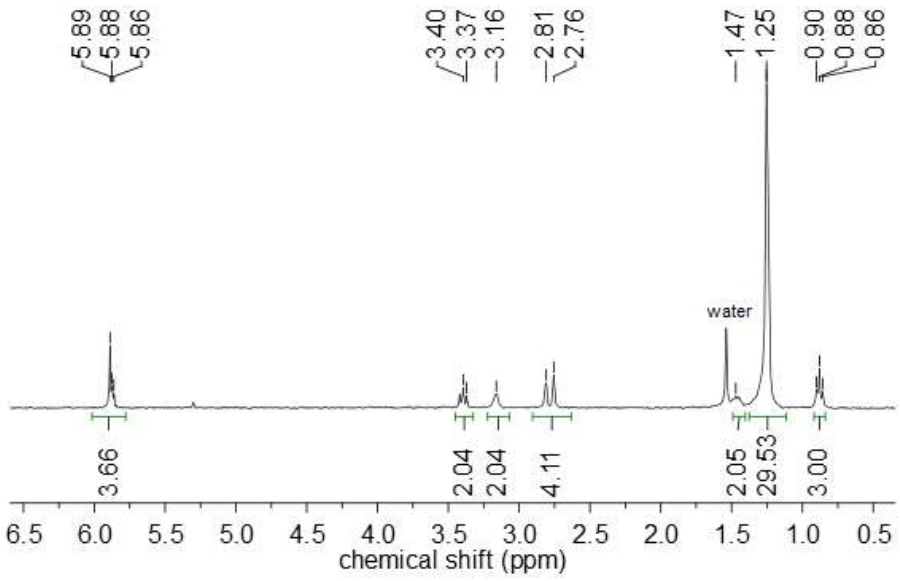

^{13}C: TD-OD

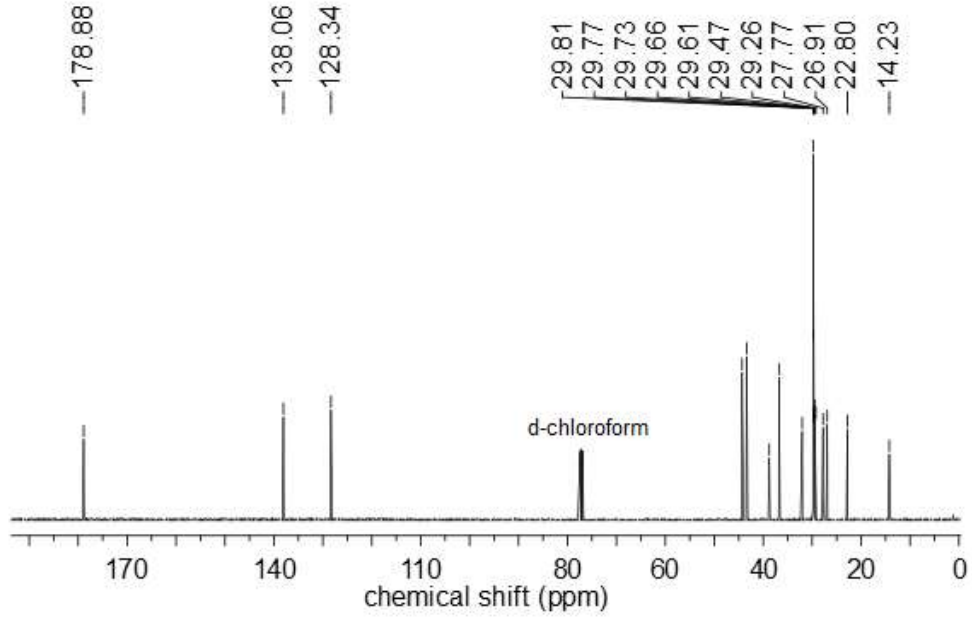

^{1}H: PTD-G0

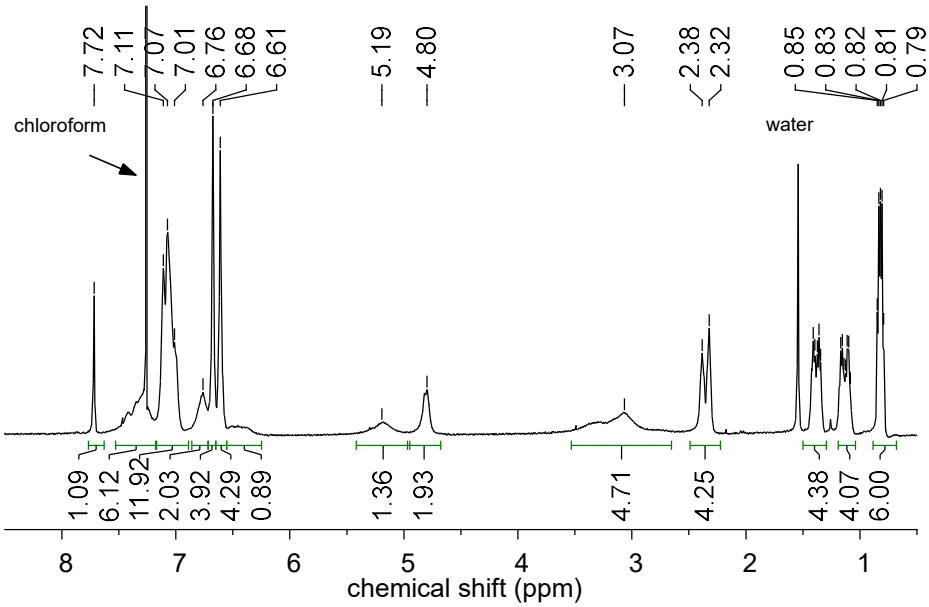

^{1}H: PTD-G1

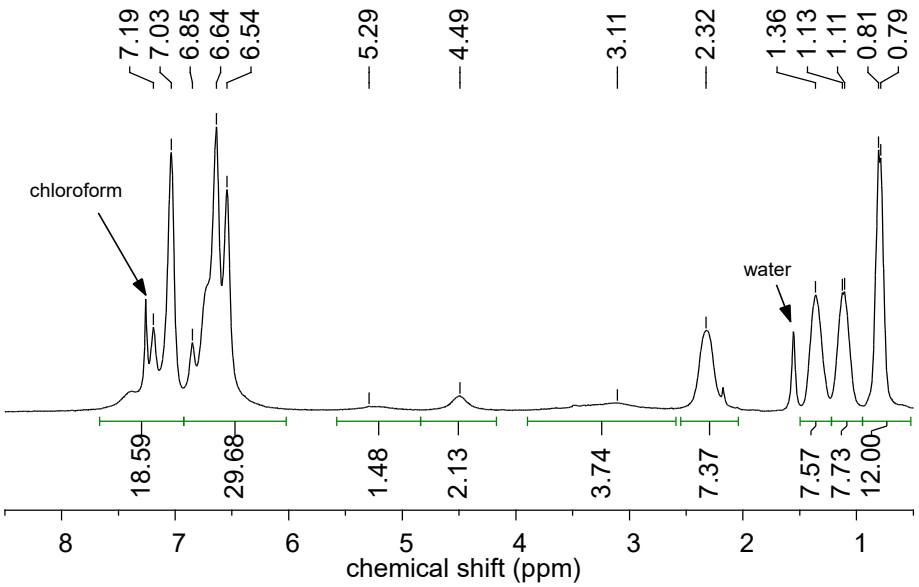

^{1}H: PTD-G2

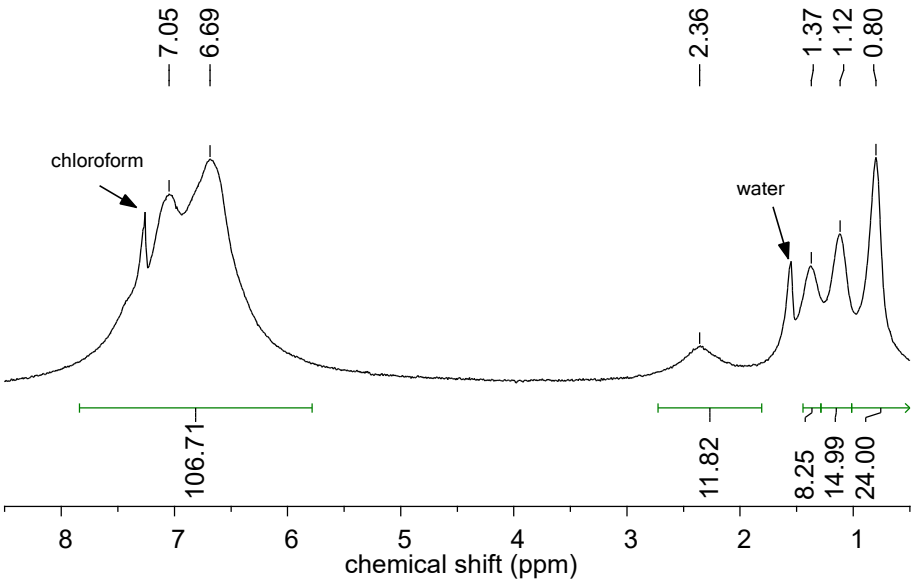

^{1}H: PTD-OD

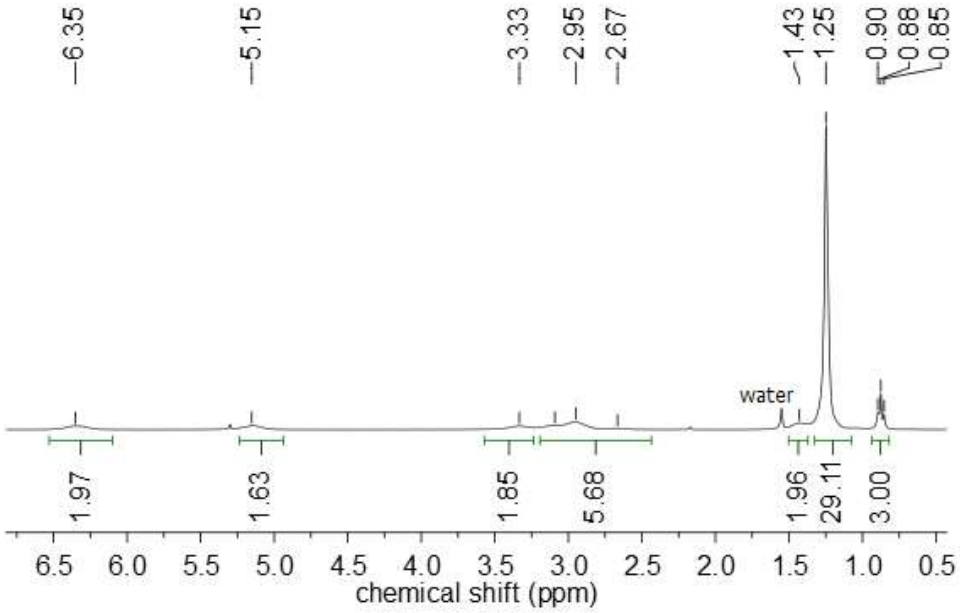

3.6 References

(1) Hammer, B. A. G.; Moritz, R.; Stangenberg, R.; Baumgarten, M.; Mullen, K. *Chemical Society Reviews* **2015**, *44*, 4072.

(2) Kim, H.; Bang, K.-T.; Choi, I.; Lee, J.-K.; Choi, T.-L. *Journal of the American Chemical Society* **2016**, *138*, 8612.

(3) Setayesh, S.; Grimsdale, A. C.; Weil, T.; Enkelmann, V.; Müllen, K.; Meghdadi, F.; List, E. J. W.; Leising, G. *Journal of the American Chemical Society* **2001**, *123*, 946.

(4) Dutertre, F.; Bang, K.-T.; Loppinet, B.; Choi, I.; Choi, T.-L.; Fytas, G. *Macromolecules* **2016**, *49*, 2731.

(5) Kim, K. O.; Choi, T.-L. *Macromolecules* **2013**, *46*, 5905.

(6) Caruso, M. M.; Davis, D. A.; Shen, Q.; Odom, S. A.; Sottos, N. R.; White, S. R.; Moore, J. S. *Chemical Reviews* **2009**, *109*, 5755.

(7) Peterson, G. I.; Larsen, M. B.; Ganter, M. A.; Storti, D. W.; Boydston, A. J. *ACS Applied Materials & Interfaces* **2015**, *7*, 577.

(8) Ramirez, A. L. B.; Kean, Z. S.; Orlicki, J. A.; Champhekar, M.; Elsakr, S. M.; Krause, W. E.; Craig, S. L. *Nat Chem* **2013**, *5*, 757.

(9) Chen, Z.; Mercer, J. A. M.; Zhu, X.; Romaniuk, J. A. H.; Pfattner, R.; Cegelski, L.; Martinez, T. J.; Burns, N. Z.; Xia, Y. *Science* **2017**, *357*, 475.

(10) Thomas, J. R. *The Journal of Physical Chemistry* **1959**, *63*, 1725.

(11) Malhotra, S. L. *Journal of Macromolecular Science: Part A - Chemistry* **1986**, *23*, 729.

(12) Daraboina, N.; Madras, G. *Ultrasonics Sonochemistry* **2009**, *16*, 273.

(13) May, P. A.; Munaretto, N. F.; Hamoy, M. B.; Robb, M. J.; Moore, J. S. *ACS Macro Letters* **2016**, *5*, 177.
(14) Li, Y.; Niu, Z.; Burdyńska, J.; Nese, A.; Zhou, Y.; Kean, Z. S.; Dobrynin, A. V.; Matyjaszewski, K.; Craig, S. L.; Sheiko, S. S. *Polymer* **2016**, *84*, 178.
(15) Kim, K. O.; Choi, T.-L. *ACS Macro Letters* **2012**, *1*, 445.
(16) Kang, E.-H.; Lee, I. S.; Choi, T.-L. *Journal of the American Chemical Society* **2011**, *133*, 11904.
(17) Jung, K.; Kim, K.; Sung, J.-C.; Ahmed, T. S.; Hong, S. H.; Grubbs, R. H.; Choi, T.-L. *Macromolecules* **2018**.
(18) Kang, E.-H.; Yu, S. Y.; Lee, I. S.; Park, S. E.; Choi, T.-L. *Journal of the American Chemical Society* **2014**, *136*, 10508.
(19) Kang, C.; Kang, E.-H.; Choi, T.-L. *Macromolecules* **2017**, *50*, 3153.
(20) Ki-Young, Y.; Suyong, S.; Yong-Jae, K.; Inhye, K.; Eunji, L.; Tae-Lim, C. *Macromolecular Rapid Communications* **2015**, *36*, 1069.
(21) Florea, M. *Journal of Applied Polymer Science* **1993**, *50*, 2039.
(22) Church, D. C.; Peterson, G. I.; Boydston, A. J. *ACS Macro Letters* **2014**, *3*, 648.
(23) Gostl, R.; Sijbesma, R. P. *Chemical Science* **2016**, *7*, 370.
(24) Schaefer, M.; Icli, B.; Weder, C.; Lattuada, M.; Kilbinger, A. F. M.; Simon, Y. C. *Macromolecules* **2016**, *49*, 1630.
(25) Cotton, J. P.; Decker, D.; Benoit, H.; Farnoux, B.; Higgins, J.; Jannink, G.; Ober, R.; Picot, C.; des Cloizeaux, J. *Macromolecules* **1974**, *7*, 863.
(26) Ouali, N.; Méry, S.; Skoulios, A.; Noirez, L. *Macromolecules* **2000**, *33*, 6185.

(27) Li, J.; Hu, B.; Hu, G.; Li, X.; Lu, P.; Wang, Y. *Organic & Biomolecular Chemistry* **2012**, *10*, 8848.
(28) Förster, B.; Bertran, J.; Teixidor, F.; Viñas, C. *Journal of Organometallic Chemistry* **1999**, *587*, 67.
(29) Weil, T.; Wiesler, U. M.; Herrmann, A.; Bauer, R.; Hofkens, J.; De Schryver, F. C.; Müllen, K. *Journal of the American Chemical Society* **2001**, *123*, 8101.
(30) Stangenberg, R.; Saeed, I.; Kuan, S. L.; Baumgarten, M.; Weil, T.; Klapper, M.; Müllen, K. *Macromolecular Rapid Communications* **2014**, *35*, 152.
(31) Yoon, K.-Y.; Shin, S.; Kim, Y.-J.; Kim, I.; Lee, E.; Choi, T.-L. *Macromolecular Rapid Communications* **2015**, *36*, 1069.
(32) Potisek, S. L.; Davis, D. A.; Sottos, N. R.; White, S. R.; Moore, J. S. *Journal of the American Chemical Society* **2007**, *129*, 13808.
(33) Nikitas, P.; Pappa-Louisi, A.; Papageorgiou, A. *Journal of Chromatography A* **2001**, *912*, 13.
(34) Ying, Q.; Chu, B. *Macromolecules* **1987**, *20*, 362.
(35) Debye, P. *The Journal of Chemical Physics* **1946**, *14*, 636.

Chapter 4. Synthesis of the Defect-Free Carbon Nanodot Polymers by Controlled ROMP

4.1 Abstract

We reported the synthesis of well-defined poly(norbornene) having hexa-*peri*-hexabenzocoronene (HBC) moiety by ring-opening metathesis polymerization (ROMP). After optimization, the 3rd generation Grubbs catalyst enabled precise control of the molecular weight of the polymer with a narrow dispersity. This controlled polymerization led us to prepare the block copolymer containing HBC for the first time.

4.2 Introduction

In chapter 3, we prepared the series of the denpols having polyphenylene dendrons. It is noticed that the denpols have high soluble in organic solvents, motivating us to incorporate more challenging side groups to the backbone. We were intrigued by π-extended polycyclic aromatic hydrocarbon (PAH)[1], which is an analogue of the 'fused' polyphenylene dendron. PAHs have attracted significant attention as they are regarded as one of the smallest segments of graphene.[2] Numerous reports have been dedicated to the bottom-up synthesis of various PAHs, allowing for the precise control of their molecular structures.[3-6] They have shown great potential in the fields of nanoelectronics, spintronics, and optoelectronics.[7-12]

However, the strong π-π stacking owing to the planar structure results in poor solubility in organic solvents, which can be overcome by incorporating long and branched alkyl-chains[13] or breaking the planarity of the PAH.[14] Another method to improve the solubility is to incorporate the PAH into a polymer backbone as a pendant group, but

an additional monomer-bearing solubilizing group is necessary.[15]

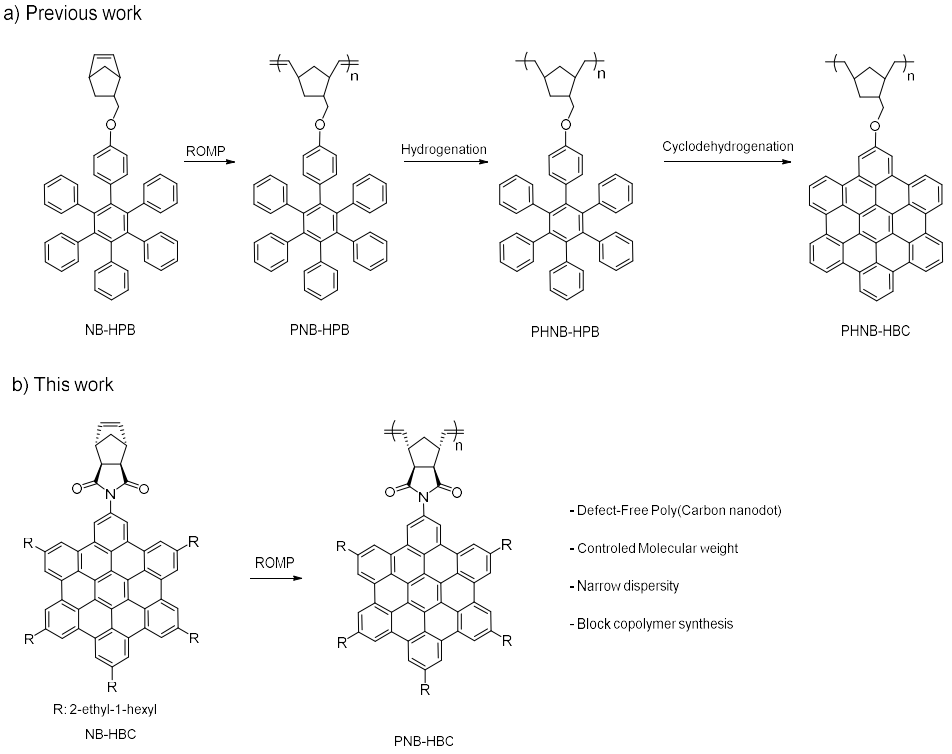

Scheme 4.1 Preparation of the polymer containing the HBC moiety.

At this point, we noticed that synthesis of the polymer with PAH groups by the controlled polymerization such as ROMP has been rarely investigated. For instance, Liaw and coworkers reported the synthesis of a polymer containing hexa-*peri*-hexabenzocoronene (HBC) by ROMP (Scheme 4.1a).[16] However, two post-modifications of the poly(norbornene) (PNB) with hexaphenylbenzene (HPB) were required. Specifically, the hydrogenation of the olefin was necessary to prevent undesired side reactions during cyclodehydrogenation with $FeCl_3$, which converted the HPB precursor to the final HBC. Moreover, the controlled polymerization of PNB containing a PAH has not been reported to date. Therefore, the simple and direct preparation of a

polymer containing HBC via controlled polymerization is desirable. Herein, we report the controlled synthesis of a well-defined carbon nanodot polymer (Scheme 4.1b) via the direct polymerization of a defect-free HBC without post-modification. Using the highly active 3rd generation Grubbs catalyst, we could control the molecular weight of the polymers with narrow dispersities by varying the monomer to initiator ratio (M/I) and prepare a block copolymer containing HBC moieties for the first time.

4.3 Result and Discussion

Scheme 4.2 Synthesis of the macromonomer

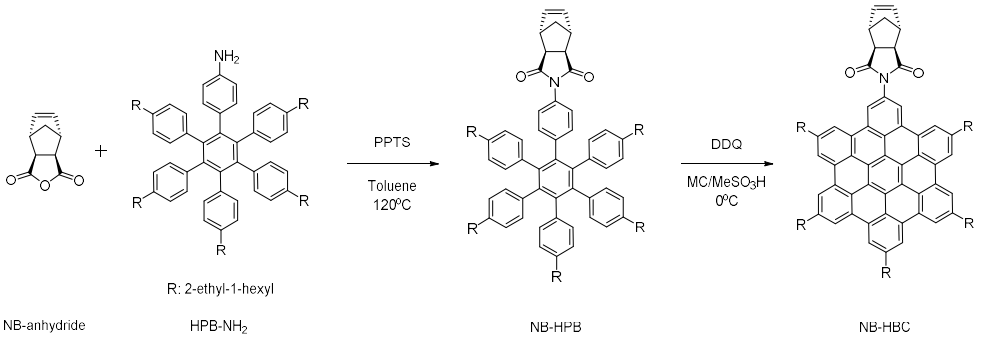

To synthesize defect-free carbon nanodot polymers, we designed a novel NB monomer containing a hexabenzocoronene (HBC) moiety (Scheme 2) because the release of the high ring strain by a highly active ruthenium catalyst could afford a defect-free polymer. A symmetrical NB containing an anhydride moiety (NB-anhydride) was selected to avoid the polymer regioregularity issue and the synthesis of NB-HBC is summarized in Scheme 4.2. First, pyridinium *p*-toluenesulfonate (PPTS) catalyzed imidization of NB-anhydride and HPB-NH_2 yielded NPB-HPB. Subsequently, the cyclodehydrogenation

of NB-HPB by 2,3-dichloro-5,6-dicyano-1,4-benzoquinone (DDQ) at 0 °C afforded the final monomer (NB-HBC). Each compound was characterized by NMR spectroscopy and matrix-assisted laser desorption/ionization-time of flight mass spectrometry (MALDI-TOF) to ensure a defect-free structure (see Experimental section for further details).

Scheme 4.3 ROMP of NB having a PAH.

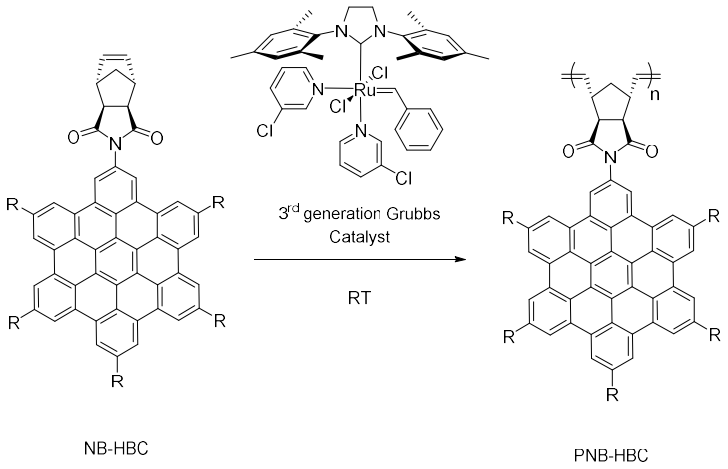

Table 4.1 Optimization of the polymerizations.

Entry	Solvent	M/I	Conc.(M)	Time(h)	Conv.(%)[a]	M_n(kDa)[b]	$Đ$ [b]
1	CF	100	0.1	2	96	116	1.36
2	CF/THF[c]	100	0.1	2	96	117	1.43
3	CF	100	0.05	2	>99	119	1.24
4	DCM	100	0.05	3	>99	141	1.38
5	CF	25	0.05	0.5	>99	32	1.17
6	CF	50	0.05	1	>99	52	1.29
7	CF	150	0.05	3	>99	164	1.37
8	CF	500	0.1	22	85	637	1.80

[a]Estimated by the relative integration of the polymer to monomer peaks. [b]Determined by SEC- MALLS in THF. [c]Volumetric ratio of CF to THF was 3 to 1.

To realize the direct polymerization of NB-HBC, ROMP was performed with a fast initiating 3rd generation Grubbs catalyst (Scheme 4.2).

Initially, we selected chloroform (CF) as a solvent since it is known to be a good solvent for HBC compounds.[17] ROMP of NB-HBC with a M/I ratio of 100 at 0.1 M afforded a polymer molecular weight (M_n) of 116 kDa with a moderate dispersity of 1.36 (Table 4.1, entry 1). To reduce this dispersity, we added a common solvent for ROMP,[18-25] THF as a co-solvent, but this increased the dispersity to 1.43 (Table 4.1, entry 2) presumably due to the strong π-π stacking of the HBC moiety, causing less ideal polymerization in the less soluble THF (Table 4.1, entry 2). To suppress the π-π interactions, we lowered the concentration to 0.05 M in CF and the polymer with a narrow dispersity of 1.24 was prepared with full consumption (Table 4.1, entry 3). We also tested dichloromethane (DCM) as an alternative solvent, but the resulting polymer showed a slightly broader dispersity of 1.38 (Table 1, entry 4). Thus, CF with a concentration of 0.05 M was the optimal condition for controlled ROMP of NB-HBC (Table 4.1, entry 3). Notably, we prepared PNB-HBC having high Mw of 637kDa, which is necessary to estimate its conformation in solution (Table 4.1, entry 8).

Scheme 4.4 Plots of M_n vs M/I ratios and the corresponding $Đ$ values.

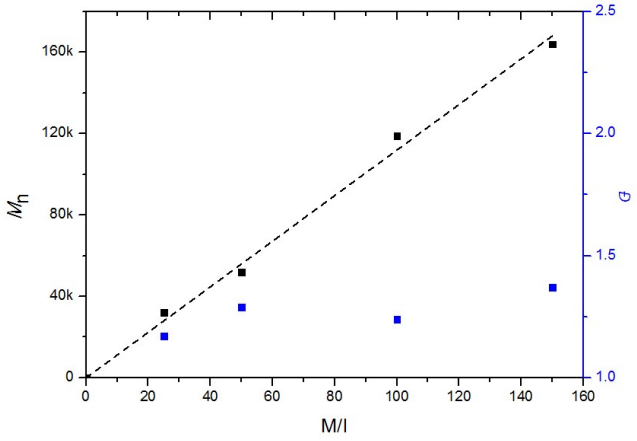

After obtaining the optimized conditions, we varied the M/I ratios from 25 to 50 to achieve the controlled polymerization of NB-HBC (Table 4.1, entries 5 and 6). The polymerizations were completed within 1 h to afford the desired polymers with narrow dispersities (M_n = 32 kDa and $Đ$ = 1.17, M_n = 52 kDa and $Đ$ = 1.29, respectively). Encouraged by these results, we increased the M/I ratio to 150, producing PNB-HBC with a M_n of 164 kDa and full consumption of the monomer (Table 4.1, entry 7). Notably, a linear increase in M_n was observed according to the M/I ratio and relatively narrow dispersity of < 1.4, demonstrating a tightly controlled polymerization (Scheme 4.4).

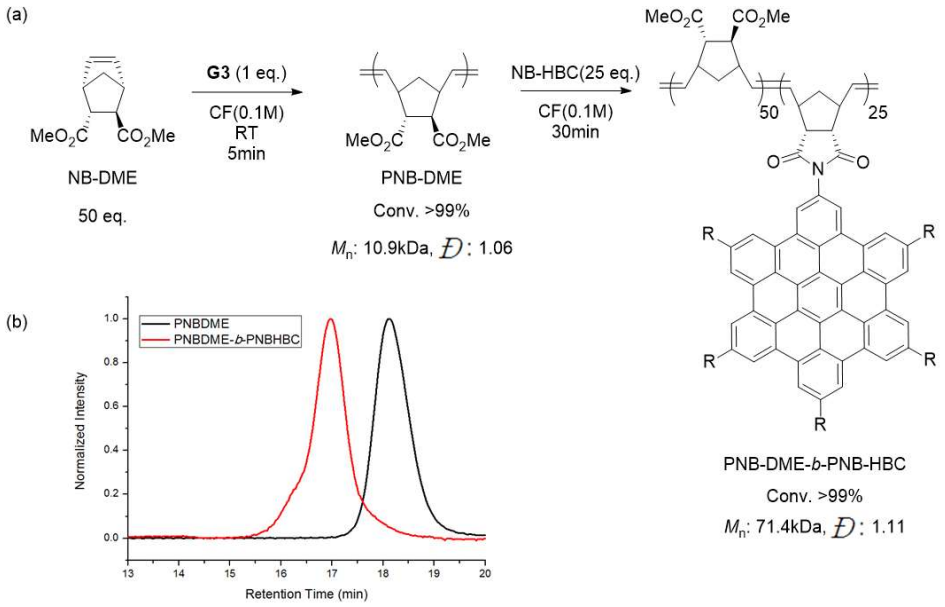

Scheme 4.5 (a) Synthesis of the block copolymer by ROMP of NB-DME and NB-HBC. (b) The corresponding SEC traces.

The successful syntheses allowed for the preparation of a block copolymer containing the HBC moiety using G3 via sequential addition of two monomers (Scheme 4.5). First, ROMP of norbornene-dimethyl ester (NB-DME) using G3 (M/I = 50/1) afforded the first block with a living chain-end. Subsequently, a solution of NB-HBC (25 eq.) was added and the full consumption of the monomer was observed after 30 min. A complete shift in the SEC trace to the high molecular weight region was observed while maintaining narrow dispersity of 1.11, indicating the successful preparation of the block copolymer. A small high molecular shoulder might arise from the bimolecular coupling.[26] Notably, the block copolymer containing an HBC unit was achieved for the first time.

Scheme 4.6 (left) Structure of PNB-EH **Table 4.2 (right)** Characteristics of polymers

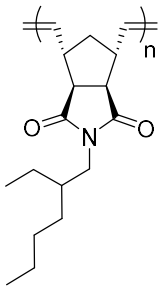

Polymer	M_n[a] (kDa)	$Đ$[a]	v[a]	l_p(nm)[b]
PNB-HBC[c]	637	1.80	0.37	2.2
PNB-EH	410	1.33	0.46	3.6

[a] Determined by SEC-MALLS in THF. [b] Obtained from SEC-MALLS data fitting using Benoit Doty equation. [c] Corresponds to entry 8, Table 4.1.

Next, we examined the chain extension of the polymer in solution. It is expected that the polymer might adapt rod-like conformation due to π-π stacking between the HBC pendants. To estimate the chain extension, flory exponent (v) and persistence length (l_p) were

estimated and compared to those of PNB-EH[24] having an alkyl chain instead of the HBC unit. However, both ν and l_p value of PNB-HBC are lower than those of PNB-EH, indicating their highly entangled conformation.

4.4. Conclusion

In conclusion, we prepared well-defined PNB containing carbon nanodots by were prepared via ROMP. Direct polymerization of NB with an HBC moiety allowed for the elimination of defects in the resulting polymer. Moreover, the use of the fast-initiator, G3, enabled the molecular weight control of the polymers ranging from 32 to 164 kDa by varying the M/I ratio while retaining a narrow dispersity of < 1.4. Furthermore, we successfully synthesized a block-copolymer containing HBC for the first time. This method provides access to defect-free carbon nanodot polymers and allows to explore their conformation in solution.

4.5 Experimental Section

General Information

^{1}H and ^{13}C NMR spectra were recorded on a Varian/Oxford As-500 (500 MHz for ^{1}H and 125 MHz for ^{13}C), Agilent 400-MR (400 MHz for ^{1}H and 100 MHz for ^{13}C) spectrometers. Chemical shifts are reported in delta (δ) units, expressed in parts per million (ppm) downfield from tetramethylsilane using the residual protio-solvent as an internal standard (CD_2Cl_2, ^{1}H: 5.33 ppm and ^{13}C 53.84 ppm). Abbreviations associated with the peak assignment are as follows: s, singlet; d, doublet; m, multiplet. The molar masses of each precursor were

measured by Bruker Microflex TOF using dithranol as a matrix. High resolution mass spectroscopy (HRMS) analyses were performed by JMS-700 (JEOL, Japan) and 6890 Series (Agilent, USA) in National Center for Inter-University Research Facilities (NCIRF). SEC setup consisted of: Waters 1515 pump, manual injector with a loop volume of 50 μL, 2 Shodex GPC LF-804 size-exclusion columns maintained at 35 ºC, DAWN-HELEOS 8+ multi-angle laser light scatter and OptiLab T-rEx refractive index detectors (each from Wyatt Technologies Corporation). The mobile phase consisted of HPLC-grade THF (inhibitor free). Molecular weights were determined from light scattering using dn/dc values calculated from batch mode measurements of polymer solutions at different concentrations. UV/Vis spectra were obtained by Jasco Inc. UV-vis Spectrometer V-650. Emission spectra were obtained by Cary Eclipse Fluorescence spectrophotometer (Varian Associates). Thermogravimetric analysis (TGA) and differential scanning calorimetry (DSC) were carried out under N^2 gas at a scan rate of 10 °C/min with Q50 and Q10 model devices, respectively, from TA Instruments.

Materials

All reagents which are commercially available from Sigma-Aldrich®, Tokyo Chemical Industry Co. Ltd., Acros Organics, Alfa Aesar®, without additional notes, were used without further purification. The catalyst[27] and NB-DME[28] were prepared according to the literatures. THF was distilled from sodium and benzophenone. The solvents for the polymerization were degassed by three freeze-pump-thaw cycles. DCM-d^2 (99.90% D, 0.75mL) was purchased from Euriso-top® and

used without further purification.

Synthesis of NB-HBC

General procedure for the Grignard reagent

Mg (84 mmol, 1 eq.) was suspended in THF (42 ml) under Ar atmosphere and heated to 70 ºC for 30min. Then, 2-ethyl-1-hexyl bromide (84 mmol, 1 eq.) was added dropwise. After 2 h, the reaction solution was cooled to RT and used for further reactions.

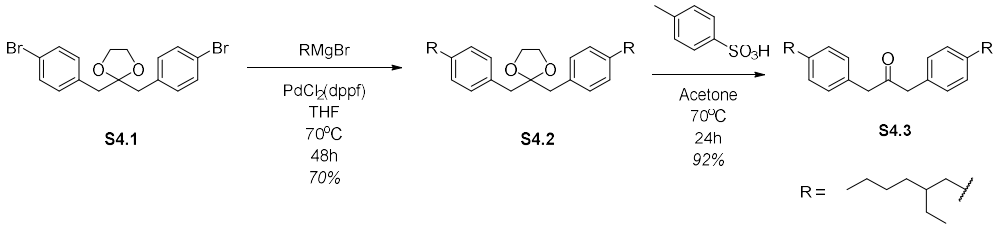

Scheme S4.1 Synthesis of S4.3

Synthesis of **S4.2**

S4.1 (21 mmol, 1 eq., prepared as previously described[29]) and [1,1-bis (diphenylphosphino)ferrocene]dichloropalladium (0.84 mmol 0.04 eq.) were dissolved in THF (100 ml) under an Ar atmosphere. Then, the Grignard solution (42 ml, 4 equiv.) was added dropwise and heated to 70 ºC. After 48h, the reaction solution was cooled to RT and quenched by excess amount of methanol. The solvent was removed under reduced pressure and the crude product was purified by flash column chromatograph on silica gel (*n*-hexane/dichloromethane = 3/1). The product was obtained in 70% yield. ^{1}H NMR (500 MHz, CD_2Cl_2, δ): 7.15 (d, *J* = 7.9 Hz, 4H), 7.06 (d, *J* = 7.9 Hz, 4H), 3.45 (s, 4H), 2.87 (s, 4H), 2.51 (d, *J* = 7.1 Hz, 4H), 1.56 (m 2H), 1.29 (m, 16H), 0.87 (m, 12H).

^{13}C NMR (125 MHz, CD_2Cl_2, δ): 140.27, 134.42, 130.91, 129.04, 111.41, 65.73, 44.49, 41.63, 40.19, 32.83, 29.31, 26.04, 23.48, 14.30, 11.05. MS (MALDI-TOF, *m/z*): $[M]^+$ calcd for $C_{33}H_{50}O_2$, 478.381; found, 478.929.

Synthesis of **S4.3**

S4.2 (14.4 mmol, 1 eq.) and *p*-toluenesulfonic acid (1.44 mmol, 0.1 eq.) were dissolved in acetone (15 ml) and stirred for 12 h at 70 ºC under an Ar atmosphere. After, the solvent was removed under reduced pressure and the crude product was purified by flash column chromatograph on silica gel (*n*-hexane/ethyl acetate = 20/1). The product was obtained in 92% yield. ^{1}H NMR (500 MHz, CD_2Cl_2, δ): 7.12 (d, *J* = 8.0 Hz, 4H), 7.05 (d, *J* = 8.0 Hz, 4H), 3.71 (s, 4H), 2.54 (m, 4H), 1.65 – 1.52 (m, 2H), 1.37 – 1.18 (m, 16H), 0.90 (t, *J* = 7.4 Hz, 12H). ^{13}C NMR (125 MHz, CD_2Cl_2, δ): 206.28, 141.11, 131.93, 129.84, 129.72, 49.15, 41.58, 40.14, 32.83, 29.32, 25.93, 23.52, 14.34, 11.02. MS (MALDI-TOF, *m/z*): $[M]^+$ calcd for $C_{31}H_{46}O$, 434.355; found, 434.261.

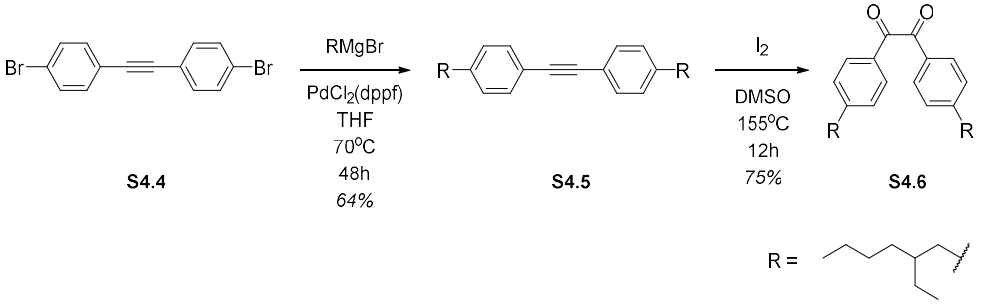

Scheme S4.2 Synthesis of S4.6

Synthesis of **S4.5**

S4.4 (7 mmol, 1 eq., prepared as previously described[29]) and [1,1-bis

(diphenylphosphino)ferrocene]dichloropalladium (0.35 mmol 0.05 eq.) were dissolved in THF (30 ml) under an Ar atmosphere. Then, the Grignard solution (10.5 ml, 3 equiv.) was added dropwise and heated to 70 ºC. After 48h, the reaction solution was cooled to RT and quenched by excess amount of methanol. The solvent was removed under reduced pressure and the crude product was purified by flash column chromatograph on silica gel (*n*-hexane). The product was obtained in 64% yield. ^{1}H NMR (500 MHz, CD_2Cl_2, δ): 7.44 (d, *J* = 8.1 Hz, 4H), 7.17 (d, *J* = 8.1 Hz, 4H), 2.57 (d, *J* = 7.1 Hz, 4H), 1.59 (m, 2H), 1.38 – 1.20 (m, 16H), 0.90 (m, 6H). ^{13}C NMR (125 MHz, CD_2Cl_2, δ): 142.98, 131.62, 129.73, 120.91, 89.29, 41.54, 40.46, 32.77, 29.26, 25.93, 23.47, 14.32, 11.00. MS (MALDI-TOF, *m/z*): $[M]^+$ calcd for $C_{30}H_{42}$, 402.329; found, 402.020.

Synthesis of S4.6

S4.5 (4.4 mmol, 1 eq.) and iodine (2.2 mmol, 0.5 eq.) were dissolved in DMSO (22 ml) and stirred for 12 h at 155 ºC under an Ar atmosphere. the reaction solution was cooled to RT and quenched by excess amount of saturated sodium thiosulfate aqueous solution. After extraction with DCM twice, the combined organic layer was dried over $MgSO_4$ and the solvent was removed under reduced pressure. The crude product was purified by flash column chromatograph on silica gel (*n*-hexane/dichloromethane = 4/1). The product was obtained in 75% yield. ^{1}H NMR (500 MHz, CD_2Cl_2, δ): 7.88 (d, *J* = 8.3 Hz, 4H), 7.33 (d, *J* = 8.2 Hz, 4H), 2.64 (d, *J* = 7.1 Hz, 4H), 1.70 – 1.59 (m, 2H), 1.40 – 1.18 (m, 16H), 0.89 (m, 12H). ^{13}C NMR (125 MHz, CD_2Cl_2, δ): 195.05, 150.83, 131.36, 130.30, 130.18, 41.54, 40.87, 32.84, 29.26, 26.00,

23.44, 14.30, 10.98. MS (MALDI-TOF, *m/z*): $[M]^+$ calcd for $C_{30}H_{42}O_2$, 434.318; found, 436.230.

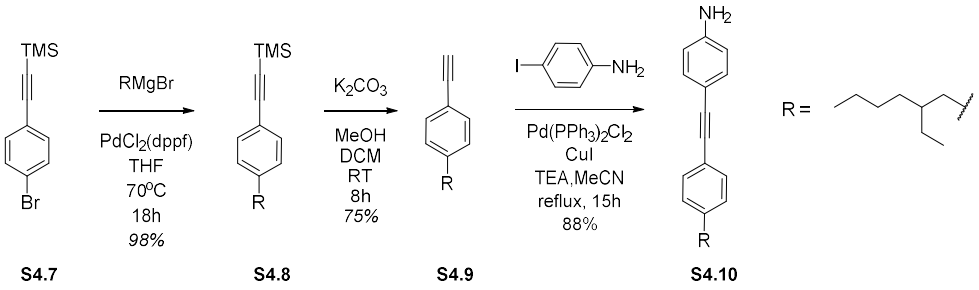

Scheme S4.3 Synthesis of S4.10

Synthesis of **S4.8**

S4.7 (8.3 mmol, 1 eq., prepared as previously described[29]) and [1,1-bis (diphenylphosphino)ferrocene]dichloropalladium (0.42 mmol 0.05 eq.) were dissolved in THF (24 ml) under an Ar atmosphere. Then, the Grignard solution (8.3 ml, 2 equiv.) was added dropwise and heated to 70 ºC. After 18h, the reaction solution was cooled to RT and quenched by excess amount of methanol. The solvent was removed under reduced pressure and the crude product was purified by flash column chromatograph on silica gel (*n*-hexane). The product was obtained in 98% yield. ^{1}H NMR (400 MHz, CD_2Cl_2, δ): 7.36 (d, *J* = 8.1 Hz, 2H), 7.12 (d, *J* = 8.1 Hz, 2H), 2.54 (d, *J* = 7.1 Hz, 2H), 1.65 – 1.48 (m, 1H), 1.38 – 1.15 (m, 8H), 0.88 (m, 6H), 0.36 – 0.17 (s, 9H). ^{13}C NMR (100 MHz, CD_2Cl_2, δ): 143.40, 131.97, 129.62, 120.62, 105.70, 93.66, 41.50, 40.44, 32.72, 29.22, 25.90, 23.45, 14.31, 10.99, 0.11. HRMS (ESI, *m/z*): $[M]^+$ calcd for $C_{19}H_{30}Si$, 286.2117; found, 286.2114.

Synthesis of **S4.9**

S4.8 (4.1 mmol, 1 eq.) and potassium carbonate (0.82 mmol, 0.2 eq.) were dissolved in DCM (10 ml) and Methanol (10 ml) and stirred for 8 h at RT under an Ar atmosphere. . After extraction with DCM twice, the combined organic layer was dried over $MgSO_4$ and the solvent was removed under reduced pressure. The crude residue was purified by flash column chromatograph on silica gel *n*-hexane). The product was obtained in 75% yield. ^{1}H NMR (500 MHz, CD_2Cl_2, δ): 7.40 (d, *J* = 8.1 Hz, 2H), 7.14 (d, *J* = 8.1 Hz, 2H), 3.09 (s, 1H), 2.55 (d, *J* = 7.1 Hz, 2H), 1.67 – 1.49 (m, 1H), 1.40 – 1.16 (m, 8H), 0.88 (m, 6H). ^{13}C NMR (125 MHz, CD_2Cl_2, δ): 143.74, 132.23, 129.69, 84.18, 76.76, 41.51, 40.46, 32.77, 29.25, 25.92, 23.45, 14.29, 10.98. HRMS (ESI, *m/z*): $[M]^+$ calcd for $C_{16}H_{22}$, 214.1722; found, 214.1722.

Synthesis of **S4.10**

S4.9 (3.1 mmol, 1 eq.), 4-iodoaniline (3.4 mmo., 1.1 eq.), copper(I) iodide (0.15 mmol, 0.05 eq.), and bis-(triphenylphosphine)palladium(II)dichloride (0.15 mmol, 0.05 eq.) were dissolved in trimethylamine (1.24ml) and acetonitrile (12.4ml) and stirred for 15 h at 80 ºC under an Ar atmosphere. . After extraction with diethyl ether twice, the combined organic layer was dried over $MgSO_4$ and the solvent was removed under reduced pressure. The crude residue was purified by flash column chromatograph on silica gel (*n*-hexane/DCM = 3/1). The product was obtained in 88% yield. ^{1}H NMR (500 MHz, CD_2Cl_2, δ): 7.40 (d, *J* = 8.2 Hz, 2H), 7.32 (d, *J* = 8.6 Hz, 2H), 7.15 (d, *J* = 8.2 Hz, 2H), 6.65 (d, *J* = 8.6 Hz, 2H), 3.91 (br, 2H), 2.56 (d, *J* = 7.1 Hz, 2H), 1.59 (m, 1H), 1.31 (m, 8H), 0.90 (m, 6H). ^{13}C NMR (125 MHz, CD_2Cl_2, δ): 147.43, 142.44, 133.16, 131.35, 129.66,

121.34, 114.97, 112.81, 89.80, 87.65, 41.51, 40.40, 32.74, 29.23, 25.89, 23.45, 14.30, 10.98. MS (MALDI-TOF, *m/z*): $[M]^+$ calcd for $C_{22}H_{27}N$, 305.214; found, 304.979.

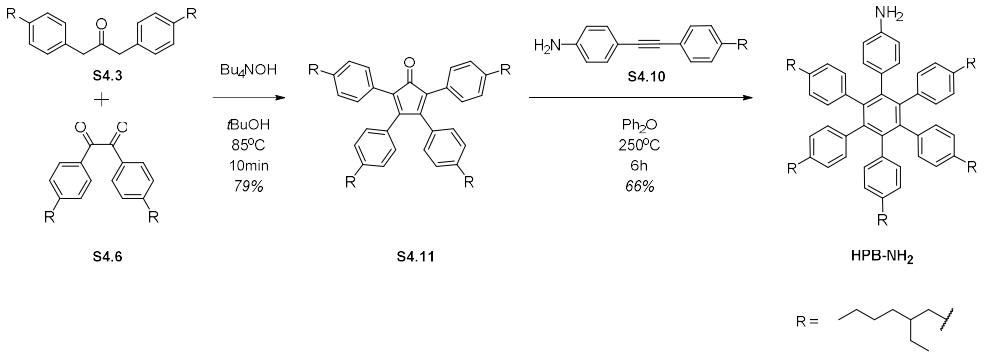

Scheme S4.4 Synthesis of **HPB-NH_2**

Synthesis of **S4.11**

S4.3 (4.73 mmol, 1 eq.) and **S4.6** (4.73 mmol, 1 eq.) were dissolved in 4.73 mL of *tert*-butanol and heated to 80 ºC for 30 min. Then, tetrabutylammonium hydroxide in methanol (1M, 3.26ml, 0.69 eq.) was added dropwise. After 1 h, the reaction solution was cooled to RT. The solvent was removed under reduced pressure and the crude product was purified by flash column chromatograph on silica gel (*n*-hexane/DCM = 3/1). The product was obtained in 79% yield. ^{1}H NMR (500 MHz, CD_2Cl_2, δ): 7.20 (d, *J* = 8.2 Hz, 4H), 7.08 (d, *J* = 8.2 Hz, 4H), 7.00 (d, *J* = 8.1 Hz, 4H), 6.87 (d, *J* = 8.1 Hz, 4H), 2.68 – 2.45 (m, 8H), 1.59 (m, 4H), 1.42 – 1.14 (m, 32H), 1.04 – 0.81 (m, 24H). ^{13}C NMR (125 MHz, CD_2Cl_2, δ): 201.49, 154.97, 142.98, 141.75, 131.36, 130.32, 129.26, 129.13, 129.07, 125.30, 41.71, 41.59, 40.65, 40.48, 32.94, 29.39, 29.37, 26.31, 26.14, 23.55, 14.41, 11.28, 11.14. MS (MALDI-TOF, *m/z*): $[M]^+$ calcd for $C_{61}H_{84}O$, 832.652; found, 833.296.

Synthesis of **HPB-NH_2**

S4.10 (3.25 mmol, 1 eq.) and **S4.11** (3.25 mmol, 1 eq.) were dissolved in 5ml of diphenyl ether and heated to 250 ºC. After 6 h, the reaction solution was cooled to RT and purified by flash column chromatograph on silica gel (*n*-hexane/DCM = 4/1). The product was obtained in 66% yield. ^{1}H NMR (400 MHz, CD_2Cl_2, δ): 6.83 – 6.50 (m, 22H), 6.18 (d, *J* = 8.2 Hz, 2H), 3.39 (s, 2H), 2.45 – 2.17 (m, 10H), 1.44 – 1.02 (m, 45H), 0.96 – 0.61 (m, 30H). ^{13}C NMR (100 MHz, CD_2Cl_2, δ): 144.07, 141.01, 140.82, 140.62, 140.50, 139.03, 138.80, 138.75, 138.73, 132.85, 131.73, 131.59, 127.71, 127.63, 113.57, 41.48, 41.40, 40.02, 32.65, 29.17, 25.68, 23.50, 14.40, 11.13, 11.05. MS (MALDI-TOF, *m/z*): $[M]^+$ calcd for $C_{82}H_{117}N$, 1109.872; found, 1109.719.

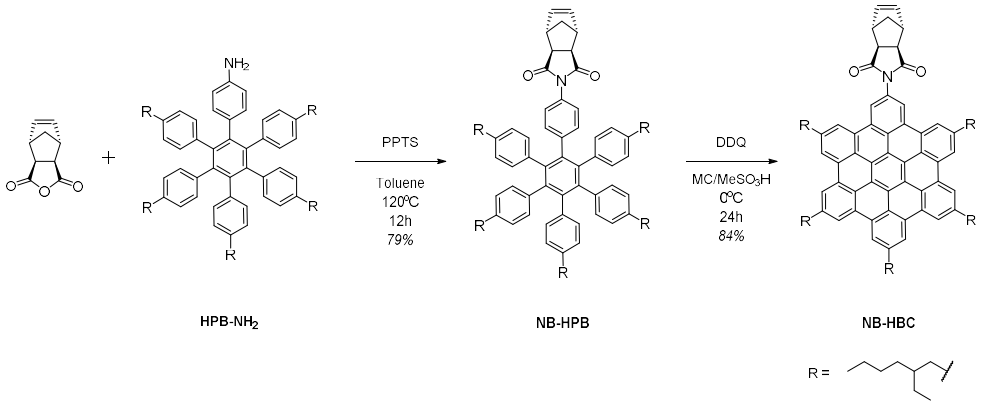

Scheme S4.5 Synthesis of NB-HBC

Synthesis of **NB-HPB**

HPB-NH_2 (0.97 mmol, 1 eq.), *cis*-5-Norbornene-*exo*-2,3-dicarboxylic anhydride (1.07 mmol, 1.1 eq.) and pyridinium p-toluenesulfonate (0.097 mmo, 0.1 eq.) were dissolved in 5ml of toluene and heated to 250 ºC. After 12 h, the reaction solution was cooled to

RT and purified by flash column chromatograph on silica gel (*n*-hexane/DCM = 1/1). The product was obtained in 79% yield. ^{1}H NMR (400 MHz, CD_2Cl_2, δ): 6.93 (d, *J* = 8.1 Hz, 2H), 6.70 (m, 22H), 6.32 (s, 2H), 3.28 (s, 2H), 2.72 (s, 2H), 2.43 – 2.17 (m, 10H), 1.55 – 1.44 (m, 2H), 1.40 – 0.97 (m, 43H), 0.87 (m, 15H), 0.83 – 0.68 (m, 15H). ^{13}C NMR (100 MHz, CD_2Cl_2, δ): 176.91, 141.85, 141.27, 141.01, 140.67, 139.49, 139.13, 138.87, 138.54, 138.48, 138.36, 138.29, 132.44, 131.62, 129.61, 128.93, 128.84, 128.66, 124.53, 48.09, 46.18, 43.25, 41.36, 41.32, 39.98, 39.85, 32.60, 29.12, 25.64, 25.45, 23.46, 23.44, 14.36, 11.01, 10.93. MS (MALDI-TOF, *m/z*): $[M]^+$ calcd for $C_{91}H_{117}NO_2$, 1255.908; found, 1255.940.

Synthesis of NB-HBC

NB-HPB (0.08 mmol, 1 eq.) and 2,3-dichloro-5,6-dicyano-*p*-benzoquinone (0.96 mmol, 12 eq.) were dissolved in 14.4ml of DCM and cooled to 0 ºC for 30 min. Then 1.6 ml of methanesulfonic acid was added. After 24 h, the reaction mixture was quenched by excess amount of water and washed by DCM twice. The solvent was removed under reduced pressure and the crude product was purified by flash column chromatograph on silica gel (*n*-hexane/DCM/ethyl acetate = 8/1/1). The product was obtained in 84% yield. ^{1}H NMR (400 MHz, CD_2Cl_2, δ): 8.83 (s, 2H), 8.56 (s, 2H), 8.42 (s, 2H), 8.36 (s, 2H), 8.32 (s, 2H), 8.25 (s, 2H), 6.61 (s, 2H), 3.74 (s, 2H), 3.26 (s, 2H), 3.17 – 2.99 (m, 6H), 2.93 (m, 4H), 2.15 (d, *J* = 10.1 Hz, 1H), 1.99 (m, 3H), 1.90 (m, 2H), 1.77 – 1.34 (m, 40H), 1.20 – 1.02 (m, 15H), 0.97 (m, 15H). ^{13}C NMR (125 MHz, CD_2Cl_2, δ): 178.05, 139.57, 139.26, 138.72, 131.49, 130.89, 129.65, 129.57, 129.53, 129.23, 129.15, 125.00, 123.20,

123.03, 122.73, 122.58, 122.32, 122.14, 119.93, 119.72, 119.46, 118.77, 49.00, 46.63, 44.06, 42.01, 41.86, 41.75, 41.70, 41.45, 33.06, 32.93, 32.82, 29.44, 29.31, 26.09, 26.03, 23.77, 23.75, 23.71, 14.55, 14.52, 11.21, 11.20, 11.15. MS (MALDI-TOF, *m/z*): $[M]^+$ calcd for $C_{91}H_{105}NO_2$, 1243.815; found, 1244.463.

General polymerization procedure

2-mL sized screw-cap vial with septum was charged with NB-HBC (c.a. 20 mg) and a magnetic bar. The vial was purged with argon four times, and a dried and degassed solvent was added purged with Ar, and then dissolved in dried and degassed solvent. The initiator solution was added at once to the monomer solution under vigorous stirring. After c.a. 2h, the polymerization was quenched with by excess ethyl vinyl ether and partally precipitated in acetone, remaining small amount of crude mixture (c.a. 2 mg). Obtained solid was filtered and dried under reduced pressure.

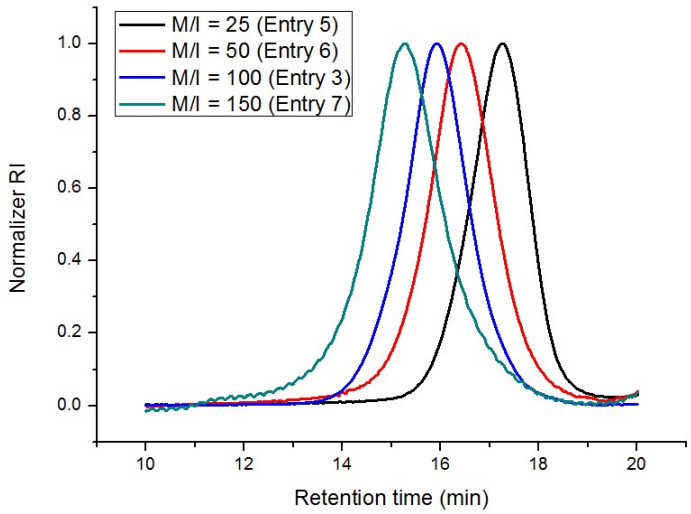

Figure S4.1 SEC traces of polymers obtained by controlled

polymerization.

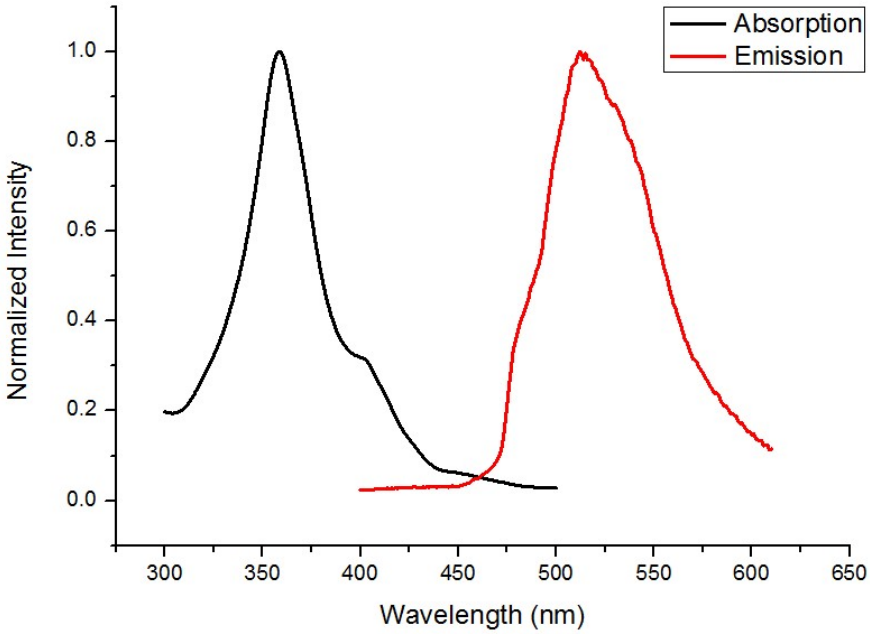

Figure S4.2 Absorption and emission spectra of PNB-HBC (M_n: 117kDa, $Đ$: 1.43) in DCM solution (10μg/ml)

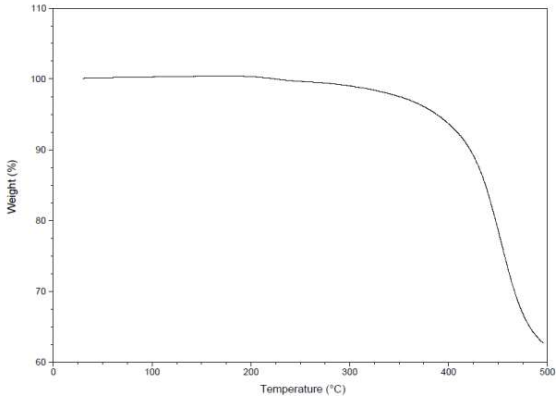

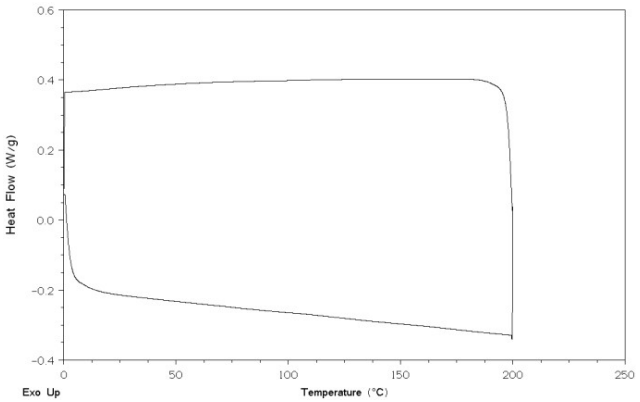

Figure S4.3 TGA (left) and DSC (right) data for PNB-HBC (M_n: 52kDa, $Đ$: 1.29)

NMR Spectra for New Compounds

^{1}H: S4.2

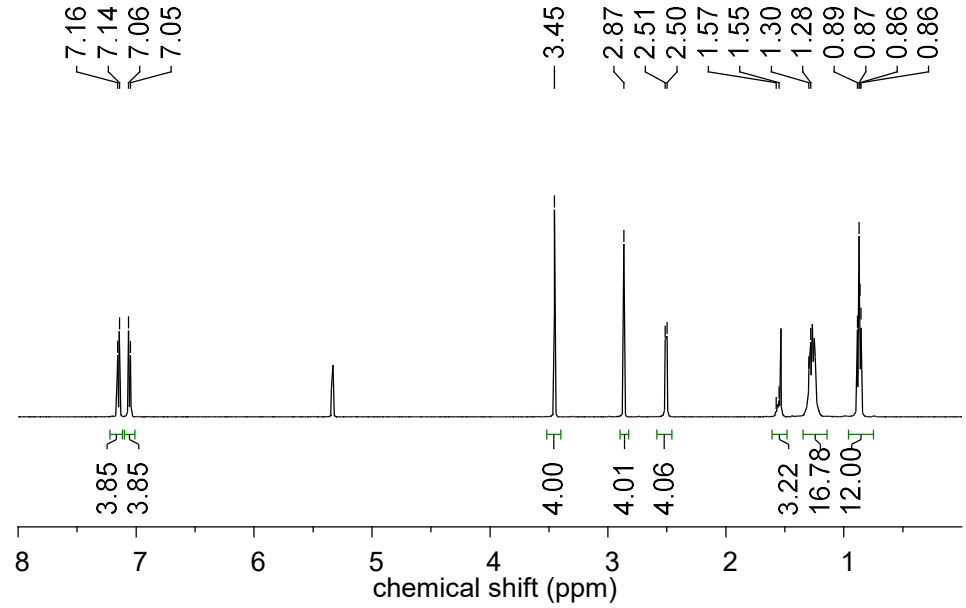

^{13}C: S4.2

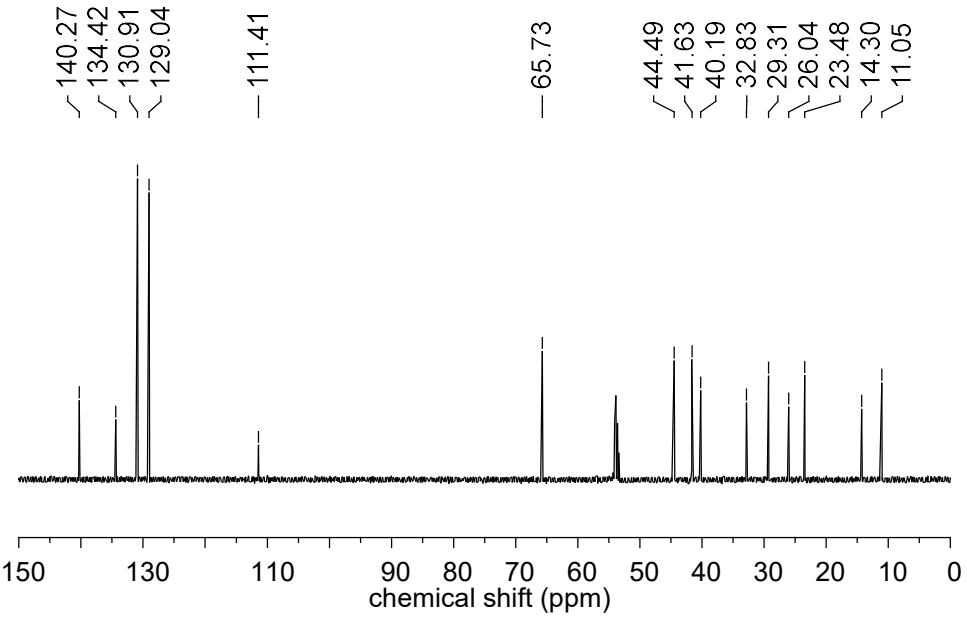

^{1}H: S4.3

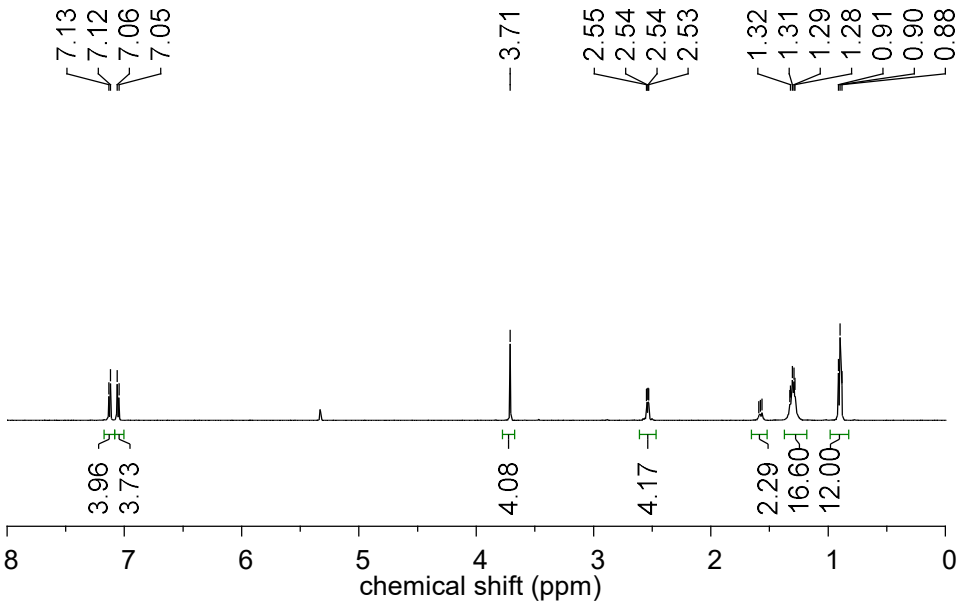

^{13}C: S4.3

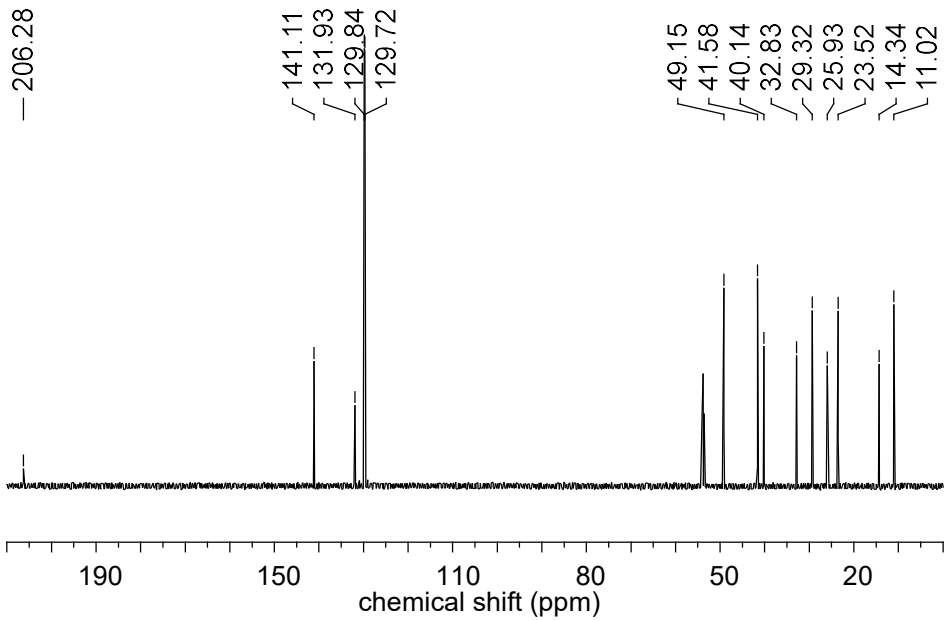

^{1}H: S4.5

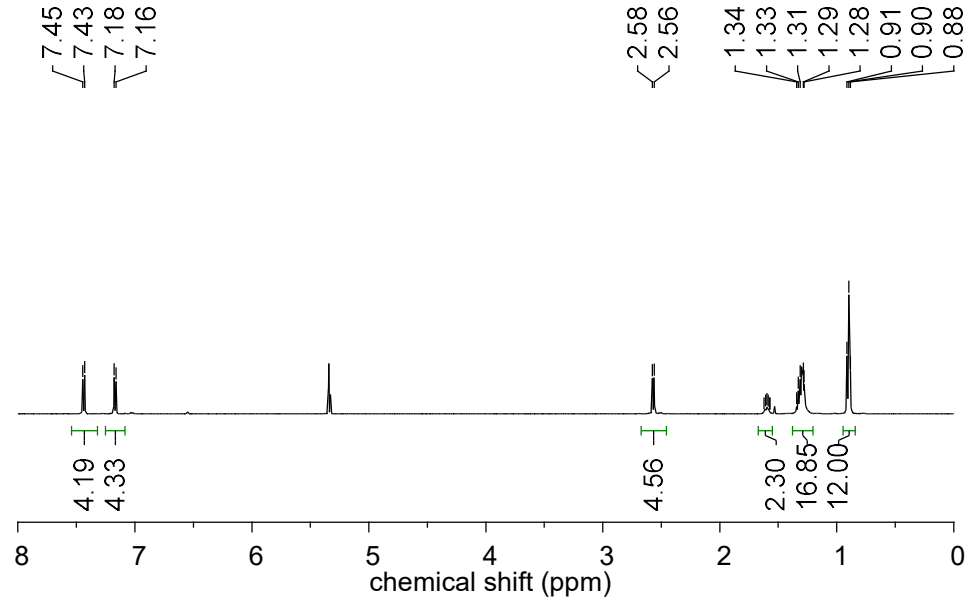

^{13}C: S4.5

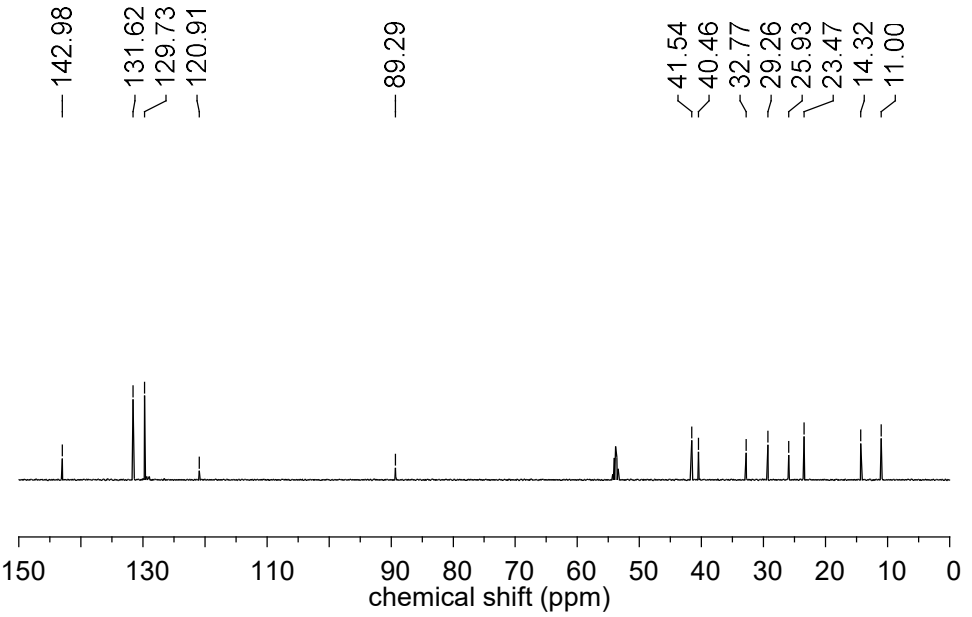

^{1}H: S4.6

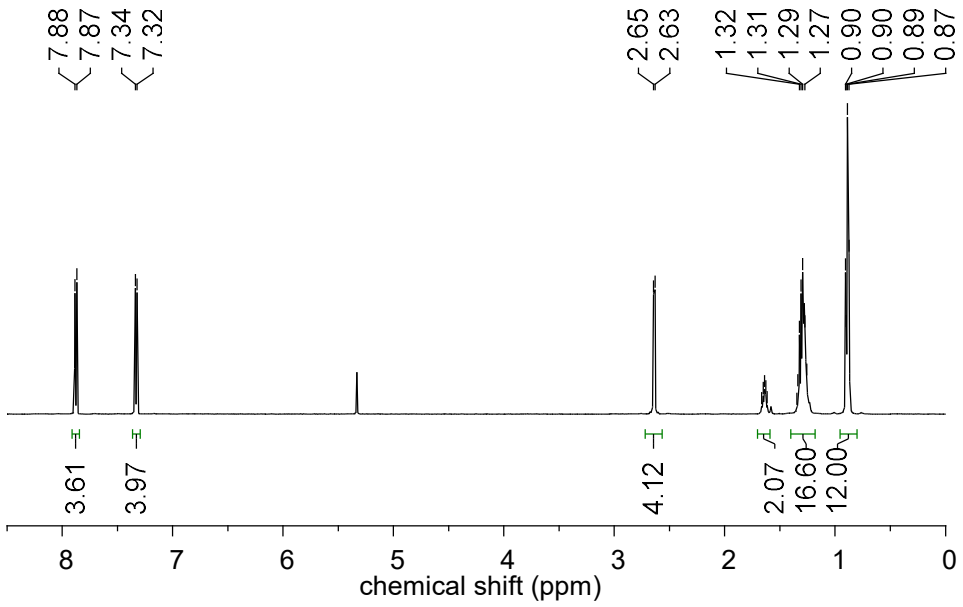

^{13}C: S4.6

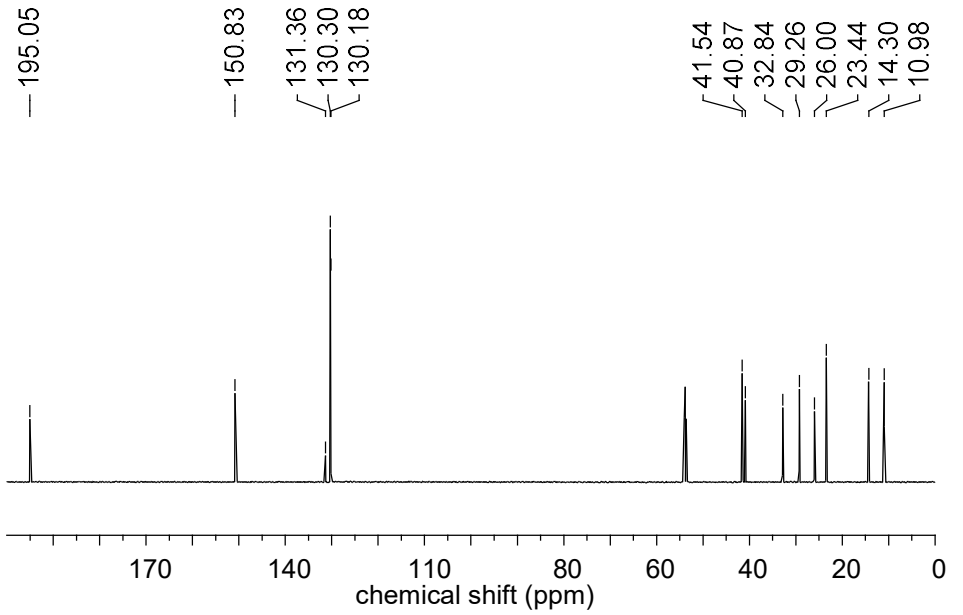

^{1}H: S4.8

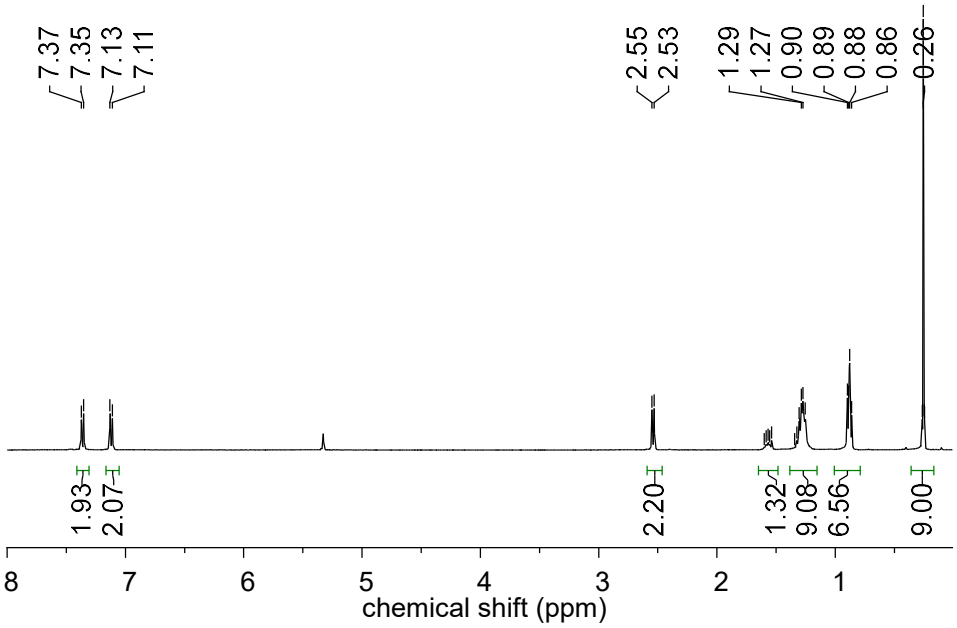

^{13}C: S4.8

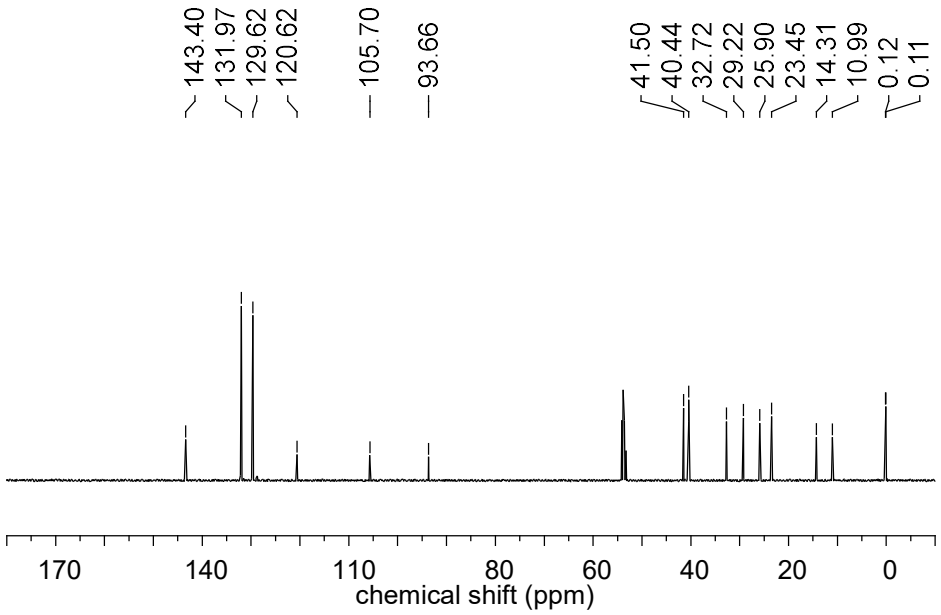

^{1}H: S4.9

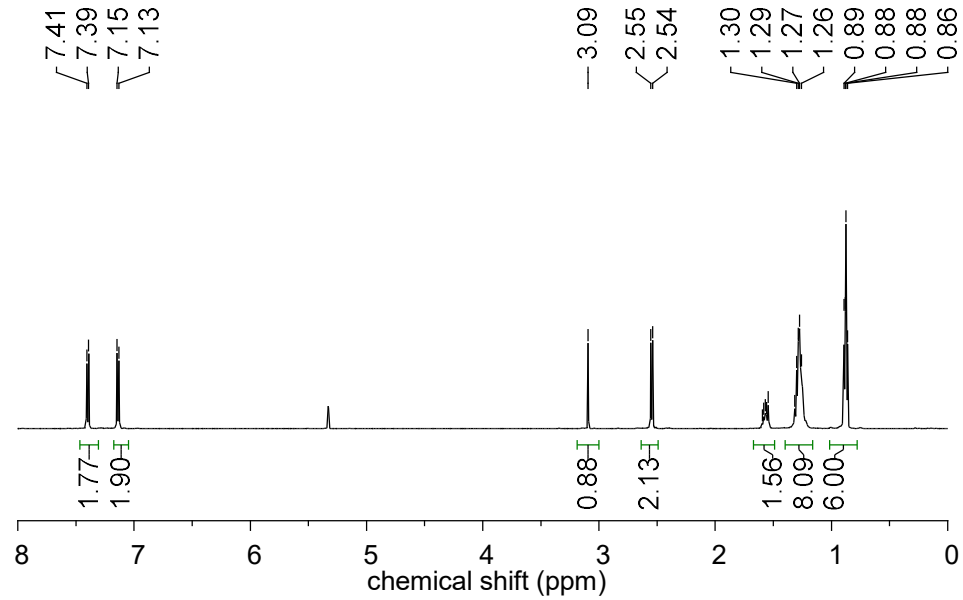

^{13}C: S4.9

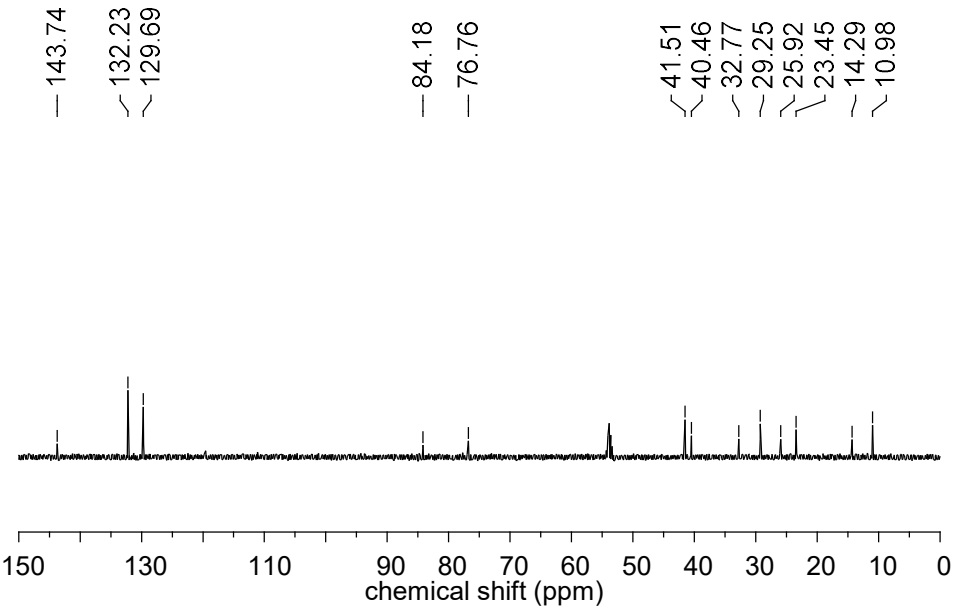

^{1}H: S4.10

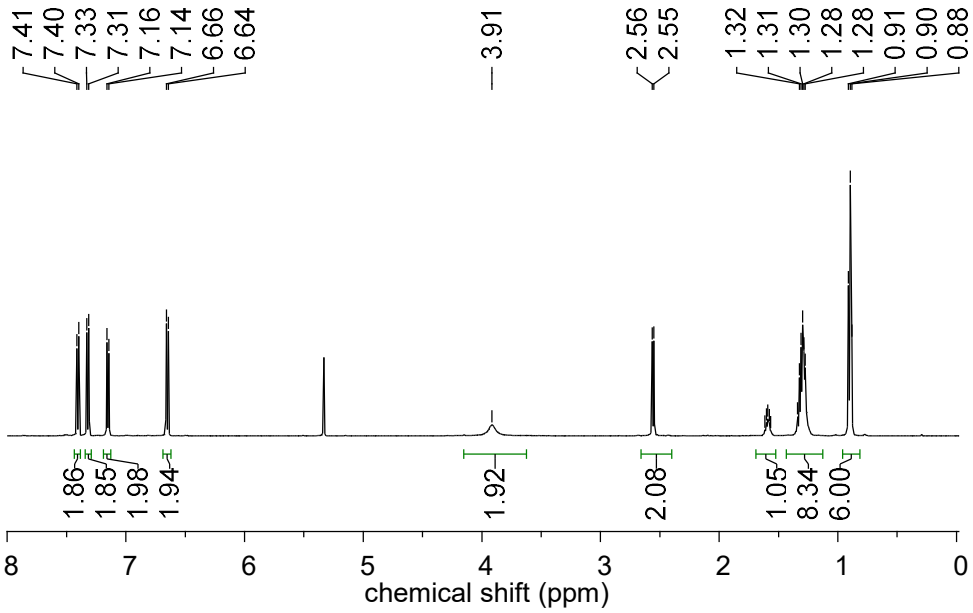

^{13}C: S10

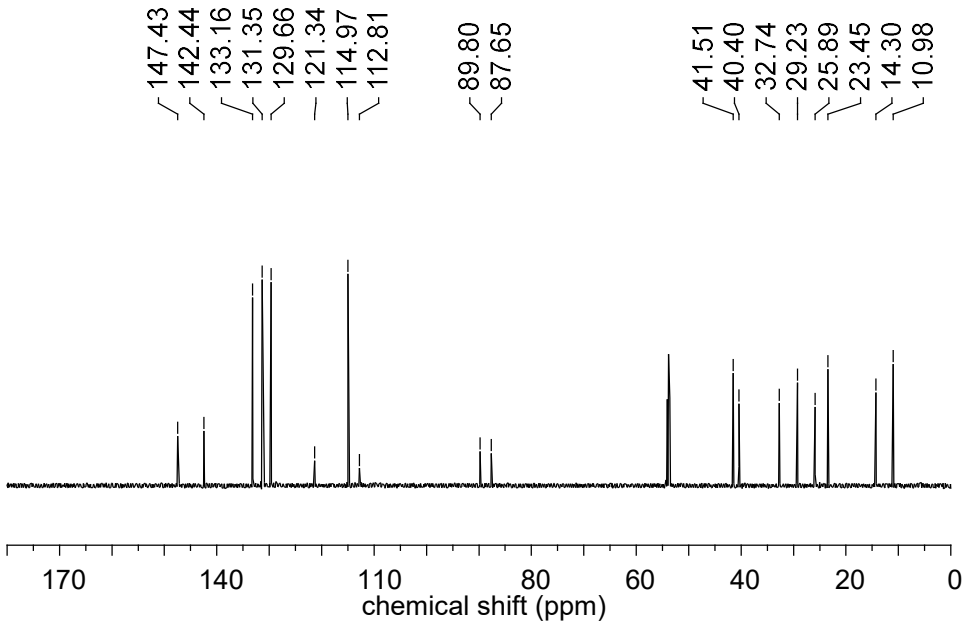

^{1}H: S4.11

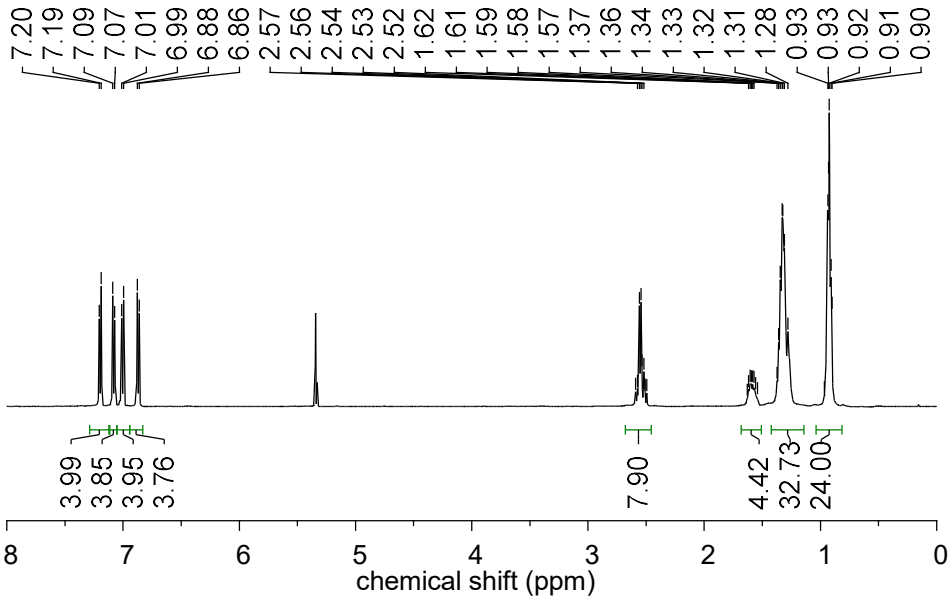

^{13}C: S11

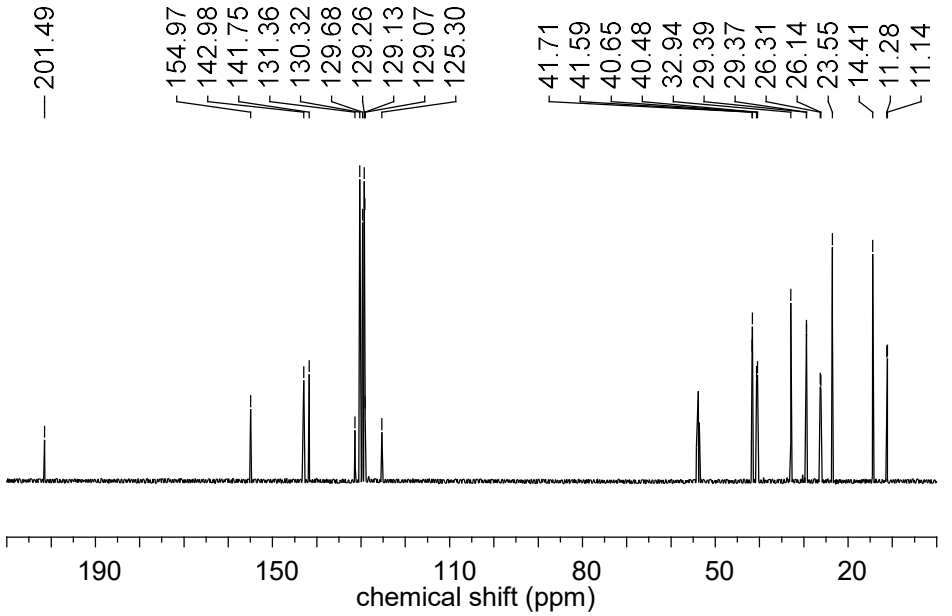

^{1}H: HPB-NH_2

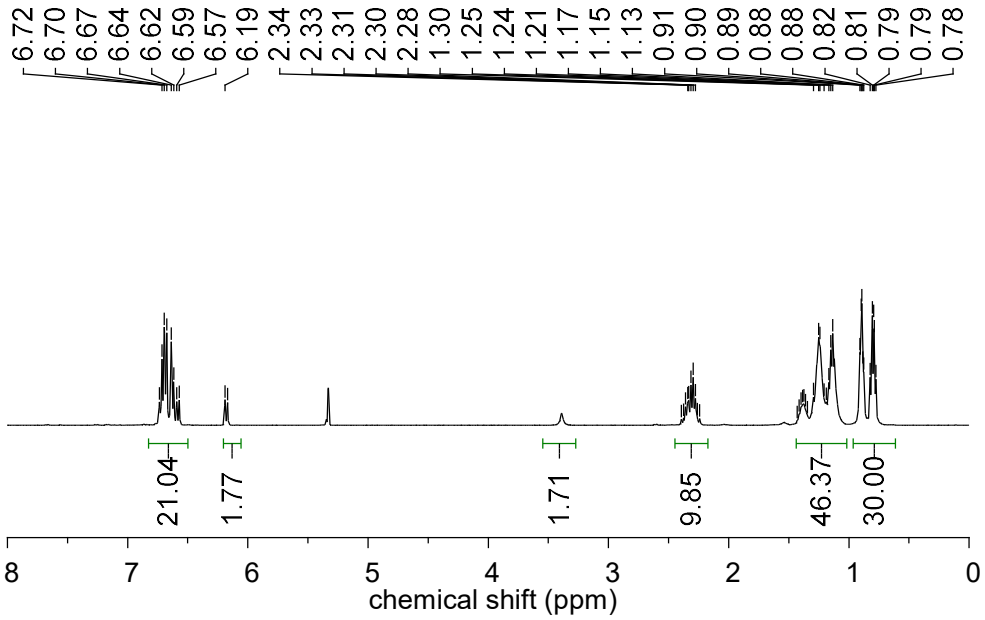

^{13}C: HPB-NH_2

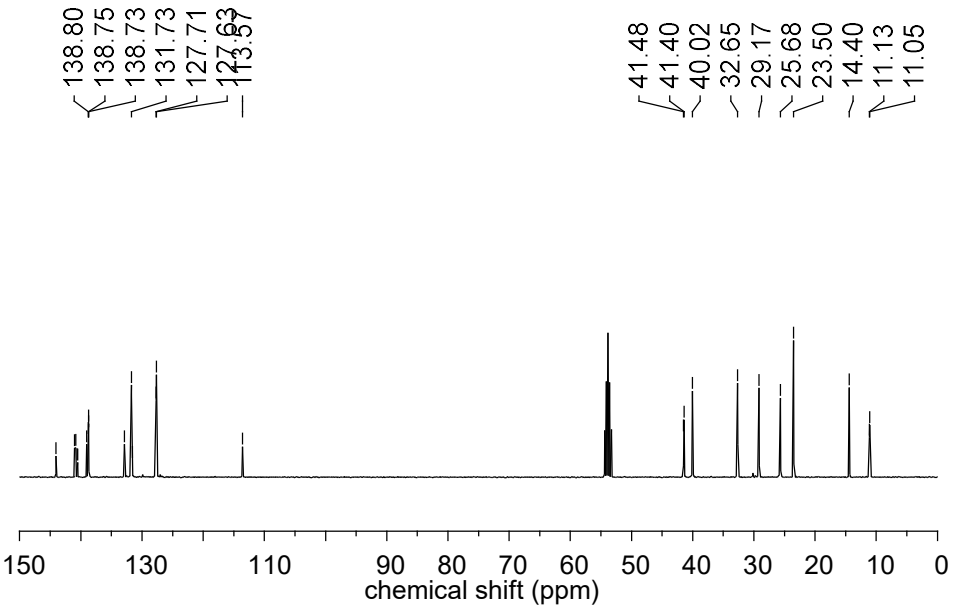

^{1}H: NB-HPB

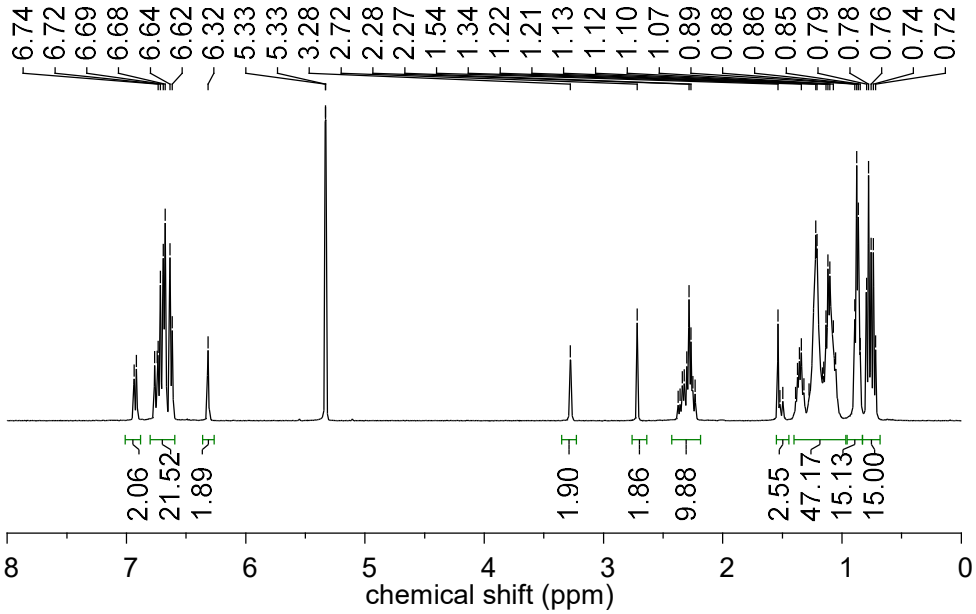

^{13}C: NB-HPB

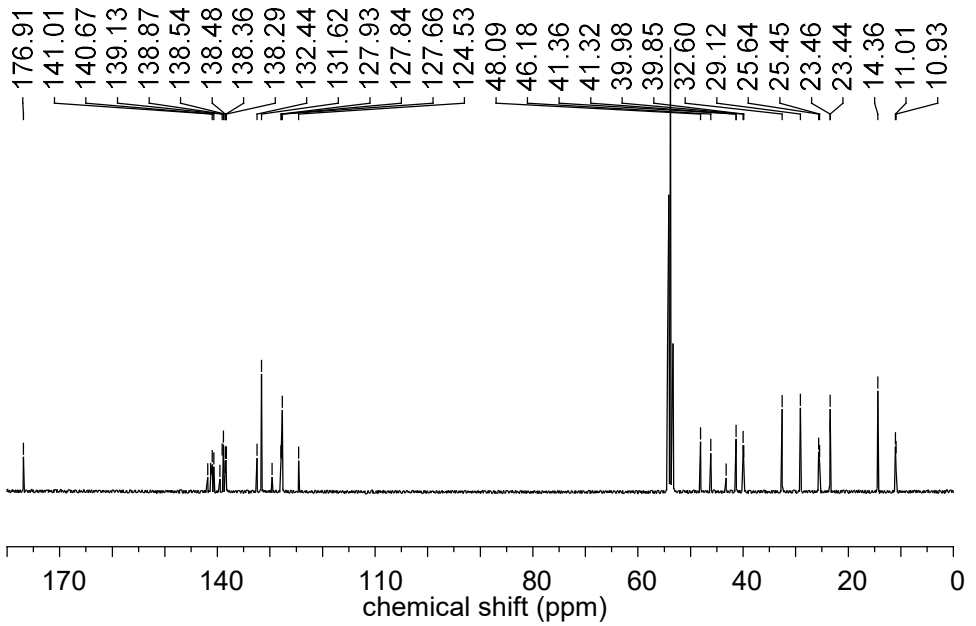

^{1}H: NB-HBC

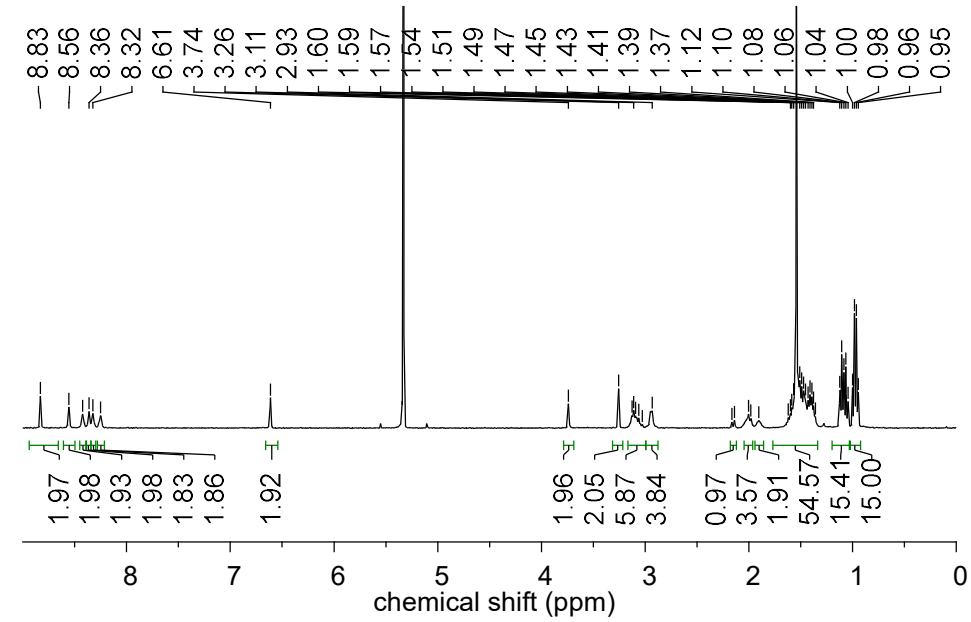

^{13}C: NB-HBC

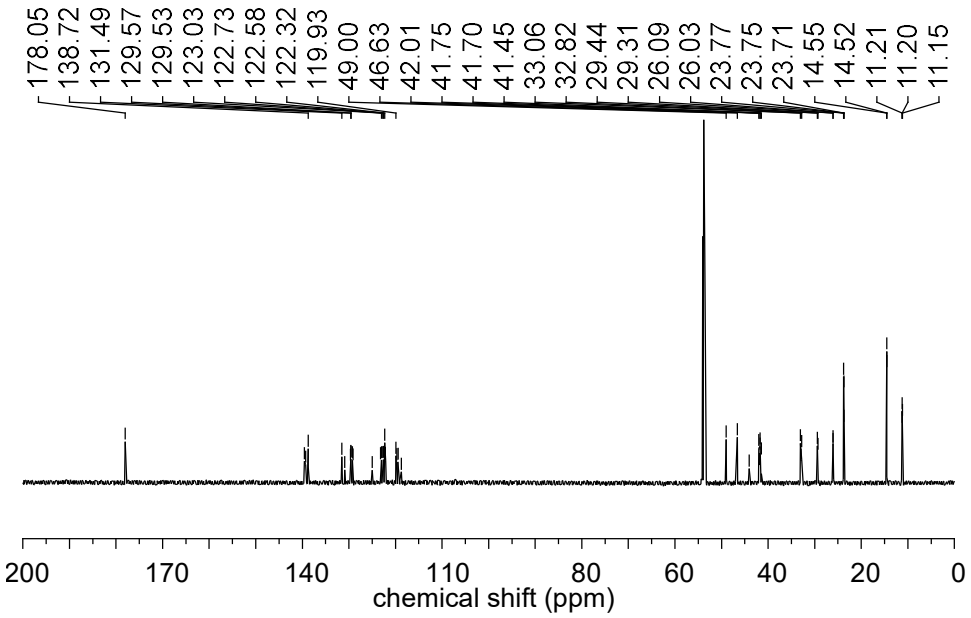

4.6. References

(1) Narita, A.; Wang, X.-Y.; Feng, X.; Müllen, K. *Chemical Society Reviews* **2015**, *44*, 6616.

(2) Anthony, J. E. *Chemical Reviews* **2006**, *106*, 5028.

(3) Chen, L.; Hernandez, Y.; Feng, X.; Müllen, K. *Angewandte Chemie International Edition* **2012**, *51*, 7640.

(4) Narita, A.; Feng, X.; Müllen, K. *The Chemical Record* **2015**, *15*, 295.

(5) Segawa, Y.; Maekawa, T.; Itami, K. *Angewandte Chemie International Edition* **2015**, *54*, 66.

(6) Zhang, X.; Xu, Z.; Si, W.; Oniwa, K.; Bao, M.; Yamamoto, Y.; Jin, T. *Nature Communications* **2017**, *8*, 15073.

(7) Yan, X.; Li, L.-s. *Journal of Materials Chemistry* **2011**, *21*, 3295.

(8) Baldridge, K. K.; Siegel, J. S. *Angewandte Chemie International Edition* **2013**, *52*, 5436.

(9) Ball, M.; Zhong, Y.; Wu, Y.; Schenck, C.; Ng, F.; Steigerwald, M.; Xiao, S.; Nuckolls, C. *Accounts of Chemical Research* **2015**, *48*, 267.

(10) Pisula, W.; Feng, X.; Müllen, K. *Chemistry of Materials* **2011**, *23*, 554.

(11) Morita, Y.; Suzuki, S.; Sato, K.; Takui, T. *Nature Chemistry* **2011**, *3*, 197.

(12) Sun, Z.; Zeng, Z.; Wu, J. *Chemistry – An Asian Journal* **2013**, *8*, 2894.

(13) Wu, J.; Grimsdale, A. C.; Müllen, K. *Journal of Materials Chemistry* **2005**, *15*, 41.

(14) Lin, H.-A.; Sato, Y.; Segawa, Y.; Nishihara, T.; Sugimoto, N.; Scott, L. T.; Higashiyama, T.; Itami, K. *Angewandte Chemie International Edition* 2018, *57*, 2874.
(15) Wang, P.-I.; Pisula, W.; Müllen, K.; Liaw, D.-J. *Polymer Chemistry* 2016, *7*, 6211.
(16) Tsai, C.-Y.; Zhang, Q.; Wang, Y.-Z.; Shyong, J.; Chen, H.-L.; Liaw, D.-J. *Polymer Chemistry* 2017, *8*, 3327.
(17) Hu, Y.; Dössel, L. F.; Wang, X.-Y.; Mahesh, S.; Pisula, W.; De Feyter, S.; Feng, X.; Müllen, K.; Narita, A. *ChemPlusChem* 2017, *82*, 1030.
(18) Shin, S.; Menk, F.; Kim, Y.; Lim, J.; Char, K.; Zentel, R.; Choi, T.-L. *Journal of the American Chemical Society* 2018, *140*, 6088.
(19) Shin, S.; Gu, M.-L.; Yu, C.-Y.; Jeon, J.; Lee, E.; Choi, T.-L. *Journal of the American Chemical Society* 2018, *140*, 475.
(20) Kawamoto, K.; Zhong, M.; Gadelrab, K. R.; Cheng, L.-C.; Ross, C. A.; Alexander-Katz, A.; Johnson, J. A. *Journal of the American Chemical Society* 2016, *138*, 11501.
(21) Guo, Z.-H.; Le, A. N.; Feng, X.; Choo, Y.; Liu, B.; Wang, D.; Wan, Z.; Gu, Y.; Zhao, J.; Li, V.; Osuji, C. O.; Johnson, J. A.; Zhong, M. *Angewandte Chemie International Edition* 2018, *57*, 8493.
(22) Kim, K. O.; Choi, T.-L. *Macromolecules* 2013, *46*, 5905.
(23) Kim, K. O.; Choi, T.-L. *ACS Macro Letters* 2012, *1*, 445.
(24) Dutertre, F.; Bang, K.-T.; Loppinet, B.; Choi, I.; Choi, T.-L.; Fytas, G. *Macromolecules* 2016, *49*, 2731.
(25) Peterson, G. I.; Bang, K.-T.; Choi, T.-L. *Journal of the American Chemical Society* 2018, *140*, 8599.

(26) Bailey, G. A.; Foscato, M.; Higman, C. S.; Day, C. S.; Jensen, V. R.; Fogg, D. E. *Journal of the American Chemical Society* 2018, *140*, 6931.
(27) Kang, E.-H.; Lee, I. S.; Choi, T.-L. *Journal of the American Chemical Society* 2011, *133*, 11904.
(28) Hickey, S. M.; Ashton, T. D.; Boer, G.; Bader, C. A.; Thomas, M.; Elliott, A. G.; Schmuck, C.; Yu, H. Y.; Li, J.; Nation, R. L.; Cooper, M. A.; Plush, S. E.; Brooks, D. A.; Pfeffer, F. M. *European Journal of Medicinal Chemistry* 2018, *160*, 9.
(29) Albert, S. K.; Sivakumar, I.; Golla, M.; Thelu, H. V. P.; Krishnan, N.; K. L, J. L.; Ashish; Varghese, R. *Journal of the American Chemical Society* 2017, *139*, 17799.

국문초록

자연계의 고분자를 모방하고 넘어설 수 있는 정교한 구조를 가진 거대한 고분자의 합성은 고분자화학 분야에서 중요한 목표다. 특히 그라프트 고분자의 경우 선형의 고분자(linear polymer)가 곁사슬로써 주 사슬에 도입된 고분자이다. 하지만 고분자 곁사슬이 가지는 결함과 분포 문제로 인해, 거대분자의 구조(architecture)를 정밀하게 조절하는 데 있어 아직 한계가 존재한다. 본 논문에서는 잘 정립된 거대분자들의 합성 및 그 특징에 대해 다음 세 장에 걸쳐 소개한다.

2장에서는 높은 세대의 덴드론화 고분자 합성을 보고한다. 덴드론화 고분자는 주 사슬에 부채형태의 곁사슬인 dendron이 도입된 독특한 고분자다. 고리개환복분해중합(ring opening metathesis polymerization, ROMP)을 이용해서 지금까지 grafting-through 방법으로 합성된 덴드론화 고분자 중 가장 높은 세대인 6세대의 에스터 덴드론을 가진 결함이 없는 덴드론화 고분자를 합성했다. Size-exclusion chromatography multi-angle laser light scattering (SEC-MALLS) 및 small-angle neutron scattering (SANS) 분석 기법을 통해 덴드론화 고분자의 반지름, 구조(conformation) 및 grafting density간의 상관관계를 규명했다.

3장에서는 polyphenylene dendron기반의 덴드론화 고분자합성을 보고한다. 조절된 ROMP방법을 통해 최대 1484kDa의 분자량과 1.3이하의 좁은 분포도를 가진 덴드론과 고분자를 합성했다. 초음파 분해기법을 이용해 합성한 덴드론화 고분자의 기계화학적 반응에 대해 연구했다. 이 연구를 통해 덴드론화 고분자에서 주사슬이 펴진 정도와 분해속도간의 정량적인 관계를 파악했다.

4장에서는 카본 나노닷 고분자의 합성을 보고한다. 나노그래핀을 포함한 노보넨(norbornene)의 고분자화 반응을 통해 결함이 없는 카본 나노닷

고분자를 합성했다. Grubbs 3세대 촉매를 이용해 1.4이하의 좁은 분산도를 유지하면서 고분자의 분자량을 32 kDa에서 164 kDa까지 조절할 수 있었다. 또한 이 방법을 이용해 나노그래핀을 포함한 블록 공중합체를 처음으로 합성했다.

주요어: 고리개환복분해중합, 덴드론화 고분자, 다각도광산란기법, 구조, 기계화학, 나노그래핀

학번:2014-21252